VOLUME 34 JULY 1956 NUMBER 7

Canadian Journal of Physics

Editor: G. M. VOLKOFF

Associate Editors:

L. G. ELLIOTT, *Atomic Energy of Canada, Ltd., Chalk River*
J. S. FOSTER, *McGill University*
G. HERZBERG, *National Research Council of Canada*
L. LEPRINCE-RINGUET, *Ecole Polytechnique, Paris*
R. W. PRINGLE, *University of Manitoba*
B. W. SARGENT, *Queen's University*
Sir FRANCIS SIMON, *Clarendon Laboratory, University of Oxford*
W. H. WATSON, *University of Toronto*

Published by THE NATIONAL RESEARCH COUNCIL
OTTAWA CANADA

CANADIAN JOURNAL OF PHYSICS

(Formerly Section A, Canadian Journal of Research)

Under the authority of the Chairman of the Committee of the Privy Council on Scientific and Industrial Research, the National Research Council issues THE CANADIAN JOURNAL OF PHYSICS and six other journals devoted to the publication, in English or French, of the results of original scientific research. Matters of general policy concerning these journals are the responsibility of a joint Editorial Board consisting of: members representing the National Research Council of Canada; the Editors of the Journals; and members representing the Royal Society of Canada and four other scientific societies.

EDITORIAL BOARD

Representatives of the National Research Council

A. N. Campbell, *University of Manitoba*
G. E. Hall, *University of Western Ontario*
H. G. Thode, *McMaster University*
D. L. Thomson, *McGill University*
W. H. Watson (Chairman), *University of Toronto*

Editors of the Journals

D. L. Bailey, *University of Toronto*
T. W. M. Cameron, *Macdonald College*
J. B. Collip, *University of Western Ontario*
G. A. Ledingham, *National Research Council*
Léo Marion, *National Research Council*
R. G. E. Murray, *University of Western Ontario*
G. M. Volkoff, *University of British Columbia*

Representatives of Societies

D. L. Bailey, *University of Toronto*
Royal Society of Canada
T. W. M. Cameron, *Macdonald College*
Royal Society of Canada
J. B. Collip, *University of Western Ontario*
Canadian Physiological Society
R. G. E. Murray, *University of Western Ontario*
Canadian Society of Microbiologists
H. G. Thode, *McMaster University*
Chemical Institute of Canada
T. Thorvaldson, *University of Saskatchewan*
Royal Society of Canada
G. M. Volkoff, *University of British Columbia*
Royal Society of Canada; Canadian Association of Physicists

Ex officio

Léo Marion (Editor-in-Chief), *National Research Council*
F. T. Rosser, Director, Division of Administration, *National Research Council*

Manuscripts for publication should be submitted to Dr. Léo Marion, Editor-in-Chief, Canadian Journal of Physics, National Research Council, Ottawa 2, Canada.
(For instructions on preparation of copy, see **Notes to Contributors** (inside back cover).)

Proof, correspondence concerning proof, and orders for reprints should be sent to the Manager, Editorial Office (Research Journals), Division of Administration, National Research Council, Ottawa 2, Canada.

Subscriptions, renewals, requests for single or back numbers, and all remittances should be sent to Division of Administration, National Research Council, Ottawa 2, Canada. Remittances should be made payable to the Receiver General of Canada, credit National Research Council.

The journals published, frequency of publication, and prices are:

Canadian Journal of Biochemistry and Physiology	Bimonthly	$3.00 a year
Canadian Journal of Botany	Bimonthly	$4.00 a year
Canadian Journal of Chemistry	Monthly	$5.00 a year
Canadian Journal of Microbiology	Bimonthly	$3.00 a year
Canadian Journal of Physics	Monthly	$4.00 a year
Canadian Journal of Technology	Bimonthly	$3.00 a year
Canadian Journal of Zoology	Bimonthly	$3.00 a year

The price of single numbers of all journals is 75 cents.

Canadian Journal of Physics

Issued by THE NATIONAL RESEARCH COUNCIL OF CANADA

VOLUME 34 JULY 1956 NUMBER 7

METEORIC ECHOES OBSERVED SIMULTANEOUSLY BY BACK SCATTER AND FORWARD SCATTER[1]

BY D. W. R. MCKINLEY AND A. G. MCNAMARA

ABSTRACT

Simultaneous observations of back-scatter and forward-scatter meteoric echoes have been made by means of a high-power 33 Mc./sec. pulse transmitter at Ottawa, with identical receiving systems at Ottawa and at Scarboro, 337.8 km. distant. Two-way transmissions, employing a low-power transmitter at Scarboro, were also used to measure absolute time delays. The approximate position of each meteor was plotted from the observed time delays, which enabled corrections to be applied to the echo durations for variations in antenna patterns and other factors, and which also determined the forward-scatter angle, 2ϕ, for each meteor. In the majority of cases an enhancement was observed in the forward-scatter duration relative to the back-scatter duration. The data were divided into a short-duration or underdense group and a long-duration or overdense group. Assuming a theoretical forward-scatter enhancement proportional to $\sec^m \phi$, it was found that the exponent, m, was 1.73 for the underdense group and 1.13 for the overdense group.

INTRODUCTION

In an earlier paper (McKinley 1954), an attempt was made to predict, from available back-scatter data on meteoric echo durations, the probable performance of a forward-scatter meteoric system as a function of wavelength and sensitivity. Intrinsic in the argument was the assumption, developed theoretically by Eshleman and Manning (1954), that for a given meteor echo the ratio of the forward-scatter duration, T_F, to the back-scatter duration, T_B, is given by $T_F/T_B = \sec^2\phi$, where 2ϕ is the angle at the meteor between the incident and reflected ray. Some experimental evidence to support this hypothesis has been presented by the Stanford workers (e.g., Villard, Peterson, and Manning 1953) and also by Forsyth and others (Forsyth and Vogan 1955; Forsyth, Hines, and Vogan 1955). In those experiments a continuous-wave method was used, which provided a satisfactory record of echo amplitude but failed to yield any range resolution of individual echoes, nor was it easy to determine the value of the forward-scattering angle in each case. The pulsed radar technique provides a high degree of range resolution which can be used to locate the meteor positions, and it also simplifies the problem of operating a receiver in the near vicinity of the transmitter for recording back-scatter echoes. Accordingly, early in 1954, the 33 Mc./sec. meteor radar system at

[1]Manuscript received February 8, 1956.
Contribution from the Radio and Electrical Engineering Division, National Research Laboratories, Ottawa, Canada. Issued as N.R.C. No. 3972.

Ottawa was modified to carry out simultaneous observations of back-scatter and forward-scatter meteor echoes.

The Ottawa transmitter was rebuilt to emit 10-μsec. pulses at a peak power of about 300 kw. The average power was 300 w. (Owing to a typographical error in the earlier paper by McKinley (1954) the average power of the equipment at that time was given as 5 kw.—it should have been 500 w.) In the earlier back-scatter work at Ottawa, the transmitter and receiver each used a single half-wave dipole, mounted a quarter-wave above ground. For this experiment each dipole was enclosed by a 60° corner reflector, made of spaced wires, in order to concentrate the radiation pattern in a broad beam approximately 30° above the horizon. The calculated gain of this antenna was 12 db. relative to a dipole in free space. A scaled-down model of the antenna was built (scale 1:100) and the radiation patterns of this model, measured in the horizontal and vertical planes, are shown in Fig. 1. The transmitting and receiving an-

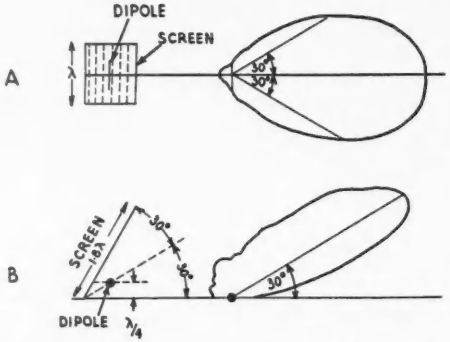

FIG. 1. Schematics and radiation patterns of corner reflector antenna. A—Horizontal plane. B—Vertical plane.

tennas at Ottawa were directed toward the station at Scarboro, Ontario, (near Toronto) on an approximate bearing of 238° from Ottawa. The great circle distance between the stations is 337.8 km. At Scarboro, an identical corner reflector antenna and a duplicate receiver and display were installed, with the antenna directed towards Ottawa so that the main axes of the Ottawa and Scarboro beams intersected at the 90 km. height level.

The conventional range–time recording technique was used at both Ottawa and Scarboro. In the early stage of the experiment the range, or delay time, calibration at both stations was done by means of the usual 20 km. range markers (spaced at intervals of 133 μsec.), which were later replaced by markers spaced at 100-μsec. intervals. Two examples selected from these records are shown in Fig. 2.

TWO-WAY TRANSMISSIONS

On the Scarboro records of Fig. 2 will be seen a stationary signal (marked *Trop.*) which was received from Ottawa for an appreciable fraction of the observing time. On some occasions this signal would remain above noise for

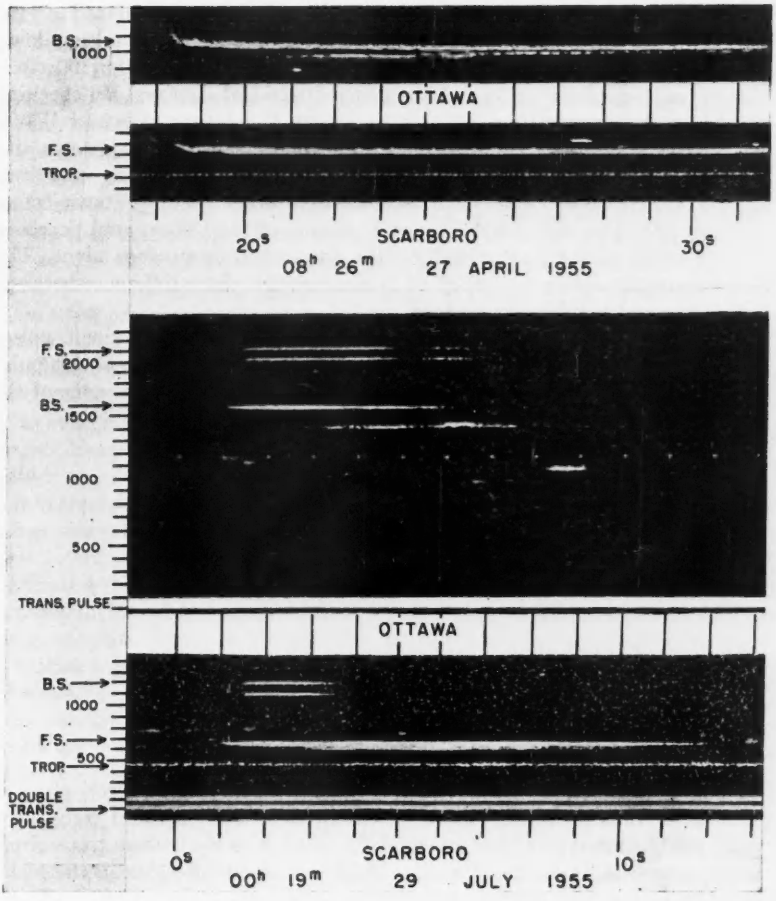

FIG. 2. Samples of the Ottawa and Scarboro records. The ordinate axis is delay time in microseconds. The records at 08h 26m, 27 April, 1955, show an approaching head echo on both films. The Scarboro transmitter was not operating at the time. The records at 00h 19m, 29 July, 1955, show both back- and forward-scattered echoes at each end of the link, from the same meteor.

several hours, though it was often absent, especially during the late afternoons and evenings, and particularly in the wintertime. In order to prove that this signal was propagated via a tropospheric path, and also to provide a means of measuring absolute delays of meteor echoes at Scarboro in the absence of this signal, a second transmitter was installed at Scarboro, operating on the same frequency as the Ottawa station.

The peak power at Scarboro was about 1 kw. and the energy was emitted in double pulses, with a spacing of 100 μsec. between the two pulses to distinguish the echoes from those produced by the Ottawa transmitter. This low-

power transmitter fed a Yagi antenna with about 10 db. gain, directed toward the mid-point of the path. High-stability quartz crystals and counting-down circuits were used at both Ottawa and Scarboro to generate the 100 c.p.s. recurrence frequencies for keying the transmitters and displays. By checking the crystal harmonics from time to time with the transmissions of WWV the relative stability of the recurrence frequencies generated at Ottawa and Scarboro could be maintained to a high degree, so that there was very little drift of the Scarboro range–time record with respect to the Ottawa transmissions. However, the relative phase or timing of the Ottawa and Scarboro records could not be determined by the one-way transmissions alone. The Scarboro transmissions permitted us to measure this phase difference between the records in the following manner.

The top line of Fig. 3 shows the Ottawa transmitter (solid single pulse) firing at an arbitrary zero reference time. A forward-scatter echo of this pulse from a meteor, which may be located anywhere in space within range of the

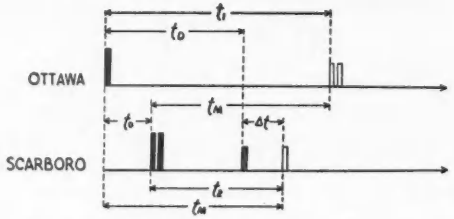

FIG. 3. Timing diagram of the two-way forward-scatter system.
Solid single pulse—Ottawa transmitter.
Solid double pulse—Scarboro transmitter.
Open single pulse—forward-scatter meteor echo received at Scarboro.
Open double pulse—forward-scatter meteor echo received at Ottawa.
Shaded single pulse—tropospheric signal received at Scarboro.

system, is received at Scarboro (bottom line—open single pulse), after an interval of time t_M which has to be determined. The Scarboro transmitter (solid double pulse) fires after an interval t_0 relative to the Ottawa transmitter, where t_0 represents the constant but unknown phase difference in the recurrence frequency. The Scarboro transmission is received at Ottawa (open double pulse) via the same meteor over the return path, after the same elapsed time, t_M. The quantities which can actually be measured from the two records are the intervals t_1 and t_2. Therefore, we have $t_0 = t_M - t_2 = t_1 - t_M$; whence $t_M = (t_1+t_2)/2$, and $t_0 = (t_1-t_2)/2$.

For each of the selected meteor echoes considered in this paper a back-scatter echo appeared at Ottawa, and in some cases a similar back-scatter echo showed at Scarboro from the low-power transmitter (see Fig. 2), but these back-scatter echoes have been omitted from Fig. 3 to avoid confusion. In Fig. 3, we have shown as a shaded single pulse on the Scarboro record a stationary signal which was received for long periods of time from the Ottawa transmitter, with a time delay, t_D, (see also the signal marked *Trop.* on the Scarboro records of Fig. 2). For each meteoric echo which appeared on both

records a time t_M could be calculated, and a value obtained of the time interval, Δt, between the tropospheric pulse and the selected meteor echo, whence $t_D = t_M - \Delta t$. When the stationary signal was first observed it was not clear whether it was a direct tropospheric pulse, or a pulse received via the ionosphere, presumably from some point or points near the mid-path, in the vertical plane containing the stations. A large number of measurements showed that $t_D = 1129$ μsec., which corresponds closely to the tropospheric path over the great circle distance of 337.8 km. between the stations. The stationary signal having thus been identified as tropospheric, with little variation in delay from day to day, it may be used as a reference timing marker on the Scarboro record.

On a few occasions a second stationary pulse has been observed at Scarboro, delayed after the tropospheric signal, but the evidence available to date is insufficient to determine whether this second pulse may have been due to ionospheric reflections at high altitudes in the vertical plane through the stations, or to reflections from an aircraft at lower altitudes (or even from a ground target) located to one side of this plane. This matter will be investigated further.

It is thus possible to determine the forward-scatter delay time, t_M, and the phase interval, t_0, for each meteor that has yielded a forward-scatter echo on both records. One may interpolate between such observations to obtain a continuous and accurate measure of the slow rate of change of t_0, in order to measure t_M for other forward-scatter echoes which appeared at Scarboro but not at Ottawa, owing to the low power of the Scarboro transmitter. This technique would be especially useful over a long base line where no tropospheric echo was observable at any time. However, since over our relatively short base line the direct tropospheric pulse was observable on the Scarboro record for a considerable percentage of the observing time—though it was rarely more than a few decibels above noise, and the return echo was never observed at Ottawa—it was more convenient to employ the time interval Δt as a measure of the meteoric forward-scatter delay time.

CONTOUR MAPS OF TIME DELAYS AND RELATIVE ECHO POWERS

If we assume the meteoric echoes to occur at a mean height of 90 km., then the position of each meteor may be plotted on a plan view of the 90 km. level, from a knowledge of the back-scatter and forward-scatter delay times. The dashed curves on the top half of Fig. 4 show the contours of back-scatter delay times relative to the Ottawa station, calculated for the 90 km. height level. The solid curves on the top half of Fig. 4 shows the contours on the 90 km. level of forward-scatter delay times, relative to the time taken for the tropospheric pulse to travel from Ottawa to Scarboro. The intersection of the two characteristic delay curves for a given meteor will locate the meteor in space. There will be a mirror-image ambiguity with respect to the line joining the stations, of course. If the actual height of the meteor is greater than 90 km. its true plan position will be nearer to the vertical plane through the stations than the plotted position, and vice versa. The effect is most pronounced for meteors nearest

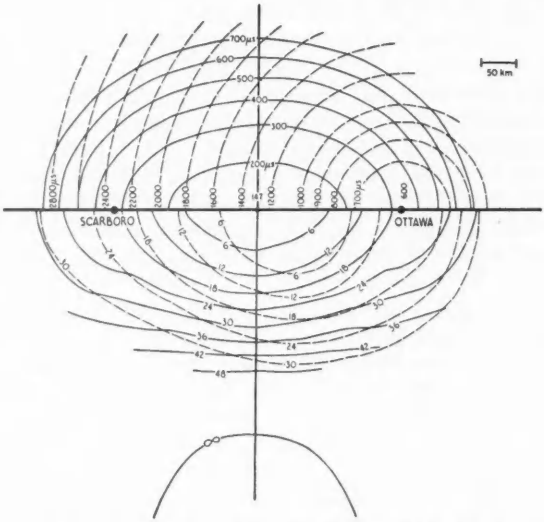

FIG. 4. *Top half.—Dashed lines* are contours of back-scatter time delay. *Solid lines* are contours of forward-scatter time delay relative to the tropospheric path.
Bottom half.—Dashed lines are contours of received back-scatter power, in decibels below the maximum value near the mid-point. *Solid lines* are contours of received forward-scatter power. All contours are drawn on the 90 km. height level.

to this vertical plane; therefore the meteor positions plotted in this immediate vicinity can only be regarded as approximate, and little reliance can be placed on their apparent distribution. The meteor positions are used to determine the power corrections to be applied to the echo durations, and, while a plotting error of this nature would represent a first-order error in either one of the power level maps described below, the plotting error results in a second-order error only in the power level differences which are actually used.

On the bottom half of Fig. 4 the dashed curves show the contours, on the 90 km. level, of constant power received back at the Ottawa station, in decibels below the maximum value which occurs near the mid-point. These were calculated as follows. The vertical antenna pattern of Fig. 1 was used to determine a series of points along the line joining the stations as projected on the 90 km. level. The inverse square law of attenuation with distance was assumed, so that this first step resulted in a one-way one-dimensional power plot. Similarly the horizontal antenna pattern was used to calculate the transverse power distribution on the right-bisector of the path, projected on the 90 km. level. The corresponding points on these two lines were then joined by smooth curves to yield a one-way power contour map. It is felt that these contours were fairly realistic over most of the area between the two stations, but they were admittedly subject to considerable error well off to either side, and to the rear of the Ottawa station where the side lobe structure was not well determined. The dashed curves of the bottom half of Fig. 4 were calculated by squaring the

power contour values of this one-way map, or by doubling the attenuation figures in decibels. Similarly, the solid curves of the bottom half of Fig. 4 were computed by first making a mirror image of the one-way map centered on Scarboro, superimposing this on the Ottawa map, and then adding point by point the decibel values of the two maps. Next, the effect of the reradiation pattern and its polarization relative to the receiving dipole was also included (Eshleman and Manning 1954), which results in one contour of infinite forward-scatter attenuation. An over-all inverse fourth power law is probably appropriate for many of the long-duration echoes that form the bulk of the observations. If an equivalent inverse cube law were assumed, as might be expected to apply to the short-duration echoes, the contours of Fig. 4 would be slightly displaced, but it was found that for purposes of this paper it made little difference which law was adopted, since we used only the power differentials between the back- and forward-scatter patterns, and not the absolute values.

Eshleman and Manning (1954) showed that, in addition to the $\sec^2\phi$ effect on echo durations, there should be an increase in the forward-scatter echo amplitude, which is proportional to $\sec\phi$ if the meteor trail lies in a plane containing the two stations, and which falls off to unity as the trail approaches the transverse orientation. In our experiment the maximum power enhancement would be about 6 db., but the average meteor echo would show much less, so this effect has been neglected. As the meteor path orientations were not known, except under some special circumstances, it would only be possible to assume an average enhancement, of about 1 or 2 db., say, which is negligible by comparison with the errors involved in computing the contours.

OBSERVATIONS AND ANALYSIS

The first records were obtained on the Ottawa–Scarboro high-power link in August, 1954. The Scarboro–Ottawa low-power link was put into operation in February, 1955, which, by confirming the tropospheric character of the stationary pulse, enabled us to use some of the earlier records as well, for purposes of this paper. The system has been operated intermittently for about a year, roughly one day a month on the average, with some attention being given to a few of the major shower periods. From the data on hand we have selected 212 meteor echoes which we believe have been observed simultaneously by forward and back scatter. The selection is by no means exhaustive because, for convenience, we have usually used only those periods during which the tropospheric pulse was present. Furthermore, the selection is biased strongly towards the longer echo durations where there was little doubt that the echoes were from the same meteor. For the shorter durations the criteria of coincidence in time and of similar echo characteristics were more difficult to apply because of the large numbers of such echoes. Therefore, no significance can be attached to any relation between numbers and duration in our selected data.

Fig. 5 shows the plan positions on the 90 km. level of the 212 selected echoes. Each echo has been plotted twice, as a mirror-image reflection about

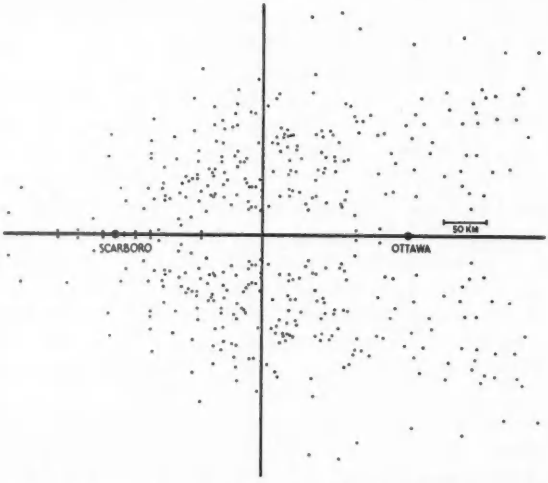

FIG. 5. Observed meteor positions plotted on the 90 km. level. There are 212 observations, and each position is plotted twice as a mirror image about the Ottawa–Scarboro line.

the center line, because we do not know which of the two positions is the correct one. Since the data have been picked from any hour of the day or night, on several days spaced some months apart, and also during some shower periods, no significant conclusions can be drawn concerning possible radiant distributions. For the longer duration echoes, too, the aspect sensitivity of the meteor trail decreases, which means that the radiant position no longer has to satisfy stringent geometrical requirements for simultaneous forward- and backscatter echoes.

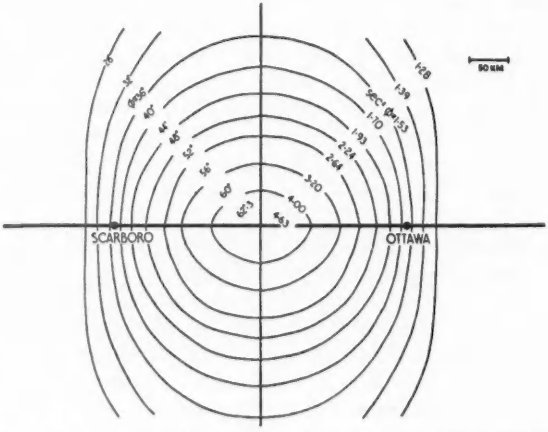

FIG. 6. Contours of constant ϕ and $\sec^2 \phi$, calculated for the 90 km. height level.

We can superimpose the position plots in Fig. 5 over the power contour maps in the lower half of Fig. 4 and, for each meteor, read the difference in power level which would be expected to occur between the forward-scatter and back-scatter echoes from the meteor in the given position. In an earlier paper (McKinley 1953*a*) there was given a set of empirical curves with which to correct observed echo durations measured above an arbitrary threshold level (the receiver noise level was used in all cases) for variations in power level. These curves were used here to correct the back-scatter duration of a given echo to a power level corresponding to that expected for the forward-scatter echo. For example, suppose an echo has a forward-scatter duration of 20 sec. and a back-scatter duration of 10 sec. and, from its plotted position, the power level difference is +10 db. in favor of the back-scatter echo, i.e. the back-scatter echo would be expected to be 10 db. stronger than the forward-scatter echo. In this case the correction curves indicate that the back-scatter duration for an echo 10 db. weaker than the one actually observed would be about 7 sec., which may then be compared directly with the 20 sec. forward-scatter duration. Conversely, if the power level differential were found to be −10 db., the corrected back-scatter duration would be about 13 sec. In the analysis that follows, T_F will refer to the observed forward-scatter duration, and T_B to the corrected back-scatter duration.

Of the 212 echoes in the original data shown in Fig. 5 it is apparent that some lie behind the Ottawa station, or in regions where the calculated power contours are susceptible to rather large errors. We have therefore selected 178 echoes which lie within the area on the power contour map that we feel is reasonably well charted. Fig. 7 shows the individual plots of log T_F against log T_B (common logarithms) for these echoes. The straight line denotes the 1:1 relation which would exist if there were no forward-scatter enhancement

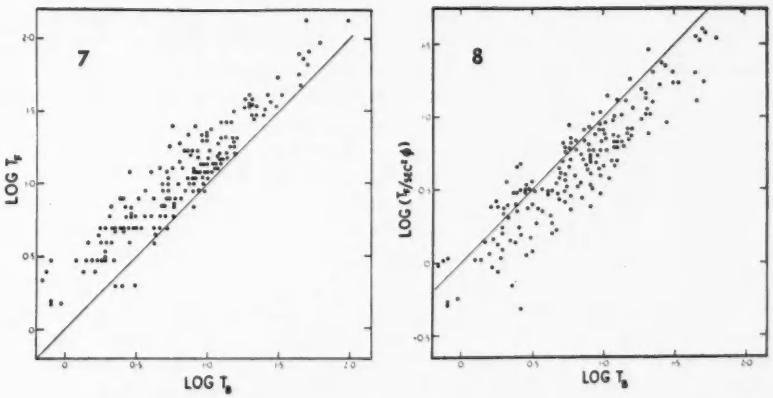

FIG. 7. Relation between log T_F and log T_B for 178 selected meteors. The straight line represents the 1:1 relation, assuming no forward-scatter enhancement.

FIG. 8. Relation between log(T_F/sec^3 ϕ) and log T_B for 178 selected meteors. The straight line represents the 1:1 relation, assuming a forward-scatter enhancement proportional to sec^3 ϕ for all meteor durations.

of the echo, and it is obvious that for essentially all the echoes there is some forward-scatter enhancement. Earlier experience with the same 33 Mc. experimental equipment (McKinley 1953*b*) has indicated that the transition from underdense to overdense meteor trails should occur for back-scatter durations of 3 to 4 sec. ($\log T_B = 0.55$), and a casual inspection of Fig. 7 does suggest that there may be a greater enhancement for the short-duration echoes, that is, for $\log T_B < 0.55$.

In Fig. 6 we have plotted the calculated contours of ϕ and $\sec^2 \phi$ on the 90 km. level, for our station spacing. By superimposing the observed meteor position plots of Fig. 5 over Fig. 6 the value of $\sec^2 \phi$ can readily be found for each meteor. The theory of Eshleman and Manning (1954) implies that $T_F/\sec^2 \phi$ should be equal to T_B, for the underdense trails at least. Fig. 8 shows the individual observations plotted on this basis: the straight line now indicates the 1:1 relationship that one could expect from theory of underdense trails. In the short-duration region the points do appear to be distributed about this line, but they tend to lie below it for the longer durations.

We shall assume that the observed forward-scatter enhancement may be expressed by the factor $\sec^m \phi$ where the exponent m is to be determined from the relation $T_F/\sec^m \phi = T_B$. We may compute the value of m from the data for each echo and consider the distribution of these m values. For this purpose we have divided the observations into two groups: the underdense group for which $\log T_B < 0.55$, containing 50 echoes, and the overdense group for which $\log T_B > 0.55$, containing 128 echoes. The histograms for these cases are shown in Fig. 9. Even intuitively, each of the two distributions appears to be

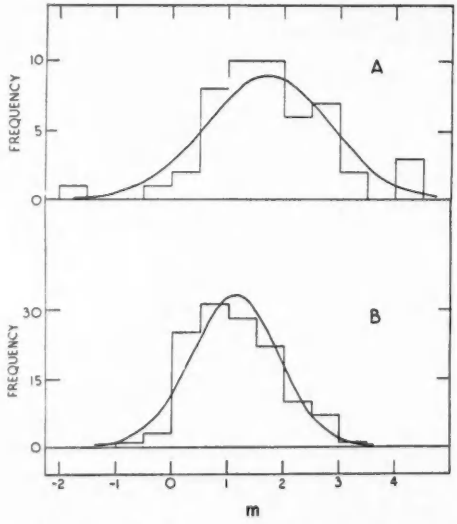

FIG. 9. Frequency distribution of m, where m is the exponent of $\sec^m \phi$ computed for each observation. A—Distribution of m(u) for the underdense trails. B—Distribution of m(o) for the overdense trails. Gaussian error curves, calculated from the observational data, have been fitted to the observed histograms.

reasonably symmetrical about a mean value, which therefore supports our initial assumption that the observations should follow a normal error distribution in terms of the quantity m. Gaussian error curves, computed from the observational data, have been superimposed on the histograms of Fig. 9 as a visual aid in assessing the reliability of the assumption. A more precise verification can be made from a formal application of statistical theory (Cramer 1955), and the results of this are shown in Table I.

TABLE I

Characteristics of the distributions	Underdense group	Overdense group
Number of meteors in the group	50	128
Mean value of m	m(u) = 1.730	m(o) = 1.125
Standard deviation	1.12	0.78
Skewness[a]	−0.024	+0.38
Excess[b]	+0.97	−0.24
Probable error of the mean	0.11	0.05

[a]Skewness is defined by m_3/σ^3 where m_3 is the central moment of order 3, and σ is the standard deviation.
[b]Excess is defined by $(m_4/\sigma^4)-3$ where m_4 is the central moment of order 4.

One might ask first if the two values, m(u) = 1.730 for the underdense group and m(o) = 1.125 for the overdense group, are significantly different. The formal probability tests of significance here show that the observed difference in the mean values of the exponent is significant at the 0.004% level, or that the odds are 25,000:1 against a difference of this magnitude or greater occurring at random. Therefore, we may safely assume the difference is real.

In more detail we can now determine whether our observed value of m(u) = 1.730 could be compatible with the theoretical value m(u) = 2.000, and it is found that the two values are within the confidence interval at the 9% level. If we adopt the customary value of 5% as a standard significance level it follows that the theoretical value does fall well inside this, and hence could reasonably be considered possible within the spread of the observations. If anything, one would expect the observed value of m(u) to be somewhat less than the theoretical value because our underdense group is doubtlessly contaminated with members from the other group owing to overlap and the arbitrary division. Because of the difficulty in correlating the very-short-duration echoes the underdense group is deficient at the short-duration end of the range. The theoretical value of 2 applies strictly to the limiting case of an idealized underdense trail of very small diameter in which each electron scatters independently.

A theoretical value of m(o) for the overdense trails does not appear to be well established in the literature. It may be, of course, that the functional dependence cannot be expressed in the simple form $\sec^m \phi$, but a consideration of our observations does suggest that such an assumption might be satisfactory as a first approximation at least. Eshleman (1955) has shown that for overdense electron concentrations of various shapes, each having a gaussian gradient of ionization, the dependence of the back-scatter duration on wavelength should vary as $\lambda^{4/3}$ for spherical clouds, as λ^2 for cylindrical clouds, and as λ^4 for

laminal clouds. Depending on the degree of isotropy assumed in the scattering, the expected values of $m(o)$ might range from zero to 4. It is probably most unsound to attempt to apply the wavelength dependence to forward-scatter echoes with long durations in a manner analogous to that carried out by Eshleman and Manning for the short-duration trails, but we shall take this step tentatively for purposes of argument. We have already shown that the spread about our observed mean value of $m(o)$ is highly unlikely to include the value $m(u) = 1.730$; hence, *a fortiori*, our observations rule out the possibilities that the meteoric clouds may be overdense cylinders for which we are tentatively assuming $m(o) = 2$, or laminal sheets for which $m(o) = 4$. Therefore, if we assume the long-duration echoes to be due to meteoric clouds of roughly spherical shape, the expected value of $m(o)$ would be 1.333. Comparing this with our observed value, $m(o) = 1.125$, we find that the confidence level is 0.3%, which is well outside the arbitrary 5% level. On the other hand, the confidence level of $m(o) = 1$ happens to be 7% in this case, though there is no apparent theoretical reason why one would consider a value of unity for $m(o)$. In the absence of a sound theory we can only suggest that our observations seem to favor a spherical shape of the meteoric clouds associated with long-duration echoes, in preference to cylindrical or laminal forms.

In this connection Eshleman has suggested in private correspondence that, for the long-duration group of overdense trails, one might expect the observed values of m to decrease with increasing values of ϕ, or sec ϕ. In Fig. 10 we have

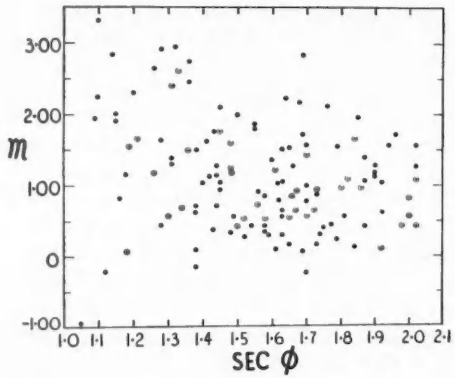

FIG. 10. Relation between m and sec ϕ for the 128 overdense trails. The 36 circled points represent the subgroup of extra-long-duration meteors for which $T_B \geqslant 15$ sec.

plotted m against sec ϕ for the 128 members of the long-duration group. Furthermore, we have circled the 36 points for which $T_B \geqslant 15$ sec. Considering all the points together the scatter of the diagram is so great that it is doubtful if any significant trend can be discerned. However, an examination of the extra-long-duration subgroup of 36 circled points does appear to show a relation between m and sec ϕ of the form proposed by Eshleman, though we would

not like to fit a curve to so few data. The mean value of m for the subgroup is 1.007, which does indicate that for the very-long-duration echoes the forward-scatter enhancement is smaller, though still quite appreciable.

In summing up, it may be of interest to note that the formally computed odds against m being zero or negative are fantastically large, i.e. they are 10^{57}:1 for the overdense case, and 10^{27}:1 for the underdense case. One may therefore conclude unequivocally that there is certainly an average enhancement in the duration of the forward-scatter echo relative to the back-scatter echo, for all echo durations. Assuming the angular dependence of the forward-scatter echo duration to vary as $\sec^m \phi$ we have shown that for the underdense meteor trails the exponent m lies in the neighborhood of 1.73, and for the overdense trails it is near 1.13. In this paper we have confined our attention to one aspect only of the information available in the records. Future papers will examine, among other things, the statistical relations between integrated durations of forward- and back-scatter echoes, including the diurnal variation.

ACKNOWLEDGMENTS

We are indebted to Mr. B. E. Bourne, Mr. A. Petch, and Mr. F. D. MacDonald for assistance in designing and constructing the equipment, and in carrying out observations. Mr. W. A. Cumming designed the corner reflector antenna and measured the radiation patterns on a model range. Dr. Peter M. Millman contributed much helpful advice.

REFERENCES

CRAMER, H. 1955. The elements of probability theory. John Wiley & Sons, Inc., New York.
ESHLEMAN, VON R. 1955. Trans. Inst. Radio Engrs., Professional Group on Antennas and Propagation, **AP-3**: 32.
ESHLEMAN, VON R. and MANNING, L. A. 1954. Proc. Inst. Radio Engrs. **42**: 530.
FORSYTH, P. A., HINES, C. O., and VOGAN, E. L. 1955. Can. J. Phys. **33**: 600.
FORSYTH, P. A. and VOGAN, E. L. 1955. Can. J. Phys. **33**: 176.
McKINLEY, D. W. R. 1953*a*. Can. J. Phys. **31**: 758.
——— 1953*b*. Can. J. Phys. **31**: 1121.
——— 1954. Can. J. Phys. **32**: 450.
VILLARD, O. G., PETERSON, A. M., and MANNING, L. A. 1953. J. Geophys. Research, **58**: 83.

RADIATION PATTERNS OF A DIELECTRIC-COATED AXIALLY-SLOTTED CYLINDER[1]

By R. A. Hurd

ABSTRACT

The azimuthal radiation pattern of an axial slot in a dielectric-coated circular cylinder is derived. Some patterns are computed, and a comparison with experiment made.

INTRODUCTION

Slotted circular cylinders have become quite widely used as microwave radiators, and numerous studies have been made of their properties (Bailin 1953; Carter 1943; Papas 1950; Silver and Saunders 1950; Sinclair, Jordan, and Vaughan 1947; Wait and Kahana 1955; Wait, Pope, and O'Grady 1954). Of considerable interest is the axially-slotted cylinder which is surrounded by a uniform dielectric layer, Fig. 1. One would expect the dielectric layer to give

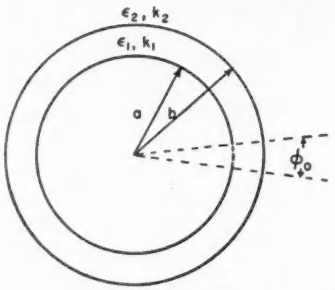

Fig. 1. Cross-section of dielectric-coated cylinder.

rise to a leaking surface wave travelling round the cylinder which would cause a substantial modification of the pattern, particularly in the shadow region of the slot. It was hoped that sufficient filling-in would be obtained to produce a substantially omnidirectional pattern.

To investigate this, expressions for the fields of an axially-slotted dielectric-coated cylinder have been derived, and some radiation patterns plotted. Although the desired omnidirectional patterns were not obtained, evidence of a substantial increase in back radiation was noted.

DERIVATION OF THE PATTERNS

The cylinder is assumed to be perfectly conducting, of radius a. In the cylinder is cut a slot of angular opening ϕ_0 centered about $\phi = 0$, Fig. 1. The dielectric layer has radius b and electrical constants ϵ_1, k_1. ($k_1 = 2\pi/\lambda_1$, λ_1 is the wavelength in the dielectric.) The region outside the dielectric is characterized by constants ϵ_2, k_2.

[1]Manuscript received March 12, 1956.
Contribution from Division of Radio and Electrical Engineering, National Research Council, Ottawa, Canada. Issued as N.R.C. No. 3980.

Across the slot we assume there exists an electric field E_0, constant in the ϕ direction. In the dielectric region the axial magnetic field must be given by an expression of the form

$$H_z^{(1)} = \sum_{n=0}^{\infty} \cos n\phi \{A_n J_n(k_1\rho) + B_n Y_n(k_1\rho)\}, \tag{1}$$

where J_n, Y_n are Bessel functions of the first and second kind respectively. Outside the dielectric the field is given by

$$H_z^{(2)} = \sum_{n=0}^{\infty} C_n \cos n\phi \, H_n^{(2)}(k_2\rho). \tag{2}$$

Here the Hankel function $H_n^{(2)}(k\rho)$ is chosen to give outgoing waves at infinity.*

The three sets of constants A_n B_n, C_n are now chosen to satisfy the boundary conditions:

(i) $E_\phi^{(1)} = i/\omega\epsilon_1 . \partial H_z^{(1)}/\partial\rho = E_0$, $\quad |\phi| < \phi_0/2, \ \rho = a;$

$E_\phi^{(1)} = 0$, $\quad |\phi| \geqslant \phi_0/2, \ \rho = a;$

(ii) $H_z^{(1)} = H_z^{(2)}$, $\quad \rho = b;$

(iii) $E_\phi^{(1)} = E_\phi^{(2)}$, $\quad \rho = b.$

For the far fields we are interested only in the coefficients C_n, which are found to be

$$C_n = \frac{i\omega\epsilon_1 E_0 \phi_0 \delta_n}{\pi^2 k_1^2 b} \frac{\sin(n\phi_0/2)}{n\phi_0/2} \{(\epsilon_1/\epsilon_2)^{\frac{1}{2}} U_n H_n^{(2)'}(k_2 b) - V_n H_n^{(2)}(k_2 b)\}^{-1}, \tag{3}$$

where

$$\delta_n = 1 \text{ for } n = 0,$$

$$= 2 \text{ for } n > 0,$$

$$U_n = J_n'(k_1 a) Y_n(k_1 b) - J_n(k_1 b) Y_n'(k_1 a),$$

$$V_n = J_n'(k_1 a) Y_n'(k_1 b) - J_n'(k_1 b) Y_n'(k_1 a).$$

The usual far-field approximation is now made for the Hankel function, i.e.

$$H_n^{(2)}(k\rho) \simeq (2/\pi k_2\rho)^{\frac{1}{2}} \exp[-i(k_2\rho - n\pi/2 - \pi/4)].$$

The far field is then

$$E_\phi^{(2)} = \frac{iE_0\phi_0}{\pi^2 k_2 b}\left(\frac{2}{\pi k_2\rho}\right)^{\frac{1}{2}} \exp[-i(k_2\rho - \pi/4)] \times \sum_{n=0}^{\infty} \delta_n i^n \frac{\sin(n\phi_0/2)}{n\phi_0/2} \cos n\phi \{(\epsilon_1/\epsilon_2)^{\frac{1}{2}} U_n H_n^{(2)'}(k_2 b) - V_n H_n^{(2)}(k_2 b)\}^{-1}. \tag{4}$$

It can be verified without difficulty that when either $\epsilon_1 \to \epsilon_2$ or $b \to a$

$$E_\phi^{(2)} \to \frac{E_0\phi_0}{2\pi i}\left(\frac{2}{\pi k_2\rho}\right)^{\frac{1}{2}} \exp[-i(k_2\rho - \pi/4)] \sum_{n=0}^{\infty} \delta_n i^n \frac{\sin(n\phi_0/2)}{n\phi_0/2} \times \cos n\phi \{H_n^{(2)'}(k_2 a)\}^{-1}, \tag{5}$$

*Time dependence $e^{i\omega t}$, m.k.s. units employed.

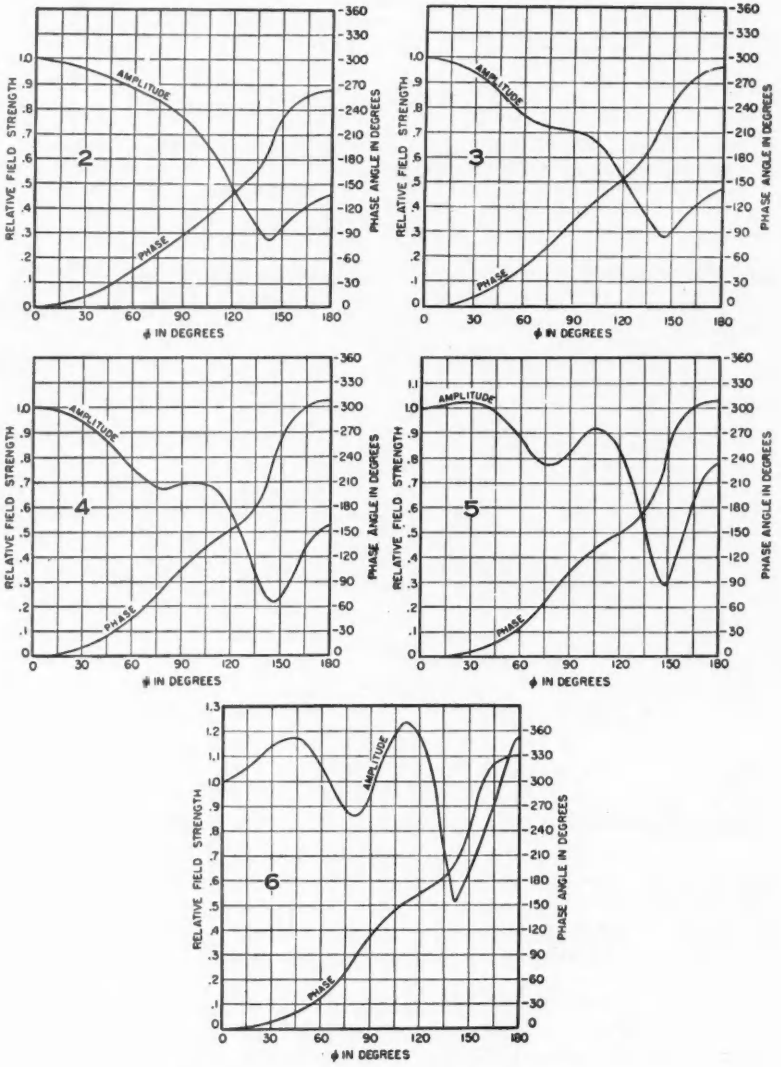

FIG. 2. $h = 0$, $a = 0.238\lambda$, $(\epsilon_1/\epsilon_2)^{\frac{1}{2}} = 1.6$.
FIG. 3. $h = 0.0637\lambda$, $a = 0.238\lambda$, $(\epsilon_1/\epsilon_2)^{\frac{1}{2}} = 1.6$.
FIG. 4. $h = 0.127\lambda$, $a = 0.238\lambda$, $(\epsilon_1/\epsilon_2)^{\frac{1}{2}} = 1.6$.
FIG. 5. $h = 0.191\lambda$, $a = 0.238\lambda$, $(\epsilon_1/\epsilon_2)^{\frac{1}{2}} = 1.6$.
FIG. 6. $h = 0.240\lambda$, $a = 0.238\lambda$, $(\epsilon_1/\epsilon_2)^{\frac{1}{2}} = 1.6$.

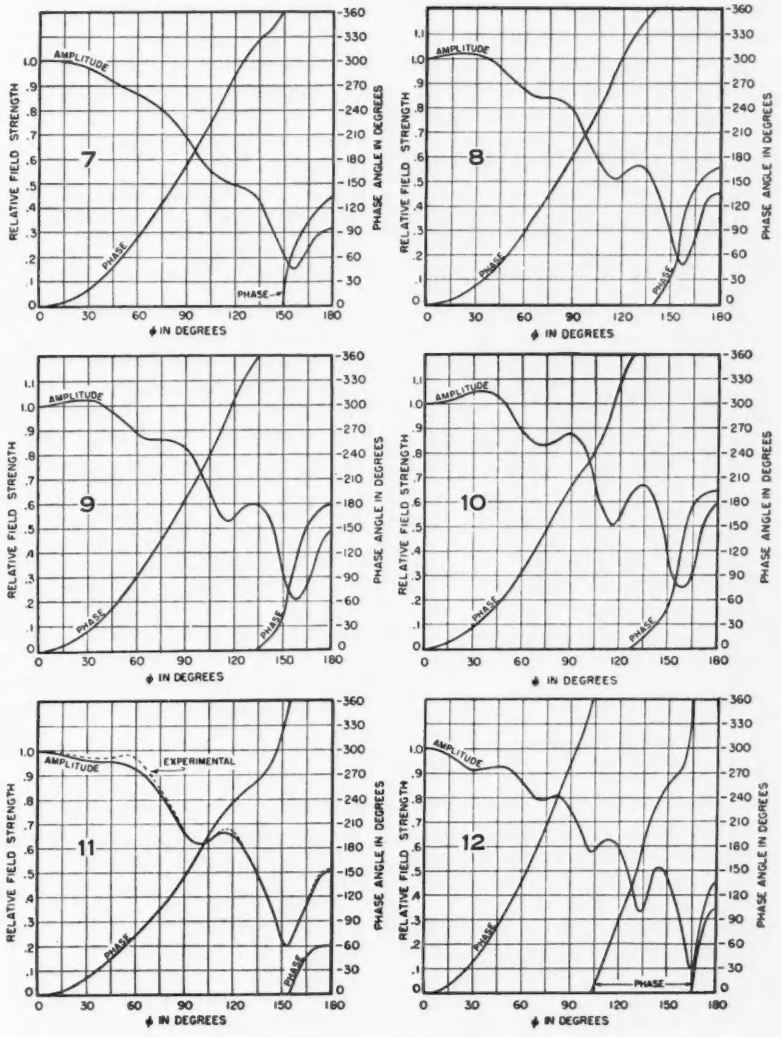

FIG. 7. $(\epsilon_1/\epsilon_2)^{\frac{1}{2}} = 1.00$, $a = 0.477\lambda$, $h = 0.0637\lambda$.
FIG. 8. $(\epsilon_1/\epsilon_2)^{\frac{1}{2}} = 1.40$, $a = 0.477\lambda$, $h = 0.0637\lambda$.
FIG. 9. $(\epsilon_1/\epsilon_2)^{\frac{1}{2}} = 1.60$, $a = 0.477\lambda$, $h = 0.0637\lambda$.
FIG. 10. $(\epsilon_1/\epsilon_2)^{\frac{1}{2}} = 2.00$, $a = 0.477\lambda$, $h = 0.0637\lambda$.
FIG. 11. $a = 0.358\lambda$, $h = 0.0637\lambda$, $(\epsilon_1/\epsilon_2)^{\frac{1}{2}} = 1.6$.
FIG. 12. $a = 0.732\lambda$, $h = 0.0637\lambda$, $(\epsilon_1/\epsilon_2)^{\frac{1}{2}} = 1.6$.

which is equivalent to the result for the circular cylinder with no dielectric, as given by Sinclair, Jordan, and Vaughan (1947).

If we assume that the slot angle ϕ_0 is so small that $n\phi_0/2 \ll 1$, for all n such that the individual terms of the series are significant, then $\sin(n\phi_0/2)/(n\phi_0/2) \simeq 1$, and therefore

$$(6)\quad E_\phi^{(2)} \simeq \frac{iE_0\phi_0}{\pi^2 k_2 b}\left(\frac{2}{\pi k_2 \rho}\right)^{\frac{1}{2}} \exp[-i(k_2\rho - \pi/4)]$$

$$\times \sum_{n=0}^{\infty} \delta_n i^n \cos n\phi \{(\epsilon_1/\epsilon_2)^{\frac{1}{2}} U_n H_n^{(2)'}(k_2 b) - V_n H_n^{(2)}(k_2 b)\}^{-1}.$$

THE RADIATION PATTERNS

A number of patterns have been computed using Eq. (6). Since the patterns are functions of three parameters, viz. a, b, and $(\epsilon_1/\epsilon_2)^{\frac{1}{2}}$, the preparation of a comprehensive set of patterns would involve a very large amount of work. Attention has therefore been focused on a relatively small range of the various parameters.

Figs. 2 to 6 show the effect of varying h $(=b-a)$, with $(\epsilon_1/\epsilon_2)^{\frac{1}{2}} = 1.6$, $a = 0.238\lambda$. It is to be noted that the minima which occur near $\phi = 80°$ and $\phi = 145°$ are relatively invariant with respect to variations of h. The effect of increasing h seems to be an increase in the amplitude of the oscillations only.

In Figs. 7 to 10, $(\epsilon_1/\epsilon_2)^{\frac{1}{2}}$ is varied holding a and h constant at 0.477λ and 0.0637λ respectively. Again it is observed that the positions of the minima are relatively invariant.

In the third set, Figs. 3, 11, 9, and 12 show the effect of changing the radius with $h = 0.0637\lambda$, $(\epsilon_1/\epsilon_2)^{\frac{1}{2}} = 1.6$.

As a check on the theoretical work, a slotted dielectric-coated cylinder was built with $a = 0.358\lambda$, $h = 0.0637\lambda$, $(\epsilon_1/\epsilon_2)^{\frac{1}{2}} = 1.6$, and the pattern measured. In Fig. 11 the measured pattern is superimposed on the calculated one. It is seen that the patterns agree very well.

CONCLUSION

As was anticipated, the dielectric coating enhances the radiation in the shadow region. However the patterns are by no means omnidirectional. The patterns show oscillations in the shadow region which increase in amplitude with increasing dielectric constant and thickness, the position of the minima apparently being determined only by the size of the metal cylinder.

ACKNOWLEDGMENT

The writer would like to thank Mrs. N. McCreery for performing the computations.

REFERENCES

BAILIN, L. L. 1953. Tech. Mem. No. 309, Hughes Aircraft Co., Culver City, Calif. July.
CARTER, P. S. 1943. Proc. I.R.E. **31**: 671.
PAPAS, C. H. 1950. J. Math. and Phys. **28**: 227.
SILVER, S. and SAUNDERS, W. R. 1950. J. Appl. Phys. **21**: 153, 745.
SINCLAIR, G., JORDAN, E. C., and VAUGHAN, E. W. 1947. Proc. I.R.E. **35**: 1451.
WAIT, J. R. and KAHANA, S. 1955. Can. J. Technol. **33**: 77.
WAIT, J. R., POPE, W. A., and O'GRADY, M. 1954. Radio Physics Lab. Project Report No. 19-0-10. Nov.

ABSORPTION SPECTRA OF ETHYLENE AND ETHYLENE-d_4 IN THE VACUUM ULTRAVIOLET. II[1]

By P. G. Wilkinson

ABSTRACT

The absorption spectra of ethylene and ethylene-d_4 have been investigated in the 1300 Å to 1500 Å region using the first order of a 21-ft. vacuum grating spectrograph. Vibrational constants for the $\nu_2(a_g)$ stretching vibration and the $\nu_4(a_u)$ twisting vibration have been determined for each of the observed five Rydberg states. The torsional oscillator–rotator treatment has been applied to the observed twisting data, and potential barriers hindering free rotation of 500 to 1200 cm^{-1} were obtained. It is concluded that the stable equilibrium configuration of the Rydberg states is not of D_{2h} symmetry but is probably bent or staggered.

I. INTRODUCTION

In a previous communication (Wilkinson and Mulliken 1955), hereafter referred to as I, the high dispersion absorption spectra of ethylene and ethylene-d_4 from 1500 Å to 2050 Å were reported. The absorption spectra were first photographed by Price (1935) and Price and Tutte (1940); more recently, absorption coefficients over the 1050 Å to 2000 Å region have been reported by Zelicoff and Watanabe (1953).[2]

In the present paper, high dispersion absorption spectra of ethylene and ethylene-d_4 are reported in the 1300 Å to 1500 Å region using the krypton continuum as the absorption background (Tanaka 1955; Wilkinson 1955*b*). In I, the spectra of the $V \leftarrow N$ and the $2R \leftarrow N$ (first Rydberg) transitions were reported. In the latter system, a number of intensity and frequency anomalies involving the "twisting" vibration were discussed and some explanations were advanced for these. In the present work these discussions are extended to five more Rydberg transitions involving four different Rydberg series.

II. EXPERIMENTAL

The absorption spectra were photographed in the first order of a 21-ft. vacuum spectrograph (Wilkinson and Mulliken 1955) with a dispersion of 1.33 Å/mm. and a practical resolving power of 100,000. Vacuum distilled ethylene (99.95% pure) and ethylene-d_4 (approximately 90% pure) were flowed at low pressure into the spectrograph tank; a krypton light source (driven by microwave power at 2450 Mc./sec. and 125 watts), which produced a continuum extending from 1250 Å to 1600 Å, was used as the absorption background (Wilkinson 1955*b*). The krypton continuum and the high dispersion employed greatly facilitated observation of a number of new absorption bands not previously reported (Price 1935; Price and Tutte 1940; Zelicoff and Watanabe 1953). The wavelength standards used were CI, NI, HgI, XeI, and

[1]Manuscript received March 26, 1956.
Contribution from the Laboratory of Molecular Structure and Spectra, Department of Physics, The University of Chicago, Chicago 37, Illinois, U.S.A.
[2]For a complete literature survey, see Wilkinson and Mulliken (1955).

OI lines occurring in the light source (Wilkinson 1955*a*, 1955*b*) and it proved to be possible to estimate positions of band centers to within 5 to 20 cm^{-1} depending on the relative sharpness of the bands.

III. EXPERIMENTAL DATA

(*a*) *General*

The observed absorption bands are given in Table I for ethylene and ethylene-d_4 and most of these may be found in the microphotometer tracings of

TABLE I

ABSORPTION BANDS OF ETHYLENE AND ETHYLENE-d_4

d—diffuse; dd—very diffuse

Intensities are estimates of absorption coefficients

Ethylene				Ethylene-d_4			
Intensity (cm^{-1})	Wavelength (Å)	Wave number (cm^{-1})	Transition[b]	Intensity (cm^{-1})	Wavelength (Å)	Wave number (cm^{-1})	Transition[b]
500	1501.34	66607	$3R_{00}'$	500	1499.41	66693	$3R_{00}'$
200d	1490.81	67077	$3R_{02}'$	50dd	1493.61	66952	$3R_{02}'$
100d	1472.36	67918	$3R_{10}'$	100d	1472.51	67911	$3R_{10}'$
1000d	1438.52	69516	$3R_{00}''$	1000	1435.62	69656	$3R_{00}''$
300d	1427.86	70035	$3R_{02}''$	300	1428.83	69987	$3R_{02}''$
330d	1413.53	70745	$3R_{04}''$	50	1417.77	70533	$3R_{04}''$
310d	1410.68	70888	$3R_{10}''$	350	1408.90	70977	$3R_{10}''$
320d	1399.68	71445	$3R_{12}''$	300	1402.35	71309	$3R_{12}''$
				600	1392.67	71804	$3R_{14}''$
2000	1393.00	71788	$3R_{00}$	900	1387.99	72047	$3R_{00}$
500	1389.83	71951	*a*	1000	1386.53	72122	*a*
1770d	1385.22	72191	$3R_{02}$	2000	1383.20	72296	$3R_{02}$
1800d	1383.40	72286	$3R_{20}''$, $3R_{14}''$				$3R_{20}''$
100d	1373.85	72788	$3R_{22}''$	950	1378.44	72546	$3R_{22}''$
			$3R_{04}$	800	1374.26	72766	$3R_{04}$
1000	1369.66	73011	$4R_{00}'''$	850	1369.71	73007	$4R_{00}'''$
1200	1365.40	73239	$3R_{10}$				
1300	1363.31	73350	$4R_{02}'''$	900	1365.00	73260	$4R_{02}'''$
1300	1360.67	73493	*a*				
				1100	1361.79	73433	$3R_{10}$
1450	1357.46	73667	$3R_{12}$	1300	1357.55	73662	$3R_{12}$, $3R_{20}''$
1200	1355.95	73749	$3R_{30}''$				
500	1346.51	74266	$3R_{32}''$	800	1353.63	73875	$3R_{32}''$
			$3R_{14}$	800	1348.72	74143	$3R_{14}$
900	1342.81	74471	$4R_{10}'''$	850	1344.90	74356	$4R_{10}'''$
				900	1339.95	74630	$4R_{12}'''$
800d	1340.2	74615	$3R_{20}$	950	1337.99	74739	$3R_{20}$
1000	1335.94	74854	$4R_{12}'''$				
500	1324.31	75511	$4R_{00}'$	500d	1321.52	75670	$4R_{00}'$
600	1320.49	75730	*a*				
600	1314.76	76060	$4R_{02}'$	600d	1315.12	76040	$4R_{02}'$
				600d	1309.25	76380	$4R_{04}'$
600	1303.22	76733	$4R_{00}''$, $4R_{10}'$	600d	1301.17	76854	$4R_{00}''$, $4R_{10}'$
100d	1295.40	77196	$4R_{02}''$				
200	1288.52	77609	$4R_{00}$				
50	1286.01	77760					
180	1283.32	77923	$4R_{20}'$, $4R_{10}''$				
0d	1281.57	78029	$4R_{22}'$, $4R_{12}''$				

[a]May be members of a fifth (nR''''–A) Rydberg series.

[b]Only upper state given; ground state is N_{00}. In the present notation a Rydberg vibronic state is designated $R_{v_1'v_2'v_3'}$, where $v_1v_2v_3$, etc. are vibrational quantum numbers of the various normal vibrations listed in order numerically according to the usual ground state notation. In the present instance only upper state quanta of ν_2 and ν_4 are identified.

Figs. 1 and 2 (the lower curve A is for low pressure and the upper curve B for higher pressure, path length 42 ft.). With the present resolving power no rotational structure is observed. These data represent six Rydberg transitions belonging to four Rydberg series, each of which converge to an ionization potential of 84750 cm^{-1} (84850 cm^{-1} for ethylene-d_4) (Price and Tutte 1940),[3]

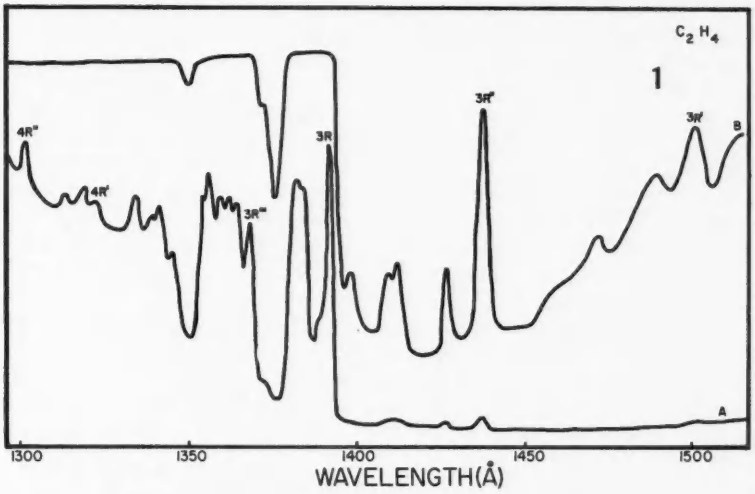

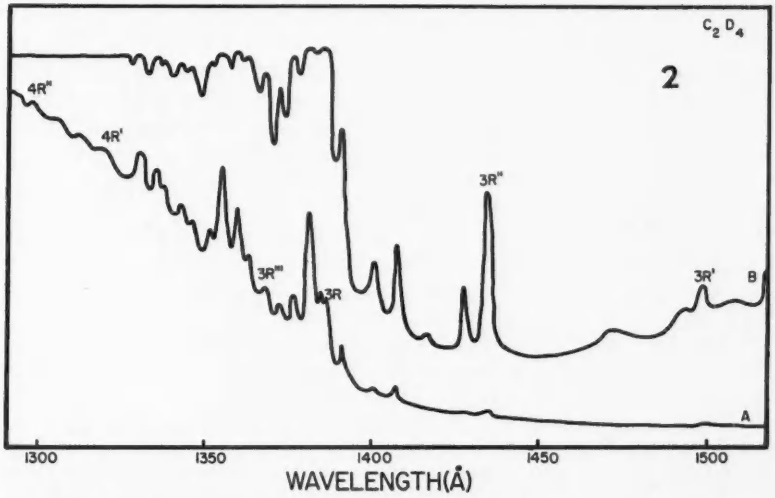

FIG. 1. Microphotometer tracings of the absorption spectra of ethylene; (A) pressure about 0.7 microns, (B) pressure about 2 microns; path length 42 ft.

FIG. 2. Microphotometer tracings of the absorption spectra of ethylene-d_4; (A) pressure about 0.6 microns, (B) pressure about 1.5 microns; path length 42 ft.

[3]Watanabe (1954) obtained 84822±80 cm^{-1} by a photoionization method.

and associated with each electronic transition, vibrational structure may be observed. We have identified four such Rydberg series (one more than given by Price and Tutte) and have named them as follows: $nR \leftarrow N$, $nR' \leftarrow N$, $nR'' \leftarrow N$, $nR''' \leftarrow N$, where the relative term values of the lowest *observed* member increase in that order. R is used as a general symbol for a Rydberg state and correlation of the various upper states with group theoretical symbols is desirable.

The ground state of ethylene belongs to point group V_h $(=D_{2h})$; group theoretically only the transitions $B_{1u} \leftarrow A_g$ (z polarized), $B_{2u} \leftarrow A_g$ (y polarized), and $B_{3u} \leftarrow A_g$ (x polarized) are permitted[4] and since the Rydberg transitions are strong, it is reasonable to attribute them to some or all of these. However, the $nR \leftarrow N$ transitions cannot be $B_{1u} \leftarrow A_g$ since the first member $2R \leftarrow N$ lies on top of the $V(B_{1u}) \leftarrow N$ continuum and very little electronic perturbation (mixing) has taken place. (It is also probable that the $nR''' \leftarrow N$ transitions can be identified with $B_{1u} \leftarrow N$ since $3R''' \leftarrow N$ is not observed although it would fall in the 1600–1700 Å region. It is presumed that $3R'''$ has mixed strongly with $V(B_{1u})$ and become very diffuse.[5])

Intensity, wavelength, wave number, and upper state identification data are given in Table I. The intensity data are rough estimates of absorption coefficients[6] at the peak of each band as obtained from photographic plate density measurements. Some bands are extremely diffuse, others are badly overlapped; frequency differences computed from these may be in considerable error (± 40 cm^{-1}).

(*b*) *Identification of Rydberg Transitions*

The location of the band system origin ("vibrationless transition") of each Rydberg transition was usually made without ambiguity from consideration of the following information: (1) this transition is expected to be the strongest in the system; (2) short wavelength isotope shift on deuteration should be approximately constant for each series; and (3) observation of expected vibrational transitions combining with each system origin. The first condition was true only for the 1500 Å system (and, of course, the 1740 Å system previously reported in I) and in general the ethylene-d_4 systems were the more unusual; failure of this condition imparts some uncertainty into the present analysis. The second condition was generally true except for the 1370 Å system (newly identified) and for the third condition, reasonable vibrational progressions were observed for all systems.

In the nomenclature employed, the number n (e.g. in $nR \leftarrow N$) is the whole number (principal quantum number) in the denominator of the Rydberg term expression,

$$R/(n-a)^2,$$

[4]The symmetry axes were chosen in accordance with the *Report on Notation for the Spectra of Polyatomic Molecules* (1955): the z axis is along the principal axis, the x axis is perpendicular to the molecular plane.

[5]These are applications of a theorem implied by Sponer and Teller (1941) and restated by Professor J. R. Platt (private communication) as follows: "Two closely adjacent absorption transitions of different intensity, structure, or diffuseness must have upper states belonging to different symmetry groups."

[6] α (atmos^{-1} cm^{-1}) $= (1/x) \log_e I_0/I$.

TABLE II

VIBRATIONAL CONSTANTS, BAND SYSTEM ORIGINS, AND C–C DISTANCES IN THE RYDBERG STATES

	Ethylene				Ethylene-d_4					Ratio C_2H_4 to C_2D_4			
Vibronic state	ν_2 $\Delta G(v_2)$ (cm^{-1})	ν_4 $\Delta_2G(1)$ (cm^{-1})	ν_4 $\Delta_2G(3)$ (cm^{-1})	Band system origin	ν_2 $\Delta G(v_2)$ (cm^{-1})	ν_4 $\Delta_2G(1)$ (cm^{-1})	ν_4 $\Delta_2G(3)$ (cm^{-1})	Band system origin (cm^{-1})	Isotope shift (cm^{-1})	ν_2 $\Delta G(v_2)$	ν_4 $\Delta_2G(1)$	ν_4 $\Delta_4G(2)$	r_0 (C–C) (Å)
$N(A_g)$	1623.3[b]	1027[a]		0	1515[b]	727[a]		0	—	1.071	1.413		1.353[f]
$2R_{00}$[c]		472	612	57336		282	431	57621	285		1.671	1.420	1.432
$2R_{10}$	1370	459	739		1295	275	454			1.058	1.669	1.628	
$3R_{00}$		403	597	71788		249	470	72047	259		1.618	1.391	1.402
$3R_{10}$	1451	428	599		1386	229[d]	481			1.047	1.87	1.446	
$3R_{20}$	1376				1306	285				1.054			
$4R_{00}$				77609									
$3R_{00}'$		470		66607		259[e]		66693	86		1.81		1.458
$3R_{10}'$	1311				1218					1.076			
$4R_{00}'$		549		75511		370	340	75670	159		1.484		1.484
$4R_{10}'$	1222				1184					1.032			
$4R_{20}'$	1190												
$3R_{00}''$		519	710	69516		331	546	69656	140		1.568	1.401	1.426
$3R_{10}''$	1372	557	841		1321	332	495			1.039	1.678	1.690	
$3R_{20}''$	1398	502			1319	250[d]				1.060			
$3R_{30}''$	1463	517			1366	213[d]				1.071			
$4R_{00}''$		463		76733				76854	122				1.507
$4R_{10}''$	1190												
$4R_{00}'''$		339		73011		253		73007			1.340		1.406
$4R_{10}'''$	1460	383			1349	274				1.082	1.398		

[a] Arnett, R. L. and Crawford, B. L. 1950. J. Chem. Phys. **18**: 118.
[b] Herzberg, G. 1945. Infrared and Raman spectra. D. Van Nostrand Company, Inc., New York. p. 326.
[c] Data taken from Wilkinson, P. G. and Mulliken, R. S. 1955. J. Chem. Phys. **23**: 1895.
[d] Measurement involves superposed bands and is probably too low.
[e] Measurement involves a weak diffuse band and is probably too low.
[f] Reference *b*, p. 439.

where R is the Rydberg constant for infinite mass (109737 cm^{-1}), and a is the "quantum defect". According to Price and Tutte (1940), for the $nR \leftarrow N$ series, $a = 0.09$ (ethylene) and $a = 0.08$ (ethylene-d_4); for the $nR' \leftarrow N$ series, $a = 0.6$; for the $nR'' \leftarrow N$ series, $a = 0.4$; and for $nR''' \leftarrow N$, the present data indicate that $a = 0.95$.

(*c*) *Identification of Vibrations*

For allowed transitions between electronic states in which the symmetry of the equilibrium configurations is the same in both, only totally symmetric vibrations are expected to appear strongly in accordance with the selection rule $\Delta v = 0, 1, 2$, etc., while non-totally-symmetric vibrations may appear with weakened intensity and according to the selection rule $\Delta v = 0, 2, 4$, etc. (Sponer and Teller 1941).

The identification of the totally symmetric $\nu_2(a_g)$ vibration in the Rydberg states of ethylene is certain from its isotope ratio (Table II), which may be predicted as $(16/14)^{\frac{1}{2}} = 1.069$ to the extent that ν_2 can be approximated by the harmonic vibration of two rigid CH_2 or CD_2 groups against each other. The magnitude of the ν_2 vibrational frequency varies over a wide range from 1190 cm^{-1} ($4R_{10}'-4R_{00}'$) to 1463 cm^{-1} ($3R_{30}''-3R_{20}''$) and shows an unusual positive anharmonicity (Table II) in the $3R''$ state. Clearly, isotope frequency ratios in the excited states may not be the same necessarily as in the ground state; though they generally are the same for totally symmetric vibrations, some wide deviations may be expected in non-totally-symmetric vibrations and this is the case here for the $\nu_4(a_u)$ "twisting" vibration. As discussed in I, the isotope ratio of ν_4 varies from 1.67 to 1.71 whereas 1.414 would be expected from simple theory. This was explained as resulting from a very unusually shaped non-harmonic potential barrier and a transitory condition in which torsional oscillation approaches free rotation. As a working rule, one may say that if a given non-totally-symmetric vibration is identified without unusual anharmonicity, and the molecule retains a geometry very similar to the ground state, the isotope ratios in excited and ground states should be nearly the same.[7] Quite often neither of these conditions holds in the ethylene Rydberg vibrations and wide deviations in isotope ratio are generally observed. The small "doublet" spacings observed must be identified with $2\nu_4$ (more properly, $\Delta_2 G(v_4)$) and ν_4 thus varies from 200 to 275 cm^{-1} in ethylene (125 to 180 cm^{-1} in ethylene-d_4) as may be seen in Table II.

As in the $2R \leftarrow N$ system, spacings which may be ascribed either to $4\nu_4$ or two quanta of a different vibration (such as ν_{10}) are frequently observed. The identification of these spacings as $4\nu_4$ (more properly, $\Delta_4 G(v_4)$) seems fairly satisfactory although $2\nu_{10}$ cannot be ruled out since in a number of instances the isotope frequency ratio (Table II) approaches 1.40 (ratio for ν_{10} in the ground state).

The $3R'' \leftarrow N$ (1438 Å) system is shown schematically in Fig. 3 for ethylene and in Fig. 4 for ethylene-d_4. The positive anharmonicity and unusual intensity

[7]This is certainly true when the vibration is the only one of a given symmetry species as is the case for the ethylene $\nu_4(a_u)$ vibration (Teller–Redlich Product Rule).

distribution in the ν_2 progression is readily seen. The maximum intensity occurs at $v_2' = 2$. The $\Delta_2G(v_4)$ spacing appears somewhat irregular; the $\Delta_4G(v_4)$ spacing is not always identified with certainty (occasionally it appears to be absent—$3R_{24}''$, $3R_{34}''$); and the unusually high intensity of $3R_{32}''$ should be noted.

For harmonic oscillations, the following intensity ratios in a non-totally-symmetric progression may be calculated (I):

$$(1a) \qquad I_{20}/I_{00} = \tfrac{1}{2}(\omega'-\omega'')^2(\omega'+\omega'')^{-2},$$

$$(1b) \qquad I_{40}/I_{00} = \tfrac{3}{8}(\omega'-\omega'')^4(\omega'+\omega'')^{-4},$$

where ω' and ω'' are the upper and lower state vibrational frequencies, respectively.

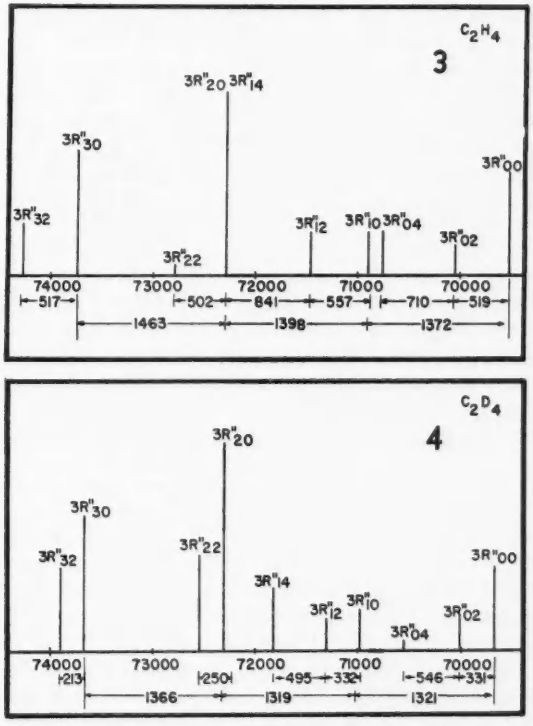

FIG. 3. Schematic diagram of the $3R''$–N system (1438 Å) in ethylene.
FIG. 4. Schematic diagram of the $3R''$–N system (1435 Å) in ethylene-d_4.

For the $3R_{00}'' \leftarrow N$, $3R_{02}'' \leftarrow N$, and $3R_{04}'' \leftarrow N$ transitions, application of equations 1*a* and 1*b*, using the data of Table II and assuming that values of $\Delta_2G(v_4)$ are to a sufficient approximation equal to $2\nu_4$, predicts the relative intensities in the ratios 1:0.18:0.05 (ethylene) and 1:0.20:0.06 (ethylene-d_4).

The actual intensities in these bands are 1:0.30:0.33 and 1:0.30:0.05, respectively.[8] At least for ethylene-d_4 there is fair agreement with (1*a*) and (1*b*) and the isotope frequency ratios are nearly harmonic (1.568, 1.426, Table II). Much greater deviations (especially in higher members of the $3R'' \leftarrow N$ system) occur in some of the other band systems and in a number of instances the vibrationless transition is weaker than the twisting bands.

(*d*) *Vibrational Constants*

In Table II are given the vibrational constants of the ground state (Herzberg 1945) and the Rydberg states observed here as well as the band origins, electronic isotope shifts, isotopic frequency ratios, and the estimated C–C distances. Since measurement frequently involved superposed bands, the values of $\Delta_2 G(v_4)$ and the corresponding isotope ratios are not always reliable; however, it may be seen that usually the ν_4 isotope ratio is greater than 1.414 (harmonic oscillator approximation).

The vibrational analysis permits, of course, no direct determination of the C–C distance. However, by use of the empirical relation, $r_0^n \omega_0 = \text{const.}$ (Herzberg 1950), using for n the value of 2.88 (obtained from O_2, which is isoelectronic with ethylene) and the ground state C–C distance (1.353 Å), estimates of r_0 in the excited states may be given (column 15, Table II). As expected, the C–C distances in the Rydberg states are somewhat larger than in the ground state.

IV. THE TORSIONAL OSCILLATOR-ROTATOR

In the electronic ground state, the potential barrier hindering internal rotation is 2.66 ev. (21500 cm^{-1}) (Rabinovitch, Douglas, and Looney 1952) whereas in the ionized and Rydberg states it should be much less than this, in fact so low that the possibility of free internal rotation must be considered (Mulliken and Roothaan 1947).

A detailed treatment of the torsional oscillator and its application to the $2R$ state was given in I. A hindering potential of the form

$$V = \tfrac{1}{2} V_0(1-\cos 2\theta) \tag{2}$$

is assumed where the top of the barrier (V_0) corresponds to the molecule in the "twisted" condition ($\theta = \pi/2$) and the bottom to the planar condition ($\theta = 0$). Substitution of this potential function into the Schroedinger equation results in Mathieu's equation, the solutions of which may be found in tables (Goldstein 1927; Ince 1932). If it is assumed that the C–H distance and the H–C–H bond angle are the same in the Rydberg states as in the ground state (probably true within 10%), numerical calculations of the barrier height may be made as follows:

$$(V_0)_D = 312\ q\ cm^{-1}, \tag{3a}$$

$$(V_0)_H = 623\ q\ cm^{-1}, \tag{3b}$$

[8]In interpreting the experimental intensities, however, one must bear in mind that photometric peak intensities for incompletely resolved bands composed of discrete lines are poor measures of true integrated absorption coefficients.

where q is a parameter in Mathieu's equation which can be calculated from the tables using experimental torsional frequencies.

In Table III values of V_0 have been calculated from Equation 3 for five Rydberg states. It may be seen that the calculated V_0 is not the same for the

TABLE III

CALCULATIONS OF BARRIER HINDERING FREE ROTATION (SEE TEXT)

Electronic state	v_2	v_4	Ethylene W (cm^{-1}) observed	Ethylene V_0 (cm^{-1}) Eq. 3	Ethylene-d_4 W (cm^{-1})	Ethylene-d_4 V_0 (cm^{-1}) Eq. 3
$3R$	0	2	403	704	249	499
	0	4	1000		719	
	1	2	428	773	229	424
	1	4	1027		710	
$3R'$	0	2	470	897	259	534
$4R'$	0	2	549	1196	370	1017
	0	4	—		710	
$3R''$	0	2	519	1072	331	846
	0	4	1229		877	
	1	2	557	1246	332	849
	1	4	1398		827	
	2	2	502	1009	250	502
$4R'''$	0	2	339	598	253	509
	1	2	383	648	274	593

two molecules (indicating that the true potential barrier is *not* of the form of equation 2) and that $W(4)$[9] shows considerable positive anharmonicity and usually lies above V_0 (i.e. in free rotation). In the only case in which V_0 is considerably larger than $W(4)$ ($4R'$), reasonable anharmonicity is exhibited, the isotope ratio (1.484) is fairly low, and the two V_0's are more nearly the same (1017 and 1196 cm^{-1}).

The necessity for assuming an unusual shape for the true potential barrier together with the high intensities in the ν_4 progressions (particularly in ethylene-d_4) probably means that the stable equilibrium configuration in the Rydberg states is not of symmetry D_{2h} but is bent or staggered in some fashion.

ACKNOWLEDGMENT

I wish to thank Professors R. S. Mulliken and J. R. Platt for many helpful discussions. I am indebted to Professor M. de Hemptinne of the University of Louvain for the gift of a sample of CD_2Br–CD_2Br, from which the ethylene-d_4 was prepared. This research was assisted in part by the Office of Ordnance Research under Project TB-2-0001 of Contract DA-11-022-ORD-1002 with The University of Chicago.

REFERENCES

GOLDSTEIN, S. 1927. Trans. Cambridge Phil. Soc. **23**: 303.
HERZBERG, G. 1945. Infrared and Raman spectra. D. Van Nostrand Company, Inc., New York.
——— 1950. Spectra of diatomic molecules. D. Van Nostrand Company, Inc., New York.

[9] $W(4)$ is used as an abbreviation for $\Delta_4 G(2) = G(v_4' = 4) - G(v_4' = 0)$.

INCE, E. L. 1932. Proc. Roy. Soc. Edinburgh, **52**: 355.
MULLIKEN, R. S. and ROOTHAAN, C. C. J. 1947. Chem. Revs. **41**: 219.
PRICE, W. C. 1935. Phys. Rev. **47**: 444.
PRICE, W. C. and TUTTE, W. T. 1940. Proc. Roy. Soc. (London), A, **174**: 207.
RABINOVITCH, B. S., DOUGLAS, J. E., and LOONEY, F. S. 1952. J. Chem. Phys. **20**: 1807.
Report on Notation for the Spectra of Polyatomic Molecules. (R. S. Mulliken) 1955. J. Chem. Phys. **23**: 1997.
SPONER, H. and TELLER, E. 1941. Revs. Mod. Phys. **13**: 89.
TANAKA, Y. 1955. J. Opt. Soc. Amer. **45**: 710.
WATANABE, K. 1954. J. Chem. Phys. **22**: 1564.
WILKINSON, P. G. 1955*a*. J. Opt. Soc. Amer. **45**: 862.
——— 1955*b*. J. Opt. Soc. Amer. **45**: 1044.
WILKINSON, P. G. and MULLIKEN, R. S. 1955. J. Chem. Phys. **23**: 1895.
ZELICOFF, M. and WATANABE, K. 1953. J. Opt. Soc. Amer. **43**: 756.

SPIN ECHOES IN ALCOHOLS AND DERIVATIVES[1]

By G. J. B. Crawford[2] and J. S. Foster

ABSTRACT

The spin echo technique has been employed to measure the relative chemical shifts and the indirect spin–electron–spin coupling constants between protons at different structural sites in ethyl, propyl, isopropyl, butyl, isobutyl, and amyl alcohols and certain of their derivatives at a Larmor frequency of 29.0 Mc./s. The separation between the two r-f. pulses applied to the sample increases regularly in accurately known steps which are controlled electronically. Thus the frequencies modulating the echo envelope have been readily measured with a precision as high as 4% in favorable cases. Relative chemical shifts found by slow passage experiments have been checked with higher accuracy, particularly for the primary alcohols. Encouraged by the implications of these earlier data, we have here analyzed the longer hydrocarbon chains on the basis of the theoretical computations of Hahn and Maxwell for only two groups of non-equivalent protons. This more precise investigation confirms the assumptions made as to where the major shifts and couplings do and do not exist in the molecular structures. In the halide molecules, it is found that the observed relative chemical shifts are linearly proportional to the paramagnetic fields arising from the valence orbits of the halogens polarized by the external field. Evidence for the particular J-coupling to the hydroxyl group in the alcohols suggests that this bond is effectively stronger in the heavier molecules which are only slightly soluble in water.

INTRODUCTION

Resonance experiments performed on molecules containing identical nuclear magnetic moments in two or more chemically non-equivalent positions reveal in general that the resonance lines are separated by an amount determined by the differences in the local fields induced at the various spin sites by the external magnetic field. The consequent differences in the Larmor precessional frequencies are called the relative chemical shifts, and are linearly proportional to the applied field. In general too, an absolute chemical shift exists, i.e. the position of a given resonance is shifted from the value a completely unshielded nucleus would reveal.

Ramsey (1950) has shown that the induced paramagnetism of the valence orbits is in many cases comparable to, or even larger than, the Lamb (1941) diamagnetic correction. In the absence of an external field, 'p' and 'd' valence orbits exert large instantaneous fields at the nucleus which have zero time average. However a slight polarization of these orbits produces an appreciable shielding (Saika and Slichter 1954) not only at their own nucleus, but also in many cases at the nuclei of the adjacent atoms. The chemical shifts reported in this paper are all examples of this latter situation.

A smaller effect has been found (Hahn and Maxwell 1951; Gutowsky *et al.* 1951, 1953) to be due to an indirect spin–electron–spin type of coupling between adjacent nuclear magnetic dipoles via their bonding electrons. The form of this interaction has been established (Ramsey and Purcell 1952; Hahn and Maxwell 1952) as $J(\mathbf{I}_1.\mathbf{I}_2)$, where J represents the strength of the J-coupling as it is often called. This coupling is independent of the external field strength.

[1]Manuscript received March 20, 1956.
Contribution from Radiation Laboratory, McGill University, Montreal, Que.
[2]Now at the Thomas A. Edison Research Laboratory, West Orange, N.J.

These two effects have been studied in a number of the alcohols and in certain of their derivatives by the spin echo method. The advantage of studying these phenomena in this way lies in its inherent ability to resolve frequencies of the order of a few cycles per second, even though the spread in Larmor frequencies over the sample due to slight inhomogeneities in the magnetic field may be several hundred times greater. Consequently, the method affords for relative chemical shifts a precision of measurement comparable to the high resolution 'slow passage' spectrometers (Anderson and Arnold 1954; Varian Associates 1955), i.e. those employing exceedingly homogeneous fields which are slowly scanned through the resonance region. While the spin echo experiment does not measure absolute chemical shifts, it is particularly suited to the detection and measurement of J-couplings.

Two papers have previously given results of a nature somewhat similar to those reported here. Both are slow passage analyses and are concerned with the chemical shifts found in the proton resonance in various organic liquids. In the first, Arnold *et al.* (1951) report the shifts measured in the primary alcohols. The resolution was such that no J-coupling was observed. In the second, Shoolery (1953) gives the results of similar experiments done on a series of substituted ethanes. Apparently the J-coupling was observed here in some instances, but no values are given for it. In the present work the relative chemical shifts and, in many cases, the J-coupling constants have been measured for a much wider range of compounds with substantially better accuracy than that obtained by either of these earlier investigators. These parameters are then discussed in relation to the various molecular structures.

EXPERIMENTAL

The procedure consists essentially in placing the sample in a coil whose axis is normal to the direction of the external magnetic field. This coil is part of a tuned circuit into which the Larmor frequency power is applied in two short intense pulses at times 0 and τ, and in which an 'echo' signal is induced at 2τ. This signal is amplified, detected, and displayed on a Tektronix oscilloscope (type 514D). As τ is regularly increased, the maximum amplitudes of these echoes, timed from the second pulse, trace out an envelope which contains a superposition of 'slow beats'. This beat structure reveals the relative chemical shift and the J-coupling constant simultaneously, if these coexist; if either is absent, no modulation is exhibited.

Unfortunately, the echo envelope decays according to the law $\exp(-2\alpha\tau - 8/3.k\tau^3)$, where $\alpha = 1/T_2$, the phase memory time; and where $k = (\gamma G)^2 D$, γ being the gyromagnetic ratio of the magnetic moment under study, G the magnetic field gradient over the sample, and D the self-diffusion constant of the spin-carrying molecule (Hahn 1950; Das and Saha 1954). This damping determines the resolution limit, and hence the magnetic field gradient should be low. For this reason, the gap of the magnet (whose pole faces are 4 in. in diameter) was set at $\frac{3}{4}$ in. and suitably shimmed. The flux of this magnet is electronically controlled to better than 1 part in 10^5 by a regulator originally built by Hunten (1951).

The pulses are applied in pairs at a rate sufficiently slow—of the order of 0.1 c.p.s.—to allow the spin system to return to equilibrium before being re-pulsed. The timing of the pulses is controlled by an electronic ratchet (Moody and Crawford 1954) which systematically increases their separation in accurately known steps. These steps are determined by the period of a relaxation oscillator which is calibrated by means of an audio signal generator whose frequency is simultaneously checked against a General Radio 1000 c.p.s. Vacuum-tube Fork (type 723-C) on an auxiliary oscilloscope. The basis of this procedure, suggested by H. J. Moody, is that a Tektronix oscilloscope supplies a square wave initiated by each cycle of its sweep circuit. This wave form is utilized to activate the ratchet once the oscilloscope has been triggered by the audio generator whose signal it displays. The ratchet oscillator output is now mixed in and thus these two oscillators are compared cycle for cycle over a hundred cycles or more. This method also served to determine the stability of the ratchet oscillator, which is of the order of 2 parts in 10^4. Consequently, the echoes can be used to provide their own time scale for the graphs on which their amplitudes are plotted.

The timing mechanism is also capable of producing three pulses per repetition cycle at manually set positions (0, τ_1, and τ_2), which are used to obtain a standard pulse width by virtue of the fact that if $\exp(-\tau_1/T_1) \approx 1$, the secondary echo at $2\tau_2-\tau_1$ vanishes sharply at $\gamma H_1 t_w = 90°$ (T_1 is the spin-lattice relaxation time, H_1 is the r-f. field intensity, and t_w is the pulse width). The pulse width normally used in these studies of protons is approximately 25 μsec.

The r-f. power is supplied by a pulsed-oscillator–gated-amplifier operating at a frequency of 29.0 Mc./s. In order to obtain the best over-all signal-to-noise ratio in the receiver and also the greatest power output during a pulse, the power stage of the amplifier and the oscillator are gated simultaneously.

The receiver has a band width of 200 kc./s., an over-all voltage gain of 120 db., and a noise figure corresponding to 0.1 μv. at the input of an otherwise noiseless system. The recovery time following a pulse is approximately 5 μsec.

Owing to the low repetition rates that must be used, the oscilloscope is fitted with a P.7 (long persistence) phosphor. Visual observation was used and the echo amplitude was recorded as a function of the number of ratchet steps taken. The time required to cover the 198 steps which constitute a normal run is about half an hour and therefore a high degree of stability is essential. This was realized by allowing the apparatus to run for a few hours.

A sample is studied through a series of runs at different ratchet settings (uniform increment by which the time between pulses is increased) in order to determine the component frequencies in the beat pattern as accurately as possible. The steps employed ranged from 500 to 1500 μsec.

Most of the chemicals used were of certified or highest purity grade. Before distillation and boiling point check, all except poisonous or lachrymatic compounds were dried—commonly with CaO, but sodium metal was used for ethyl alcohol. The compounds studied include the alcohol and selected derivatives of the ethyl, propyl, isopropyl, butyl, isobutyl, and amyl families.

THEORY AND METHOD OF ANALYSIS

Hahn and Maxwell (1952) have given equations and graphs for the echo envelopes computed for two groups of non-equivalent protons, where each group may contain one, two, or three protons. The results apply only in cases where $J \ll \delta$ if 90° pulses were used. Here $\delta/2\pi$ is the relative chemical shift in cycles per second. The general form of these envelopes may be written $V(\tau) = f_1(J\tau) + \cos(\delta\tau) . f_2(J\tau)$. Although the functions are somewhat more complex than this simple expression suggests, their important feature is that in all cases $V(\tau)$ shows a point of symmetry at $\tau = \pi/J$, the half period mark of the J modulation. This point of symmetry (see Fig. 1) was often used to check the internal consistency of a run, and in many cases in which the damping prevented a complete J period from being observed, positive identification of it led to a determination of the J value.

Indeed, since damping has been omitted from the computations, the experimental curves should be normalized for a strict comparison with the theory. Such a procedure would be valid, however, only if T_2 were the same for all the protons in the molecule—a debatable point in the more complex structures—and certainly it requires that the envelope include at least one complete J cycle—a condition that has seldom been realized. On the basis of previous work on selected molecules (Hahn and Maxwell 1952), however, it is assumed that theory and experiment do agree. The maxima and minima were obtained from the plotted data allowing for the damping. Hence the errors are determined by the spread in the measured period in terms of an integral number of ratchet steps.

Of the molecules studied, it might seem that a formula of the above type could apply only to the ethyl and isopropyl compounds. As explained below, however, the slow passage results of Arnold *et al.* (1951) suggest that the theory can also be applied to the longer hydrocarbon chains. In all primary alcohols three resonance peaks were found. The areas under these led to their identification with the proton in the OH group, the protons in the CH_2 group immediately adjoining this, and finally all those that remain. The implication is that no relative chemical shifts were observable between the 'remaining' links of the hydrocarbon chains. In the butyl structure, for example, $[CH_3CH_2CH_2]CH_2$–, the two possible chemical shifts along the bracketed portion of the chain are assumed to be zero in this simplified approach, and hence the observed slow beat is due to the third chemical shift determined largely by the short-range local magnetic field produced by the atom bonded to the structure. In other words, a "two-body" solution applies to the leading features of the observed beat pattern. Thus while the protons on the two left-hand hydrocarbon groups may not affect the 'slow beats' they do provide an exponentially decaying background on which the modulation is superimposed. Since in this case only four of the available protons are effective in producing the modulation, it is only to be expected that the amplitude of the beats will be less than those exhibited by a molecule like ethyl chloride (CH_3CH_2Cl) in which all the protons are effective. Although some small deviations will be discussed later, this interpretation applies to the gross pattern.

RESULTS AND DISCUSSION

The values obtained for the relative chemical shift and the J-coupling constant exhibited by the various compounds of the different alcohol families are listed in the following Tables I–IV. J values in parentheses are so indicated because an accurate location of the point of symmetry could not be made. The results for the compounds of the different families are discussed under the appropriate headings.

Ethyl Compounds

In Table I it will be seen that a few of the compounds contain a third group of protons. Such molecules may in general exhibit three absolute shifts, and therefore the part played by the 'extra' protons in the observed beat patterns obtained in these cases must be further clarified.

TABLE I

ETHYL COMPOUNDS
(Et– represents CH_3CH_2–)

Compound	$\delta/2\pi$ (c.p.s.)	$J/2\pi$ (c.p.s.)
EtOH	75±3	7.1±0.2
EtOCOH	88	7.1
Et_2SO_4	87	7.2
$EtOCOCH_3$	85	7.3±0.2
Et_2O	70	—
EtCl	63	—
EtNCS	69	(7.2)
EtNCO	63	—
EtBr	55	—
$EtCOCH_3$	48	—
Et_2CO	46	7.2±0.4
EtSCN	48	7.3
Et_2S	44	—
$(EtS–)_2$	44	7.3±0.4
EtSH	43	—
$EtSCH_3$	43	—
$(EtSe–)_2$	45	7.2±0.3
EtI	44±3	7.3±0.3

As pointed out above, if the J-coupling between two proton groups is absent, the chemical shift between them is not revealed by this technique. Two experiments demonstrate the limited spatial range expected of J-coupling. In the first, very high resolution, slow passage examination of dry EtOH, it is clear that no such coupling exists between the CH_3 and OH groups* (Varian Associates 1954*b*). Moreover, a spin echo run on toluene showed no modulation even though a chemical shift between the protons on the benzene ring and those of the CH_3 group is known to exist (Varian Associates 1954*a*). In other words,

*The details of the high resolution experiments performed at Stanford University were communicated by Prof. G. M. Volkoff.

then, the indirect J-coupling is effective only between neighboring groups in a molecule. Hence the third group of protons in the compounds of this type (EtOH and EtSH excepted) contribute only to the exponential background. These remarks also apply to similar compounds listed in later tables.

A further study of EtOH has been carried out to ascertain to what extent the CH_2–OH interaction may be ignored in a discussion of the present experiments. The slow passage results referred to in the last paragraph indicate that the J-coupling associated with this interaction is about 2 or 3 c.p.s. Damping prevented such a frequency from being resolved in the present experiments. The experimental approach adopted, therefore, was to add increasing amounts of water to the pure, dry alcohol while looking for any possible changes in the modulation periods. Increasing in this way the probability of chemical exchange of the OH groups between the alcohol and water molecules is to decrease the observed effective J-coupling associated with this particular interaction (Hahn and Maxwell 1952; Saika and Gutowsky 1953). The only effect observed was a decrease in the amplitude of the beats as the water content was increased, a result expected from proton loading. A typical series of these curves is shown in Fig. 1.

As a further example of this interaction, ethylene glycol ($HOCH_2CH_2OH$)

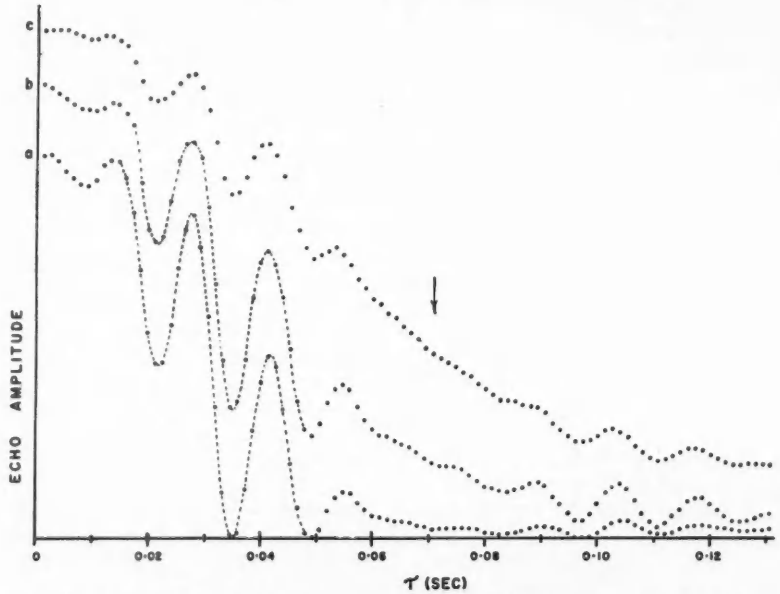

FIG. 1. The experimental plots of the echo envelopes of (*a*) anhydrous ethyl alcohol, (*b*) a mixture of 2 parts EtOH to 1 part H_2O by volume, and (*c*) a mixture of 1 part EtOH to 2 parts H_2O by volume identical to a plot obtained for Scotch Whisky. The arrow indicates the point of symmetry at π/J. The points are 1333 μsec. apart. In Figs. 1–4, the maximum echo amplitudes are plotted in arbitrary units, and for the sake of clarity convenient vertical displacements of the different plots in each figure have been introduced.

was examined. An initial water content of 0.5% all but obliterated the modulation, but after drying and vacuum distillation a relative chemical shift of 51 ± 3 c.p.s. was found. Owing to rather unexpectedly severe damping, however, only an upper limit of 3.9 c.p.s. could be placed on the J value.

It is therefore concluded that within experimental error, the OH group in ethyl alcohol plays no practical part in the pronounced modulation observed. Moreover, since sulphur has a lesser affinity for electrons than oxygen (Pauling 1948), it is very likely that the coupling of the CH_2–SH interaction in EtSH will be smaller than in EtOH, and consequently it, too, is assumed to play no part.

It is apparent from the table that the J-coupling between the two groups of protons within the ethyl structure is essentially independent of the rest of the molecule. The relative chemical shift, however, is influenced to some extent not only by the atom nearest the CH_2 group, but also by those separated from it by one, and even two spaces (e.g. EtNCS and EtNCO, EtSCN and $EtSCH_3$).

The somewhat reduced shift in Et_2O as compared with the other molecules having oxygen nearest the ethyl structure suggests that an absolute shift for the protons in the CH_3 group may be responsible. Possibly this is the result of a higher degree of association than that found in EtOH, but in any case a slow passage analysis of the ether would be of interest. In this connection, it is noted that of the compounds in Table I examined by Shoolery (1953), the halides exhibited the largest absolute shifts of the CH_3 groups.

Propyl Compounds

This family of compounds did not give very satisfactory beat patterns, a fact which is reflected in the large errors shown in Table II. Particularly in the halides, the modulation amplitudes were less than expected even though only four of the protons contribute directly to the 'slow beats'. In addition to this, all the compounds showed a greater spread in the periods of the chemical shift modulation than any other substance except the isobutyl halides.

TABLE II

PROPYL COMPOUNDS
(Pr– represents $CH_3CH_2CH_2$–)

Compound	$\delta/2\pi$ (c.p.s.)	$J/2\pi$ (c.p.s.)
PrOH	59±10	6.3±0.3
$PrOCOCH_3$	78	—
PrCl	53	6.3
PrBr	47	6.3
PrI	38±10	6.5±0.3

Propyl alcohol was studied in the same way as ethyl alcohol. However in this case the addition of water caused appreciable changes in the beat pattern. These effects are illustrated in Fig. 2. It will be seen that the high frequency beats tend to become more evenly spaced for τ less than 0.05 sec., and that a new peak appears.

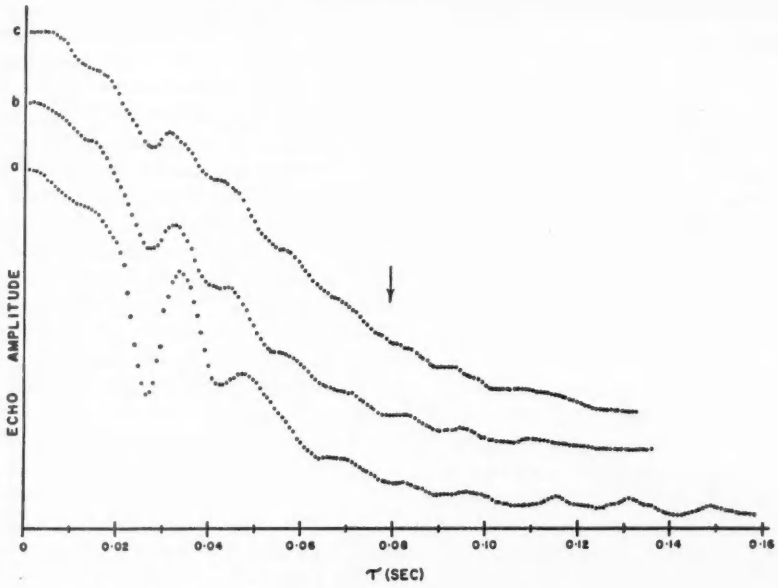

FIG. 2. The observed plots for (*a*) pure, dry propyl alcohol, (*b*) a mixture of 2 parts PrOH to 1 part H_2O by volume, and (*c*) a mixture of equal volumes of PrOH and H_2O. The point of symmetry is designated by the arrow. The points are 800 μsec. apart.

While the relaxation of the relatively weak *J*-coupling to the hydroxyl group doubtless affects the beat pattern, the persistence of small irregularities suggests that there may be a small chemical shift between the CH_3–CH_2 groups. The *J*-coupling for this interaction would presumably be equal to that found for the ethyl molecules, assuming identical bonding structures. If a second relative chemical shift does exist in the propyl molecules, it and the associated *J* value would seem to have comparable magnitudes. Such systems are described by more complex formalisms than those referred to above, and are characterized by modulations which do not depend on δ and *J* independently (Hahn and Maxwell 1952). No attempt has been made to ferret out the parameters of a possible CH_3–CH_2 interaction in the presence of the dominant CH_2–CH_2 interaction.

Isopropyl Compounds

Since the two CH_3 groups within the isopropyl structure ($\begin{matrix}CH_3\\CH_3\end{matrix}\!\!>\!CH$–) are equivalent, the situation here is considered to consist of two simultaneous CH_3–CH interactions in which the relative chemical shifts and the *J*-couplings are identical. The latter were observed only in the alcohol, but on the basis of the internal constancy of this parameter as found in other families, it is

assumed to be the same for all these compounds. The results are given in Table III.

The alcohol was treated with increasing amounts of water to find out whether or not the OH group plays an active part in the modulations. As with ethyl alcohol, no change was apparent in either the δ or the J parameters. As Figs. 9

TABLE III

ISOPROPYL COMPOUNDS

(Isopr– represents CH_3, CH_3 >CH–)

Compound	$\delta/2\pi$ (c.p.s.)	$J/2\pi$ (c.p.s.)
IsoprOH	84±3	6.0±0.2
$IsoprOCOCH_3$	111	(6.0)
$Isopr_2O$	76	—
IsoprCl	79	—
IsoprBr	76	—
$Isopr_2CO$	56	(6.0)
IsoprI	73±3	—

and 17 in Hahn and Maxwell (1952) show, the point of symmetry in this case is a maximum surrounded on either side by a small region of frequency doubling. This doubling arises from a reversal of the nuclear magnetization vector by 180° as predicted by the natures of $f_1(J\tau)$ and $f_2(J\tau)$. The only effect of adding water is to give the vectors producing the modulation a background on which to superimpose, with the result that this 'doubling' region becomes a smooth curve.

It will be seen from the table that $Isopr_2O$, like ethyl ether, has a δ-value which is unexpectedly low. A knowledge of the absolute shifts involved would be of interest here.

Butyl Compounds

The results obtained for the six butyl compounds are listed in Table IV.

TABLE IV

BUTYL COMPOUNDS

(Bt– represents $CH_3CH_2CH_2CH_2$–)

Compound	$\delta/2\pi$ (c.p.s.)	$J/2\pi$ (c.p.s.)
BtOH	63±5	5.9±0.2
$BtOCOCH_3$	76	—
Bt_3PO_4	74	6.3±0.2
BtCl	56	—
BtBr	49	—
BtI	45±5	—

Notwithstanding the fact that only four of the available protons are effective in producing the modulation, these compounds all gave much more satisfactory plots than did their propyl counterparts, both as regards amplitude and uniformity of beats. There is no evidence that suggests a possible chemical shift between the CH_3–CH_2 part of the structure.

Although water is not very soluble in butyl alcohol, a study similar to those made on the other alcohols was carried out by adding one drop of water at a time to a 1 cc. sample of dry butyl alcohol. Part of the series of curves obtained is shown in Fig. 3. Not unlike the plots for propyl alcohol, a slight but progres-

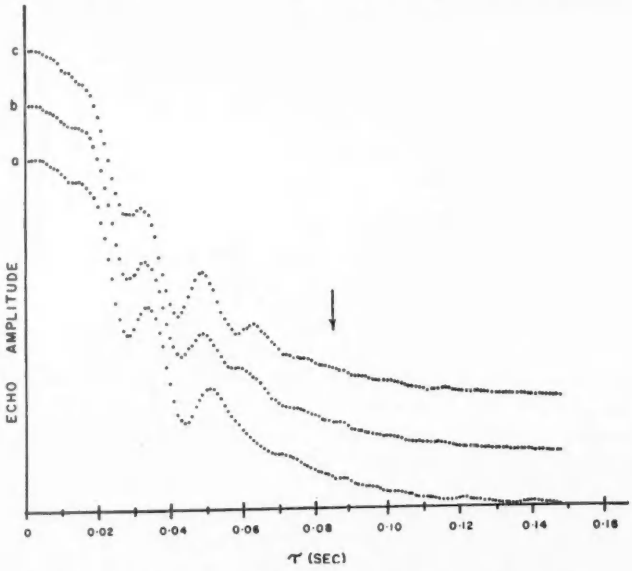

FIG. 3. The effect of adding small amounts of water to the nearly insoluble butyl alcohol. Curve (*a*) was obtained from the anhydrous alcohol. Curve (*b*) resulted from the addition of 2 drops of H_2O to 1 cc. of BtOH, and the addition of 3 more drops changed the echo envelope to that plotted as curve (*c*). The points are 1000 μsec. apart. The arrow indicates the point of symmetry at π/J.

sive change in the high frequency component occurs and a peak not present to any appreciable extent in the pure sample grows in amplitude as the water content increases. No change in the position of the point of symmetry is apparent. At the limit of solubility it would seem that the CH_2–OH interaction is still playing some part. The higher J value exhibited by the phosphate is certainly a more reliable figure for the coupling between the two CH_2 groups in the butyl structure than that indicated by the alcohol curve.

Isobutyl Compounds

It will be seen at once in Table V that, unlike the previous sets of data, the errors are much greater for the halides, a situation reminiscent of the propyl

compounds. In contrast, the other compounds in this family gave beat patterns comparable to those of the ethyl or isopropyl compounds, except of course that the amplitude of the modulation is reduced because only the three protons of the $CH–CH_2$ part of the structure are contributing to it.

TABLE V

ISOBUTYL COMPOUNDS

(Isobt– represents CH_3, CH_3 > $CH–CH_2–$)

Compound	$\delta/2\pi$ (c.p.s.)	$J/2\pi$ (c.p.s.)
IsobtOH	65±3	5.2±0.3
$IsobtOCOCH_3$	84±3	(5.2)
IsobtCl	64±10	—
IsobtBr	60±10	—
$IsobtCOCH_3$	42±4	—
IsobtI	56±10	(5.2)

Recalling the behaviors of the propyl and butyl halides leads to the general observation that in cases where CH_3 groups are immediately next to the 'beating' part of the molecule the simple modulation is interfered with, whereas in the butyl halides (in which a CH_2 group is interposed) no effect is observable. An absolute shift of the CH_3 groups has been found in the ethyl halides and a similar shift very likely occurs in the halides of these other structures as well. Slow passage analyses are needed to clarify this point. Assuming that such is the case, an explanation of the observed phenomena suggests itself. The CH_3 groups in the propyl and isobutyl halides are bonded to one of the hydrocarbon groups whose protons are taking part in the 'main' beat. Consequently the central hydrocarbon group is simultaneously engaged in two interactions, and although the one involving the CH_3 group falls into the $\delta \approx J$ category, it is still able to interfere to some extent with the high frequency modulation of the other interaction. In the butyl halides however the CH_3–CH_2 interaction is effectively buffered from the 'main' CH_2–CH_2 interaction because no chemical shift exists between the neighboring CH_2 groups of these two sets. Since the low frequencies are obscured by the damping, no evidence of its existence is afforded by experiments of this kind. This latter argument is borne out by a run on $ClCH_2CH_2Br$ in which no modulation was evident.

As Fig. 4 shows, adding water one drop at a time to isobutyl alcohol (which dissolves about the same amount of water as butyl alcohol) reduces the beat amplitude of the chemical shift modulation in those regions removed from the point of symmetry—an effect already noted. But it also causes the modulation in the immediate vicinity of this point to grow in prominence. The reasons for this effect are unknown. The actual changes in the chemical shift periods are small enough so that the approximation made by disregarding the CH_2–OH interaction is still valid.

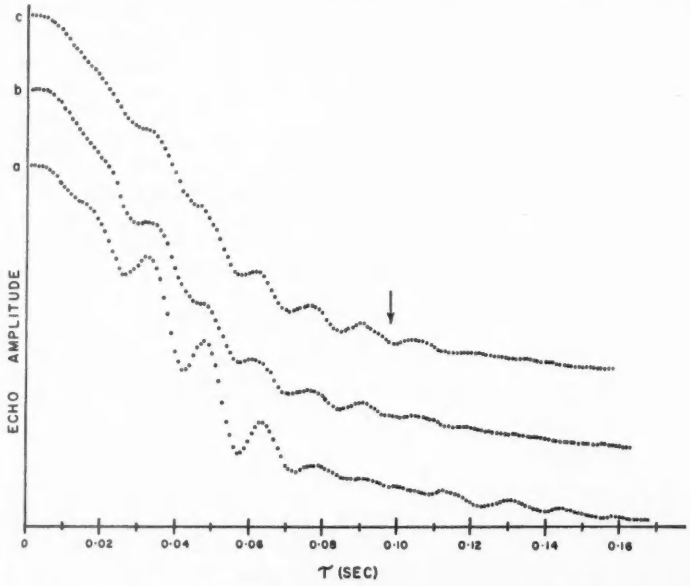

FIG. 4. Curve (*a*) is the experimental plot for dry isobutyl alcohol. It changed to curve (*b*) when 2 drops of H_2O were added to 1 cc. of the alcohol. Curve (*c*) was obtained by adding 3 more drops of H_2O. The points are 1000 μsec. apart. The point of symmetry is designated by the arrow.

The behavior of the propyl, butyl, and isobutyl alcohols when water is added suggests that the *J*-coupling in the CH_2–OH part of these molecules increases as the solubility of water in these liquids decreases. One other alcohol was examined with these effects in mind. Benzyl alcohol has a solubility in water which is even less than that of either butyl or isobutyl alcohol. Because of its structure the only beat possible occurs in the CH_2–OH appendage which is attached to a benzene ring (cf. earlier remarks on toluene). The chemical shift (37 ± 4 c.p.s.) is not important here, but the fact that $J/2\pi = 5.2\pm0.3$ c.p.s. is very interesting when the results obtained for ethylene glycol are recalled. However, assuming for the moment that decreased solubility is related to an increased *J* value, which implies a stronger or shorter bond in the CH_2–OH structure, it is still only qualitatively clear that these graded couplings affect the beats exhibited in Figs. 2, 3, and 4.

Amyl and Isoamyl Compounds

In these compounds, listed in Table VI, the overwhelming exponential background completely obscured the point of symmetry; in fact, after four cycles of the δ-modulation, the curves appear to be entirely exponential in character.

The interesting thing about these results is that the rearrangement of the 'left-hand' end of the amyl acetate molecule does not measurably change the beat frequency. Comparison with the propyl and butyl acetates, in which

TABLE VI

AMYL AND ISOAMYL COMPOUNDS

(Am– represents $CH_3CH_2CH_2CH_2CH_2$–,

Isoam– represents $\begin{matrix} CH_3 \\ \diagdown \\ \quad CH\text{–}CH_2CH_2\text{–} \\ \diagup \\ CH_3 \end{matrix}$)

Compound	$\delta/2\pi$ (c.p.s.)
AmOH	64±6
$AmOCOCH_3$	77
$IsoamOCOCH_3$	77±6

the shift likewise occurs between two CH_2 groups, reveals that in each case δ is the same. Similarly propyl, butyl, and amyl alcohols have nearly equal chemical shifts. This evidence is significant as a demonstration of the essential correctness of the assumption as to where the chemical shifts do and do not occur along the longer hydrocarbon molecular chains.

SOME FURTHER NOTES

(*a*) *On the J-Coupling*

The J values have been obtained for the indirect interactions between non-equivalent protons in cases where these are held by carbon–carbon bonds and also in cases where a carbon–oxygen bond separates them. These are the following:

CH_3–CH_2, $J/2\pi = 7.2$,	CH_3–OH, $J/2\pi = 5.0$
CH_2–CH_2, $J/2\pi = 6.3$ (6.2),	(from Hahn and Maxwell 1952),
CH_3–CH, $J/2\pi = 6.0$ (6.2),	CH_2–OH, $J/2\pi \leqslant 3.9$ (4.2),
CH–CH_2, $J/2\pi = 5.2$ (5.2),	CH–OH, $J/2\pi$ — (3.3).

It would appear that the strength of the coupling is related to the total number of protons taking part in the interaction, and one wonders whether enough information is contained in the first column to permit an estimate to be made of the unknown values in the second. If the bonding electron configurations are not changed very much from one molecular structure to another, then the J value assumed proportional to the sum of the statistical weights of all the protons in the interaction 'predicts' the values given in brackets, using the top member of each column as a reference figure. The agreement in the left-hand list suggests that possibly the figures in the other may be thought of as applying to the high solubility alcohols. The last item in this column does not at any rate contradict the behavior of isopropyl alcohol.

(*b*) *On the Relative Chemical Shifts*

Rigorous theoretical calculations of these shifts in such molecules as those investigated here are discouraged, partly because the exact wave functions are largely unknown (Ramsey and Purcell 1952) and partly because of the sensitive dependence of the final result on the particular approximation chosen, to say nothing of the complex nature of such an analysis (Saika and Slichter

1954). However something may be said by way of an interpretation of the measured changes in δ which accompany the substitution of one atom, or group of atoms, for another. It has already been noted that all the atoms in a substituted group may contribute to the observed frequency. While it is unlikely that the shielding fields arising from the carbon atoms are the same for all the protons, the indications are that any such differences are small and they will be disregarded in this semiqualitative discussion.

It will be noted that the compounds in the tables are arranged in decreasing order of the electronegativity (Pauling 1948) of the atom nearest the particular basic structure. While a rough correspondence exists between these electronegativities and the relative chemical shift (Shoolery 1953; Crawford 1954), owing to the way the former were derived, its physical significance is not too clear. The inference is that δ is proportional to the strength of the ionic part of the bond involved, although this is not the whole story.

An interesting, if oversimplified, demonstration of the relationship between the measured shifts and the induced paramagnetic fields as experienced by the protons on the hydrocarbon group nearest the substituent atom in the case of the halides is the following. The fields from the electron orbits fall off as $1/D^3$, where D is the proton–halogen distance computed from the known structures of these molecules* (Ferguson 1952; Slater 1939). As a possible correction, this quantity was also computed at the sites of the protons in the second hydrocarbon group taking part in the modulation, but was found to be negligible. Assuming that the valence orbits of the halogens are polarized to the same degree by the external field, and that each halogen has the same

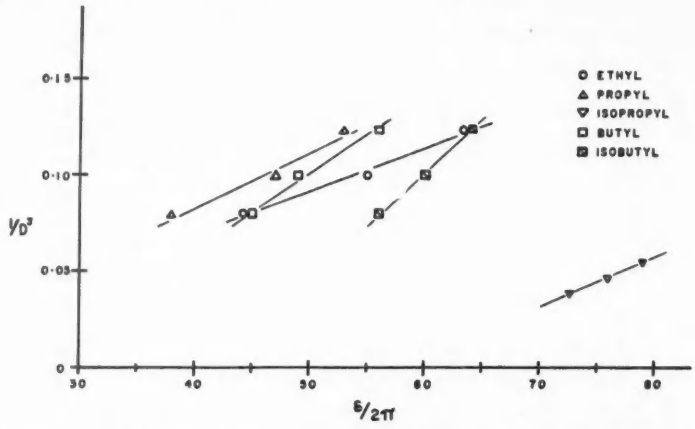

FIG. 5. The relation between the geometric dependence (D in Angstrom units) of the paramagnetic fields of the halogens for the different halide molecules and the corresponding relative chemical shift ($\delta/2\pi$ in c.p.s.). From left to right along any given line the compounds are the iodide, bromide, and chloride.

*Following a discussion with Dr. A. Taurins, Chemistry Department, McGill University, on the structures of these molecules.

number of 'p' and 'd' electrons in its molecular configuration, the proportionality constant will be the same in each case. These relationships are plotted in Fig. 5. The results are surprisingly good, and while it would be unwise to attempt to extend so simple a treatment, they demonstrate that the relative chemical shifts arise from the polarized electron orbits of the substituent group.

ACKNOWLEDGMENTS

The authors have profited from discussions with Prof. J. D. Jackson on theoretical aspects of the problem and have received advice from Dr. A. L. Thompson on chemical techniques. One of us (G. J. B. C.) gratefully acknowledges a Fellowship awarded by the National Research Council of Canada during the early part of these investigations.

REFERENCES

ANDERSON, W. A. and ARNOLD, J. T. 1954. Phys. Rev. **94**: 497.
ARNOLD, J. T., DHARMATTI, S. S., and PACKARD, M. E. 1951. J. Chem. Phys. **19**: 507.
CRAWFORD, G. J. B. 1954. Ph.D. Thesis, McGill University, Montreal, Quebec. Unpublished.
DAS, T. P. and SAHA, A. K. 1954. Phys. Rev. **93**: 749.
FERGUSON, L. N. 1952. Electron structure of organic molecules. Prentice-Hall, Inc., New York. Chap. 4.
GUTOWSKY, H. S., MCCALL, D. W., and SLICHTER, C. P. 1951. Phys. Rev. **84**: 589.
——— 1953. J. Chem. Phys. **21**: 279.
HAHN, E. L. 1950. Phys. Rev. **80**: 580.
HAHN, E. L. and MAXWELL, D. E. 1951. Phys. Rev. **84**: 1246.
HAHN, E. L. and MAXWELL, D. E. 1952. Phys. Rev. **88**: 1070.
HUNTEN, D. M. 1951. Can. J. Phys. **29**: 463.
LAMB, W. E. 1941. Phys. Rev. **60**: 817.
MOODY, H. J. and CRAWFORD, G. J. B. 1954. Can. J. Phys. **32**: 356.
PAULING, L. 1948. Nature of the chemical bond. 2nd ed. Cornell Univ. Press, Ithaca, N.Y. Chap. 2.
RAMSEY, N. F. 1950. Phys. Rev. **78**: 699.
RAMSEY, N. F. and PURCELL, E. M. 1952. Phys. Rev. **85**: 143.
SAIKA, A. and GUTOWSKY, H. S. 1953. J. Chem. Phys. **21**: 1688.
SAIKA, A. and SLICHTER, C. P. 1954. J. Chem. Phys. **22**: 26.
SHOOLERY, J. N. 1953. J. Chem. Phys. **21**: 1899.
SLATER, J. C. 1939. Introduction to chemical physics. 1st ed. McGraw-Hill Book Co., Inc., New York. Chap. 25.
VARIAN ASSOCIATES. 1954*a*. Publ. No. 1550.
——— 1954*b*. Publ. No. 76. Radio frequency spectroscopy, **1**, No. 2.
——— 1955. Publ. No. 142. Radio frequency spectroscopy, **1**, No. 3.

THE OSCILLATING SPHERE AT LARGE AMPLITUDES IN LIQUID HELIUM[1]

By C. B. Benson and A. C. Hollis Hallett

ABSTRACT

Measurements of the damping of the oscillations of a sphere which decay from an initial deflection ~10 radians show that two critical amplitudes, denoted by ϕ_c and ϕ_t, may be defined in liquid helium II. The decrement is constant at amplitudes below ϕ_c (a few tenths of a radian), and is caused by the damping due to the viscosity of the normal fluid. ϕ_c is found to be proportional to the square root of the period of oscillation. Above ϕ_c the decrement increases, the superfluid becoming involved in the motion, until it attains another constant value, which is attributed to the viscosity of a single fluid whose density is equal to the total density ($\rho_n+\rho_s$) of liquid helium II. At a larger amplitude ϕ_t (~2 radians) the decrement begins to increase linearly with amplitude, and this behavior, which is also found in liquid helium I and in helium gas at 4°K., is attributed to the onset of turbulence. Reynolds numbers calculated at ϕ_t are ~200 for helium II, helium I, and helium gas at 4°K.

1. INTRODUCTION

The oscillating disk is one of several standard methods for measuring the viscosity of liquids and vapors that has been used to study the mechanics of liquid helium below the λ-point. By its means information has been obtained on both the viscosity and the effective density of the liquid (Andronikashvili 1946, 1948; Hallett 1952). Provided that the amplitude of oscillation is small, the two-fluid model gives a satisfactory explanation of the results by attributing the increase in period (due to the moment of inertia of the carried fluid) and the damping to the density ρ_n and the viscosity η_n of the normal fluid. However, Hallett (1952) showed that if the amplitude of oscillation was increased above a certain critical value (of the order of 0.1 radian) the damping increased with the amplitude because of the action of some non-linear frictional force. He also found that the moment of inertia of the carried fluid increased with amplitude as though the superfluid was being dragged more and more into motion with the normal fluid as the amplitude increased.

The exact dependence of this critical amplitude on period of oscillation was uncertain, and it seemed likely that a more detailed study of these effects, particularly at larger amplitudes, would prove instructive. Accordingly in the present series of experiments particular attention has been paid to extending the range of amplitudes and to the investigation of effects at a number of different periods of oscillation. A sphere was used instead of a disk, however, since there was some doubt concerning the influence of the corners on the edge correction for a disk.

It has been found that the critical amplitude ϕ_c varies as the square root of the period T ($\phi_c \propto T^{\frac{1}{2}}$), and that as the amplitude is increased above ϕ_c, a range of amplitudes is found in which the fluid behaves as a single fluid with density equal to the total density of liquid helium. At still higher amplitudes (>2.0 radians) the motion of this single fluid becomes turbulent, the onset of turbulence being characterized by a Reynolds number of the order of 200.

[1]Manuscript received March 12, 1956.
Contribution from the Department of Physics, University of Toronto, Toronto, Ontario.

2. DESCRIPTION OF THE APPARATUS

An outline sketch of the apparatus is shown in Fig. 1. The sphere A was suspended from a thin quartz fiber B which was situated in the torsion head C well above the helium dewar. Rigid connection between the sphere and the

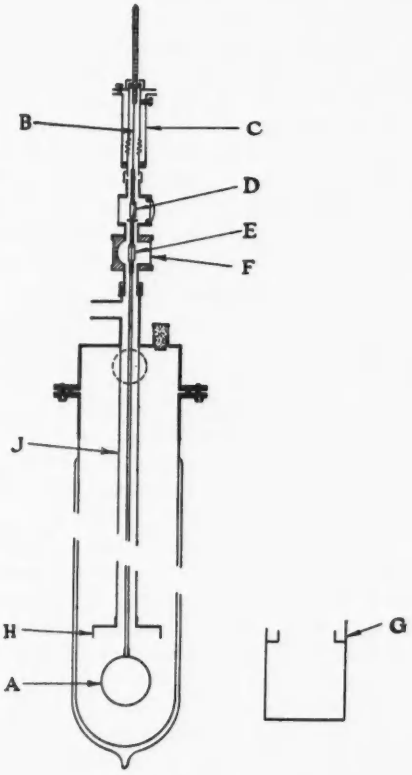

FIG. 1. The cryostat.

lower end of the quartz fiber was made by means of a quartz rod of diameter 2 mm. and length 80 cm. The sphere actually used was hollow, so that its moment of inertia was small. Consequently the weak frictional forces in the liquid produced a decay time of the system which was experimentally reasonable. The hollow sphere was constructed from thin copper sheet spun into hemispherical shape on a lathe. Two hemispheres were joined with solder round the equator to form the completed sphere which was then copper plated to a thickness of 25 microns. The sphere had a radius of 1.294 cm. and measurements of the diameter in different directions did not vary by more than 1%.

The amplitude of oscillation was observed by a lamp and scale method,

using the mirrors D and E of Fig. 1. D was a single plane mirror which was used for the observation of relatively small amplitudes, up to 0.25 radian, a converging lens being used as a window to form an image of an illuminated slit on a curved scale at a distance of 1 meter. For larger amplitudes a four-sided mirror E was used in conjunction with a semicircular scale of radius 25 cm. The window F was made from a flat strip of celluloid bent into a cylinder and sealed to the torsion head with glyptal varnish. The distortion introduced by this window was not detectable on the scale at 25 cm., although the angular deflections could be read to better than 0.001 radian.

For observations of the sphere in vacuum or in helium gas at low temperatures it was possible to isolate the oscillating system from the helium bath by means of a copper can G. This can could be sealed with mercury to the cap H on the lower end of the monel tube J. During measurements in liquid helium the can was not in place. The inside diameter of the can was 5.0 cm. and that of the helium dewar 5.6 cm.

3. EXPERIMENTAL PROCEDURE

The sphere was set into torsional oscillations by applying a magnetic field to a short piece of iron wire which was placed just below the mirror D. The field was produced by passing a current through a small pair of Helmholtz coils outside the torsion head. The system could be given an impulsive deflection by applying the magnetic field in a direction perpendicular to the iron wire for a time short compared with the period of oscillation. Alternatively the coils could be rotated about a vertical axis, thus giving the system a steady deflection before switching off the current. The subsequent behavior of the sphere was found to be independent of the method used to start the oscillations, and in practice the method of impulsive deflection was usually employed. The initial amplitude could be varied by controlling the current through the coils, and values up to about 10 radians were used.

After the initial deflection the system oscillated under the influence of the restoring couple of the quartz fiber B, and the damping forces exerted on the sphere. The decay of the oscillations produced by the damping forces was observed by recording the amplitudes of swing on each side of the position of rest until the amplitude had decayed to less than 0.05 radian.

The period of oscillation at large amplitudes was usually determined by timing a number of complete oscillations with a calibrated stop watch. At small amplitudes, however, where the results could be used to calculate the viscosity η_n of liquid helium II, it was necessary to measure this period more accurately. The period was therefore determined using a chronograph to compare the times of pulses received from a photoelectric cell placed at the zero position on the scale with pulses received every second from a standard clock. Thus by timing a number of oscillations the period was determined to an accuracy better than one part in 10^4.

For a damped oscillatory motion the decrement δ, which is proportional to the fractional energy dissipation per cycle, is given by

$$\delta = -(1/2\pi\phi).d\phi/dn,$$

where ϕ is the amplitude and n is the number of complete oscillations. For an exponentially damped oscillation this defines the same δ that appears in the expression

$$\phi = \phi_0 e^{-\delta\omega t} \sin \omega t.$$

The decrement δ was calculated from the observed amplitudes by numerical differentiation (Hartree 1952). As differences greater than the third order were unreliable because of experimental error, terms involving higher differences were ignored. The calculations were performed using FERUT, the Ferranti computer at the University of Toronto. Thus δ was obtained as a function of the amplitude ϕ.

Observations were also made in vacuum, at a pressure less than 10^{-4} mm. Hg. It was found that the vacuum decrement, which will be denoted by Δ_0, was small but could not be neglected in comparison with the decrements obtained at small amplitudes in helium II; it had therefore to be taken into account in the calculation of the viscosity η_n. It was less significant, however, at larger amplitudes, partly because of the larger values of δ which were found, and partly because Δ_0 decreased at larger amplitudes.

Temperatures were calculated from the vapor pressure over the liquid helium, using the 1949 temperature tables (van Dijk and Shoenberg 1949).

4. EXPERIMENTAL RESULTS

The variation of the decrement δ with amplitude ϕ at a number of different temperatures in liquid helium II is shown in Fig. 2. At the smallest amplitudes

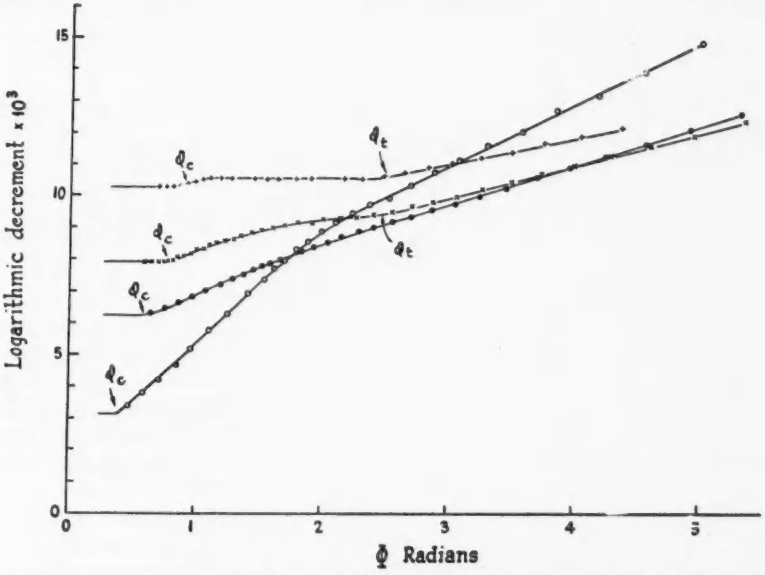

FIG. 2. The variation of the logarithmic decrement with amplitude at various temperatures in helium II.

+ at 2.175°K. × at 2.091°K. ● at 1.948°K.
○ at 1.362°K. Period of oscillation T = 25.0 sec.

δ is constant, and this is the damping produced by the viscosity of the normal fluid. It may be seen that δ is independent of amplitude only below an amplitude denoted by ϕ_c, in agreement with Hallett's observations with a disk. The constant decrement below ϕ_c may be used to calculate the viscosity η_n, and the values of the latter are in fair agreement with the results of previous workers using oscillating disks. Significant discrepancies have, however, been found and these results will be presented in a separate paper. It can be seen from Fig. 2 that for amplitudes greater than ϕ_c the decrement increases markedly. This increase is rapid at first, but as ϕ increases further, δ increases less rapidly and the curve tends to flatten. These results are in qualitative agreement with those obtained by Hallett (1952) using an oscillating disk. It can also be seen from Fig. 2 that there is another critical amplitude, of the order of 2 radians, denoted by ϕ_t, such that for amplitudes greater than ϕ_t, δ increases linearly with ϕ.

The critical amplitude ϕ_c may be determined either from the curves of log ϕ versus n, or from the curves of the decrement δ versus ϕ. The second method is unreliable since the numerical formula used in the differentiation produces a smoothing which extends over about six periods. At temperatures near the λ-point this may involve a considerable range of amplitude because of the high damping. The values of ϕ_c given in Table I are therefore all derived from the

TABLE I

VALUES OF THE CRITICAL AMPLITUDE ϕ_c AS A FUNCTION OF TEMPERATURE

(*a*) T = 25.0 sec.			(*b*) T = 10.4 sec.			(*c*) T = 6.5 sec.		
θ (°K.)	ϕ_c (radian)	$\phi_c/T^{\frac{1}{2}}$	θ (°K.)	ϕ_c (radian)	$\phi_c/T^{\frac{1}{2}}$	θ (°K.)	ϕ_c (radian)	$\phi_c/T^{\frac{1}{2}}$
2.175	1.15 (±.10)	0.230	2.176	0.60 (±.10)	0.186	2.180	>1.25	0.49
2.150	0.88 (±.03)	0.176	1.945	0.40 (±.03)	0.124	2.099	0.44 (±.03)	0.173
2.091	0.85 (±.05)	0.170	1.652	0.34 (±.02)	0.105	2.002	0.35 (±.03)	0.137
1.996	0.65 (±.05)	0.130	1.355	0.32 (±.02)	0.099	1.828	0.30 (±.05)	0.118
1.820	0.56 (±.04)	0.112	1.115	0.32 (±.02)	0.099	1.656	0.27 (±.02)	0.106
1.656	0.52 (±.03)	0.104				1.491	0.24 (±.01)	0.094
1.362	0.45 (±.02)	0.090				1.359	0.23 (±.01)	0.090
1.198	0.45 (±.02)	0.090				1.215	0.24 (±.02)	0.094
1.090	0.44 (±.01)	0.088				1.082	0.24 (±.02)	0.094

log ϕ versus n curves, and the estimated errors are also given. Measurements of ϕ_c were made at three different periods of oscillation T, and it may be seen that ϕ_c is not proportional to T but more closely to $T^{\frac{1}{2}}$. This is illustrated by the values of ϕ_c obtained at about 1.65°K. for three different periods. For periods of 25 sec., 10.4 sec., and 6.5 sec. the respective values of ϕ_c/T are 0.021 (±.001), 0.033 (±.002), and 0.041 (±.003), whereas $\phi_c/T^{\frac{1}{2}}$ is constant within the experimental errors at 0.104 (±.006), 0.105 (±.006), and 0.106 (±.006) respectively.

The dependence of the critical amplitude on temperature is shown in Fig. 3, where $\phi_c/T^{\frac{1}{2}}$ is plotted against temperature. Taking into account the probable errors a single curve may be drawn through the experimental data obtained at three periods of oscillation. Thus to within experimental error ϕ_c

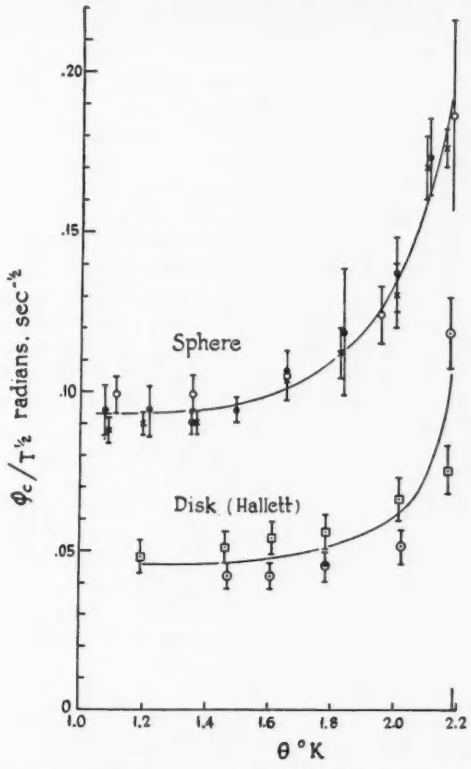

FIG. 3. The variation of $\phi_c/T^{\frac{1}{2}}$ with temperature. Comparison with the results obtained by Hallett (1952) for a disk.

is proportional to $T^{\frac{1}{2}}$ at all temperatures. As a comparison the values of $\phi_c/T^{\frac{1}{2}}$ calculated from Hallett's measurements on the oscillating disk are included in the same figure. It may be seen that again for the disk $\phi_c/T^{\frac{1}{2}}$ is constant and that the temperature variation of ϕ_c for the oscillating disk is much the same as that for the sphere. It should be noted, however, that the values of $\phi_c/T^{\frac{1}{2}}$ for the two systems do not coincide and that there must therefore be some dependence on the geometry.

At amplitudes greater than ϕ_c the exact variation of decrement with amplitude depends on the temperature, as may be seen in Fig. 2, but there are some common features which should be noticed. The first is that at temperatures just below the λ-point, for example the curve for 2.175°K., the decrement actually maintains a constant value for a considerable range of amplitudes immediately below ϕ_t. The series of curves obtained between 2.1°K. and the λ-point, given in Fig. 4, show clearly the constant value of δ just below ϕ_t, and also show how the range of amplitude for which δ is constant becomes smaller as the temperature is lowered. The second feature which is common to

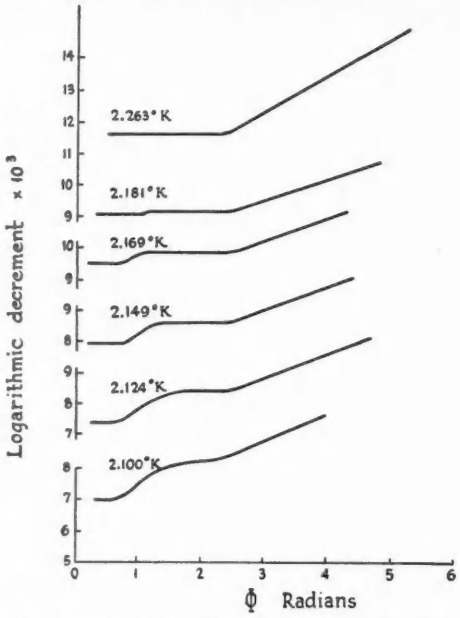

FIG. 4. The variation of the logarithmic decrement with amplitude just below the λ-point.

TABLE II

VALUES OF ϕ_t AND THE REYNOLDS NUMBERS FOR LIQUID HELIUM AND HELIUM GAS

(*a*) T = 18.5 sec. in helium II

θ (°K.)	ϕ_t (radian)	$10^3.\delta_{(\phi_t)}$	η (μpoise)	R_e
2.181	2.5±.10	9.15	21.33	220±10
2.169	2.5±.10	8.88	20.23	230±10
2.149	2.5±.10	8.60	18.95	230±10
2.124	2.5±.10	8.40	18.23	240±10
2.100	2.5±.10	8.15	17.32	240±10
2.000	2.5±.10	8.00	16.63	250±10

(*b*) T = 18.7 sec. in helium gas

θ (°K.)	ϕ_t (radian)	ρ (gm./cc.)	η (μpoise)	R_e
4.23	6.0±.20	0.0162	12.80	230±8

The kinematic viscosity $\nu = \eta/\rho = 7.9\times10^{-4}$ cm.^{2} sec.$^{-1}$

(*c*) T = 18.7 sec. in helium I

θ (°K.)	ϕ_t (radian)	ρ (gm./cc.)	η (μpoise)	R_e
2.263	2.5±.10	0.146	23.85	210±10

The kinematic viscosity $\nu = \eta/\rho = 1.63\times10^{-4}$ cm.^{2} sec.$^{-1}$

For helium gas: Viscosity from van Itterbeek and Keesom (1938).
Density from Mathias *et al.* (1925).

For helium I: Viscosity from De Troyer *et al.* (1951).
Density from Onnes and Boks (1925).

all curves is the linear increase of δ with amplitude at amplitudes greater than ϕ_t; and this is found not only in helium II but, as the curve for 2.263°K. shows, also in helium I. Similar behavior has also been found in helium gas at 4°K. Values of the amplitudes, ϕ_t, determined from the decrement versus amplitude curves, at which this behavior commences are given in Table II together with the values of the decrement $\delta_{(\phi_t)}$ found immediately below this amplitude. The form of the variation of ϕ_t with period seems to be the same as for ϕ_c, i.e. ϕ_t is proportional to $T^{\frac{1}{2}}$. The constant decrement in helium I would appear to be rather large when compared with that in helium II at the small amplitudes just below the λ-point; this effect will be discussed in a separate paper on the viscosity determination.

The period of oscillation T was found to be independent of amplitude at small amplitudes, i.e. below about 0.5 radian, but at greater amplitudes T decreased by as much as 5% at the largest amplitudes, i.e. about 10 radians. This effect was also found in vacuum measurements and is therefore attributed to a small non-linearity in the quartz suspending fibers, and is not related to the observed variation of decrement with amplitude in helium.

5. DISCUSSION OF EXPERIMENTAL RESULTS

(a) *The Amplitude* ϕ_t

The decay of the oscillations of a sphere in any normal fluid should be exponential provided that the critical Reynolds number characteristic of turbulence is not exceeded. The Reynolds number can be defined as $R_e = 2\pi R\phi l/T\nu$, where $(2\pi R\phi/T)$ is the maximum equatorial velocity of the sphere reached at the center of its swing, l is a length characteristic of the motion, and ν is the kinematic viscosity η/ρ. It seems reasonable in this type of motion to choose the penetration depth, given by $\lambda = (\eta T/\pi\rho)^{\frac{1}{2}}$, as the characteristic length, since this length defines the lateral extent of the region in which the fluid is set into motion with the sphere. The Reynolds number therefore becomes $R_e = 2R\phi(\pi\rho/\eta T)^{\frac{1}{2}}$. The critical value of this number for turbulence should be independent of the fluid used. If ϕ_t corresponds to the onset of turbulence in helium I and in helium gas, the Reynolds numbers obtained in these two fluids should agree with one another and should establish a criterion for the onset of turbulence in any other fluid under the same experimental conditions, and, in particular, in helium II.

Table II gives the Reynolds numbers calculated, according to the above definition, from the values of ϕ_t found in helium gas and in helium I, for which the viscosity and density are taken from the literature. (See Table II.) The agreement between these two numbers, 230 and 210 for helium gas and helium I respectively, is reasonably good despite the fact that the kinematic viscosities of the two fluids differ by a factor of 5.

In helium II ϕ_t occurs in the amplitude range for which the simple two-fluid model is no longer valid, since it is known (Hallett 1952) that the total density of the fluid is involved in the motion at these amplitudes. Thus in calculating the Reynolds number at the amplitude ϕ_t for helium II the total density ρ should be used, and the effective viscosity must be calculated from the constant

decrement at amplitudes just below ϕ_t. Table II shows the viscosity $\eta_{(\phi_t)}$ calculated on this basis at several temperatures between the λ-point and 2.0°K., where the constant value of δ just below ϕ_t is well defined. Below about 2.0°K. ϕ_t has not the same significance since the decrement δ does not attain a constant value until amplitudes less than ϕ_c are reached. The Reynolds numbers calculated using these values for ϕ_t and $\eta_{(\phi_t)}$ are given in column five of Table II, and it may be seen that they agree well with the Reynolds numbers obtained in helium gas and helium I. It seems reasonable, therefore, to conclude that at amplitudes greater than ϕ_t the motion of liquid helium II is turbulent.

The linear increase of δ above ϕ_t is also indicative of turbulence. It is shown in the Appendix that a decrement of the form $\delta = \delta_0 + B\phi$ can result from the inclusion of a resistance proportional to the square of the velocity in the differential equation of motion of the sphere. Since a resistance of this form is known to be a common characteristic of turbulence, it would seem to be quite definite that, for amplitudes above ϕ_t, there is turbulent motion in the boundary layer close to the sphere.

The magnitude of the Reynolds numbers found in these experiments (~200) is less than that normally found under similar conditions in fluids at room temperature (~1000). It is known, however, that the onset of turbulence is facilitated by any asymmetry in the system, and may occur at lower Reynolds numbers than 1000 under some conditions. It is also conceivable that the critical Reynolds number is a function of temperature, as suggested by Betchov (1955), although this seems unlikely.

(*b*) *The Amplitude* ϕ_c

It is evident that the amplitude ϕ_c is the amplitude at which some hydrodynamical variable has reached a critical value, so that at larger amplitudes than ϕ_c the fraction ρ_s/ρ begins to be involved in the motion. It should, however, be noted that the ϕ_c given by the experiment was actually the amplitude at which ρ_s ceased to be involved in the motion, since the amplitude always decayed from a larger value. However, provided that the relevant relaxation time is less than a time of the order of a minute, the value of ϕ_c determining the onset of the dragging of ρ_s will not be significantly different from the value given by the experiment.

It has been seen that ϕ_c is proportional to $T^{\frac{1}{4}}$ within the limits of experimental error, and this fact seems to eliminate the possibility of an actual critical velocity given by $V_c = 2\pi R\phi_c/T$ (i.e. $\phi_c \propto T$), as has been suggested by Dash (1954, 1955). A comparison with ϕ_t, which is also proportional to $T^{\frac{1}{4}}$, would suggest the possibility of a critical dimensional number being reached at ϕ_c, such as the Reynolds number; but the question of what value to choose for the kinematic viscosity then arises. The kinematic viscosity of the normal fluid η_n/ρ_n is one possibility, but this leads to a Reynolds number at ϕ_c which decreases by a factor of 30 between the λ-point and 1.1°K. This is not surprising, however, since it is known that the superfluid becomes in some way involved in the motion at ϕ_c, while a constant Reynolds number, involving

η_n/ρ_n, could indicate no more than the breakdown of laminar motion for the normal fluid. Possibly the creation of vorticity in the superfluid is responsible for the occurrence of ϕ_c, as suggested by Feynman (1955). The quantized vortex lines created in the fluid would be unstable and could therefore provide a mechanism for the dissipation of kinetic energy as heat (rotons). This is closely analogous to the onset of turbulence, but the analogy is not complete since the superfluid has zero viscosity and therefore no boundary layer exists, and a Reynolds number has no significance. If, however, the vorticity is quantized, the creation of a vortex line requires a finite expenditure of energy and thus may explain the existence of a finite critical amplitude. It is possible that the creation of vorticity may be facilitated by the presence of corners on the solid surface, and the consequent abrupt changes in the velocity profile. If that is so a qualitative explanation of the difference between the values of ϕ_c found with the disk and the sphere may be provided.

The explanation of observed critical velocities on the basis of Feynman's ideas would seem to be worthy of closer investigation, particularly in view of the fact that there is no other satisfactory explanation of these phenomena.

We are indebted to the National Research Council of Canada and to the Ontario Research Foundation for their grants in aid of research. These grants have provided the facilities which have made this research possible. One of us (C. B. B.) is indebted to the Garnet W. McKee – Lachlan Gilchrist Fund for the grant of a Scholarship. We are also indebted to Professor W. H. Watson for numerous discussions.

APPENDIX

An additional damping term proportional to the square of the angular velocity is introduced into the differential equation for damped simple harmonic motion as follows:

$$\ddot{\alpha}+\lambda\dot{\alpha}+\gamma\dot{\alpha}|\dot{\alpha}|+\omega^2\alpha = 0,$$

where $\dot{\alpha}|\dot{\alpha}|$ is used rather than $(\dot{\alpha})^2$ since the couple must change sign with $\dot{\alpha}$. The solution of this equation can be put in the form $\alpha = \varphi(t)\sin\omega t$; but if the decrement is small, so that the motion can be considered to a first approximation as periodic, then α can be written as $\alpha = \varphi \sin \omega t$.

The energy is given by $E = \phi^2\omega^2/2$, and the rate of loss of energy $dE/dt = \phi\omega^2\dot{\phi}$. Also the energy dissipation per cycle is given by the integration over a complete cycle of the sum of the damping couples:

$$dE/dt = -1/T \,.\, \int_0^{2\pi} [\lambda\phi^2\omega\cos^2 x+\gamma\phi^3\omega^2\cos^2 x|\cos x|]\,dx,$$

where $x = \omega t$. Therefore

$$\dot{\phi} = -\lambda\phi/2\pi \,.\, \int_0^{2\pi} [\cos^2 x+\gamma\phi/\lambda \,.\, \omega\cos^2 x|\cos x|]\,dx,$$

$$\dot{\phi} = -\lambda\phi/2-4\gamma\omega\phi^2/3\pi.$$

Now $\dot{\phi} = d\phi/dt = d\phi/dn \,.\, dn/dt;$

therefore

$$\dot{\phi} = 1/T.d\phi/dn,$$

$$\dot{\phi}/\phi = 1/\phi T.d\phi/dn = 1/T.d \log \phi/dn,$$

$$d \log \phi/dn = -\lambda T/2 - 8\gamma\phi/3.$$

But the decrement $\delta = -1/2\pi.d \log \phi/dn;$

therefore $\delta = \lambda T/4\pi + 4\gamma\phi/3\pi.$

or $\delta = \delta_0 + B\phi.$

REFERENCES

ANDRONIKASHVILI, E. L. 1946. J. Phys. (U.S.S.R.), **10**: 201.
——— 1948. J. Exptl. Theoret. Phys. (U.S.S.R.), **18**: 424, 429.
BETCHOV, R. 1955. Private communication.
DASH, J. G. 1954. Phys. Rev. **94**: 825, 1091.
——— 1955. Phys. Rev. **97**: 1038.
VAN DIJK, H. and SHOENBERG, D. 1949. Nature, **164**: 151.
FEYNMAN, R. P. 1955. Progress in low temperature physics. Vol. I. North-Holland Pub. Co., Amsterdam. Chap. 2.
HALLETT, A. C. H. 1952. Proc. Roy. Soc. (London), A, **210**: 404.
HARTREE, D. R. 1952. Numerical analysis. Oxford at the Clarendon Press. p. 118.
VAN ITTERBEEK, A. and KEESOM, W. H. 1938. Physica, **5**: 257.
MATHIAS, E., CROMMELIN, C. A., ONNES, H. K., and SWALLOW, J. C. 1925. Proc. Acad. Sci. Amsterdam, **28**: 526.
ONNES, H. K. and BOKS, J. D. A. 1925. Communs. Kamerlingh Onnes Lab. Univ. Leiden, No. **170b**.
DE TRØYER, A., VAN ITTERBEEK, A., and VAN DEN BERG, G. J. 1951. Physica, **17**: 50.

ON THE DISTRIBUTION OF THE PRODUCT OF DIODE DETECTOR WAVEFORMS[1]

By E. L. R. Webb

ABSTRACT

The probability distribution of the product of two waveforms such as come from the diode second detectors of radio receivers is examined over the whole range of signal to noise ratios. Computed curves of probability density are given for small and moderate values of signal to noise ratio and the limiting form for large signal to noise indicated. The pure noise case is the only one immediately available in terms of tabulated functions. Compared to the Rayleigh distribution it rises much faster, reaches its maximum sooner and lower, and decays much more slowly. The very large signal to noise ratio case approaches an impulse function. Estimates of mean and variance are given.

I. INTRODUCTION

The concept of correlation implies that a product of two variables is averaged in some sense. This kind of operation occurs quite frequently in modern electronics where the variables are, or can be made into, waveforms, and the operation is usually aimed at improved detection of weak signals masked by noise. The derivation of the general form for the distribution of the product of two random variables is outlined in Section II. The distribution functions for the particular input signals to be considered are stated in Section III. These cover the entire range of signal to noise ratios from zero to infinity ($-\infty$ db. to $+\infty$ db.) and since we are dealing with a product, we will have to examine a two-dimensional field. Fortunately it will suffice to cover the first quadrant only, since, by definition, signal to noise ratios are never negative.

The noise–noise case is quite easy and is treated fairly completely in Section IV. Signal is next introduced, but in one channel only, in Section V. The general case of signals in both channels is examined in Section VI. It is unfortunate that the resulting expressions do not appear to be readily available in tabulated form. The main attention is given to the important practical region of signal to noise ratios near unity and typical distributions are given graphically. The very large signal to noise ratio case is considered separately in Section VII, by means of impulse functions.

II. GENERAL FORM FOR PRODUCT DISTRIBUTIONS

The distribution of the product of two random variables is a special case of a rather general principle covering *functions of random variables* having individual distributions $\phi_1(x)$ and $\phi_2(y)$. The best attack appears to be by means of joint distributions and coordinate transformations; thus our point of departure is

$$\phi(x, y)dxdy = \phi[x(r, s), y(r, s)]\left|\frac{\partial(x, y)}{\partial(r, s)}\right| drds = \phi_t(r, s)drds$$

[1]Manuscript received March 14, 1956.
Contribution from the Radio and Electrical Engineering Division, National Research Council, Ottawa. Issued as N.R.C. No. 3981.

and for our purpose we set $s = xy$ and $r = x$, then

$$\left|\frac{\partial(x, y)}{\partial(r, s)}\right| \equiv \begin{vmatrix} \frac{\partial x}{\partial r} & \frac{\partial y}{\partial r} \\ \frac{\partial x}{\partial s} & \frac{\partial y}{\partial s} \end{vmatrix} = \begin{vmatrix} 1 & -\frac{s}{r^2} \\ 0 & \frac{1}{r} \end{vmatrix} = \frac{1}{r} = \frac{1}{x},$$

with the result that

$$\phi_t(r, s)drds = \phi(x, s/x)\frac{dx}{x}ds.$$

The next step is made by means of the notion of marginal distribution, which allows us to say

$$\phi(s)ds = ds\int \phi(x, s/x)\frac{dx}{x}.$$

For *independent* inputs the joint distribution may be written as a product

$$\phi_1(x) \cdot \phi_2(y)$$

and so we finally arrive at

$$\phi(s)ds = ds\int_0^\infty \phi_1(x)\phi_2(s/x)\frac{dx}{x}$$

provided that we make the assumption that neither x nor y is ever less than zero.

This result is not too widely known but it has been published at least once, by Huntington (1939), who derived it by a different and somewhat intuitive method.

III. INPUT DISTRIBUTIONS CONSIDERED

When the input to a diode second detector is the sum of narrow band Gaussian noise of mean square value σ^2 and a sinusoid of peak amplitude A, then the output waveform will always be positive (or negative), and, in the absence of further filtering, will have the well-known distribution

$$\phi(x) = \frac{x}{\sigma^2}\exp\left(-\frac{x^2+A^2}{2\sigma^2}\right) I_0\left(\frac{xA}{\sigma^2}\right).$$

For small signal to noise ratios, the Bessel function may be approximated by the first few terms of its series

$$1+\left(\frac{xA}{\sigma^2}\right)^2+\frac{1}{2!\,2!}\left(\frac{xA}{\sigma^2}\right)^4+\ldots$$

and for pure noise $A = 0$ so that

$$\phi(x) \to \frac{x}{\sigma^2}\exp\left(-\frac{x^2}{2\sigma^2}\right),$$

the well-known Rayleigh distribution.

On the other hand for very large signal to noise ratios, the asymptotic expansion for I_0 leads to

$$\phi(x) \simeq \frac{1}{\sqrt{2\pi\sigma^2}}\sqrt{\frac{x}{A}}\exp\left[-\frac{1}{2}\left(\frac{x-A}{\sigma}\right)^2\right]$$

in which the Gaussian portion dominates and, in the limit $\sigma \to 0$, becomes one of the well-known forms for the unit impulse function. Thus for purely sinusoidal IF waves the diode detector yields the amplitudes as expressed by

$$\phi(x) = u_0(x-A).$$

These will be all the distributions used in the following treatment. The numerical subscripts will refer to the channels 1 and 2 whose product is under consideration. In particular the signal to noise ratio will be written $s_i^2 = A_i^2/2\sigma_i^2$, where i may be 1 or 2.

IV. THE NOISE–NOISE CASE

Using the Rayleigh distribution twice in the general form for the product distribution derived in Section II, we have almost immediately:

$$\phi(s)ds = \frac{sds}{(\sigma_1\sigma_2)^2}\int_0^\infty \exp\left[-\frac{s}{2\sigma_1\sigma_2}\left(\frac{\sigma_2}{\sigma_1}\frac{r^2}{s}+\frac{\sigma_1}{\sigma_2}\frac{s}{r^2}\right)\right]\cdot\frac{dr}{r}.$$

The output, normalized with respect to $\sigma_1\sigma_2$, will be denoted by $x = s/\sigma_1\sigma_2$. It will also be a practical step to write $(\sigma_2/\sigma_1)(r^2/s) = e^{2\theta}$; then $dr/r = d\theta$ and the probability becomes

$$\phi(s)ds = xdx\int_{-\infty}^{\infty}\exp(-x\cosh 2\theta)d\theta = xdx\int_0^\infty \exp(-x\cosh\theta)d\theta.$$

This is a well-known definite integral and is given by the modified Bessel function of the second kind and zero order, thus

$$\phi(s)ds = xK_0(x)dx.$$

As a check, $\int_0^\infty \phi(s)ds = 1$, which is a necessity for a correct distribution function. Sometimes $(2/\pi)K_0(x)$ is tabulated as $jH_0^{(1)}(jx)$ as in Jahnke and Emde (1945). We also note that although $K_0(x)$ is infinite at the origin, the product $x\,K_0(x)$ is of the form $0.116x+x\ln(1/x)$ which goes to zero rather steeply as x approaches zero.

This noise–noise product distribution is plotted in Fig. 1 along with the Rayleigh distribution for comparison. The dotted curve is the result of taking only the first term of the asymptotic expansion of $K_0(x)$ and it is a remarkably good approximation even for small values of x. The fall-off at large values of the random variable is essentially e^{-x} as contrasted with $e^{-x^2/2}$ for the Rayleigh curve. The product distribution also rises much faster than the Rayleigh curve and reaches its maximum sooner and lower. The location and value of the maximum may be found by solving

$$\frac{d}{dx}[xK_0(x)] = K_0(x)-xK_1(x) = 0.$$

This was done graphically, yielding $\phi_{max} = 0.467$ at $x = 0.595$ as compared to 0.607 at $x = 1$ for the Rayleigh curve.

The moments about the origin may be found through partial integration and the recursion properties of Bessel functions. Thus it may be shown that

$$\int_0^\infty x^n\phi(x)dx = \int_0^\infty x^{n+1}K_0(x)dx$$

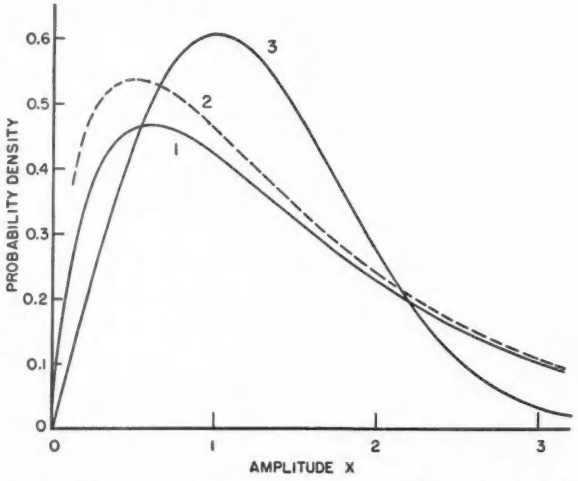

FIG. 1. Curve 1: The "noise–noise" product distribution, $xK_0(x)$, obtained by multiplying the output from two receivers each having an input of pure noise.
Curve 2: The asymptote $\sqrt{\pi x/2}\, e^{-x}$.
Curve 3: The Rayleigh distribution, $x\exp(-\frac{1}{2}x^2)$, for the output of an individual channel.

has the values $\frac{1}{2}\pi$, 1, $\frac{1}{2}\pi$, 4, and $9\pi/2$ for $n = -1$, 0, 1, 2, and 3 respectively, so that the mean is $\frac{1}{2}\pi = 1.571$, the variance

$$\sigma^2\{x\} = M\{x^2\} - M^2\{x\} = 4 - \tfrac{1}{4}\pi^2 = 1.533,$$

and the r.m.s. fluctuation $\sigma = 1.238$. These may be compared with the corresponding values for the Rayleigh curve, which has a mean of $\sqrt{\frac{1}{2}\pi} = 1.253$, and r.m.s. fluctuation of 0.655.

V. SIGNAL IN ONE CHANNEL ONLY

The case of sinusoidal signal plus noise in one channel, and noise alone in the other, is symmetrical with respect to channels but for definiteness we will use $A_2 = 0$ but $A_1 \neq 0$. With the definitions already made we have:

$$\phi(s)ds = xdx \int_{-\infty}^{\infty} \exp(-s_1{}^2 - x\cosh 2\theta)\; I_0(\sqrt{2x}\, s_1\, e^{\theta})d\theta.$$

The Bessel function may be written

$$\sum_0^{\infty} \frac{(\frac{1}{2}xs_1{}^2)^r e^{2r\theta}}{r!\, r!}.$$

Also $e^{2r\theta}$ may be written as the sum of an even and an odd function of 2θ and since we are integrating from $-\infty$ to $+\infty$ the odd part contributes nothing. The even part may be integrated term by term after interchanging the order of integration and summation:

$$\phi(s)ds = xdx\, e^{-s_1{}^2} \sum_{r=0}^{\infty} \frac{(\frac{1}{2}xs_1{}^2)^r K_r(x)}{r!\, r!},$$

where $K_r(x)$ is the modified Bessel function of the second kind. At $s_1^2 = 0$ we regain the noise–noise distribution as before.

Some general remarks are made possible by considering limiting cases of the Bessel functions.

For small x,

$$K_0(x) \to 0.116 + \ln \frac{1}{x} \text{ and } K_r(x) \to \frac{(r-1)!}{2}\left(\frac{2}{x}\right)^r,$$

so that

$$\phi(s)ds \doteq x\,dx\, e^{-s_1^2}\left[\left(0.116 + \ln \frac{1}{x}\right) + \sum_1^\infty \frac{{s_1}^{2r}}{2r \cdot r!}\right].$$

For small s_1^2 the K_0 term dominates and gives a rapid initial rise; but for large s_1^2 the curve is more linear—with slope

$$e^{-s_1^2} \sum_1^\infty \frac{{s_1}^{2r}}{2r \cdot r!}.$$

For large x,

$$K_r(x) \simeq \sqrt{\frac{\pi}{2x}}\, e^{-x};$$

then

$$\phi(s)ds \simeq \sqrt{\frac{\pi x}{2}}\, dx \exp(-{s_1}^2 - x)\, I_0(\sqrt{2x}\, s_1),$$

which demonstrates the powerful selective action of $\exp(-x \cosh 2\theta)$ in the integral, acting as a sort of impulse function. If we replace the Bessel function by its asymptote, $\phi(s) \sim \exp[-{s_1}^2 + s_1\sqrt{2x} - x]$. The exponent has a pair of complex roots at $\sqrt{x} = s_1 \exp(\pm j\pi/4)$ but since we are confined to real values, the exponent is never zero, but has a minimum value of $s_1^2/2$ at

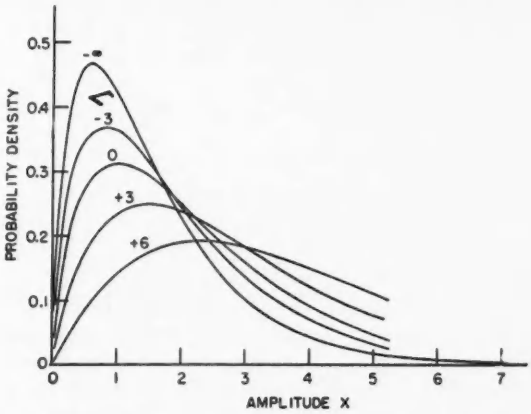

FIG. 2. The product distributions obtained with a signal to noise ratio s_1 in one channel and pure noise in the other. The five curves are for s_1 values ranging from $-\infty$ db. (pure noise) to +6 db.

$x = s_1^2/2$. This should give rise to a broad but low hump of probability in this vicinity. Thus we can say in a general way that signal (whether it be wanted or not) in just one channel will multiply with the noise in the other channel to give a diffuse output in the vicinity of $s_1^2/2$.

For intermediate values of s_1^2 (say ± 3 db.) a direct computation is practical if tabulated values of $K_r(x)$ are available in the orders 0 to 10 and in the range 0 to 5 such as in Watson (1952). If only the orders 0 and 1 were available, it would still be possible to use recursion properties akin to Lommel polynomials. We have used a desk calculator to compute points at $x = 0.2, 0.5, 1, 2, 3, 4, 5$ on the curves for $s_1^2 = \frac{1}{2}$, 1, 2, and 4, corresponding to signal to noise ratios of -3 db, 0 db, $+3$ db, and $+6$ db. respectively, which are plotted in Fig. 2.

Each curve has a single maximum whose value decreases as s_1 increases. The location of the maximum also moves to the right and shows signs of agreement with $s_1^2/2$. Since every curve has unit area beneath it, it is obvious that they must become progressively broader. It is also fairly safe to say each falls off essentially as e^{-x} for large values. The onset of exponential decay is delayed by the presence of $+s_1\sqrt{2x}$ in the exponential or its equivalent. An estimate of the mean and variance of some of the computed curves was made by an analogue method described in Appendix II. These results are contained in Table II.

VI. GENERAL CASE

The general case of arbitrary signal plus noise in each channel requires more effort. Here we are faced with

$$\phi(s)ds = xdx\, e^{-s_1^2-s_2^2} \int_{-\infty}^{\infty} \exp(-x\cosh 2\theta)\, I_0(\sqrt{2x}\, s_1 e^{\theta})\, I_0(\sqrt{2x}\, s_2 e^{-\theta}) d\theta$$

wherein we have used several earlier definitions. The definite integral is shown in Appendix I to be expressible in terms of modified Bessel functions of the second kind and another set of functions which do not appear to be widely available. The final expression for the distribution is

$$xdx\, e^{-s_1^2-s_2^2}\left[K_0(x)W_0(s_1s_2x)+\sum_{r=1}^{\infty} 2\cosh r\beta\, K_r(x)W_r(s_1s_2x)\right]$$

where

$$2\cosh r\beta = (s_1/s_2)^r+(s_2/s_1)^r.$$

Some of the properties of the $W_r(x)$ functions are given in Appendix I, including a table of values sufficient for a survey of the problem. However, it may be appropriate to point out here that although both $K_r(x)$ and $W_r(x)$ are rapidly varying functions, the products $K_r(x)W_r(\alpha x)$ are quite well behaved, and with the exception of the zeroth order, all are finite at the origin. These products are very convenient quantities to plot for the purpose of clearing out computational mistakes, and may also be useful for interpolation of $W_r(\alpha x)$ where $K_r(x)$ is available. To compute the probability distribution it is necessary to sum quantities proportional to $xK_r(x)W_r(\alpha x)$. Curves for $\alpha = \frac{1}{2}$, 1, and 2 are given in Figs. 3, 4, and 5 respectively. It appears that these quantities each have a single maximum and for a given α, they decrease monotonically with increasing order r.

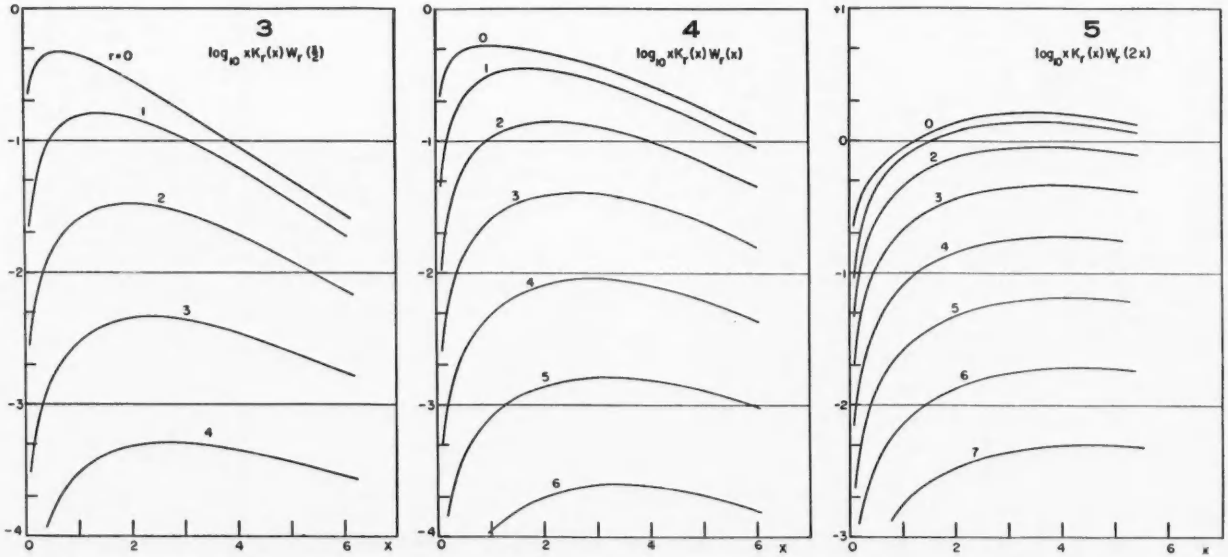

FIG. 3. The functions $\log_{10} xK_r(x)W_r(\frac{1}{2}x)$ used in computing distributions for which $s_1s_2 = \frac{1}{2}$. The case of $s_1 = s_2$ corresponding to -3 db. in both channels may be found by summing, provided double weight is given each curve of order r greater than zero.

FIG. 4. The functions $\log_{10} xK_r(x)W_r(x)$ used in computing distributions for which $s_1s_2 = 1$. The special case of unity (0 db.) signal to noise ratios in both channels may be found by summing as for Fig. 3.

FIG. 5. The functions $\log_{10} xK_r(x)W_r(2x)$ used in computing distributions for which $s_1s_2 = 2$. The case of $s_1 = s_2$, corresponding to $+3$ db. in both channels, may be found by summing as for Fig. 3.

Returning to the expression for probability density it is evident that there is complete symmetry in s_1 and s_2, the signal to noise ratios of the individual channels. Furthermore if we set $s_1 s_2 = s^2$, and $s_1/s_2 = e^{\beta}$ as before, then $\exp(-s_1^2 - s_2^2)$ may be written as $\exp(-2s^2 \cosh \beta)$ and will have a maximum at $\beta = 0$. There will be a coincident minimum for every $2 \cosh r\beta$, and we might hope that, in this region, the complete expression will be varying quite slowly with β.

This is in fact the case, as was discovered accidentally, and it is very useful since it extends the usefulness of the $s_1 = s_2$ case. There is considerable simplification (at least for manual computation) when $\beta = 0$, for then every $\cosh r\beta$ goes to unity and we are left with

$$\left[xK_0(x)W_0(s^2x) + 2\sum_1^{\infty} xK_r(x)W_r(s^2x) \right] e^{-2s^2}.$$

Summing the curves of Figs. 3, 4, and 5 (with the appropriate numerical factors) we obtain the corresponding distributions for equal signal to noise ratios in both channels. These curves, which are for -3 db., 0 db., and $+3$ db. respectively, are plotted in Fig. 6 along with the noise–noise case for comparison. As indicated above, each curve, except the noise–noise one, is valid in a symmetrical range of about ± 3 db.

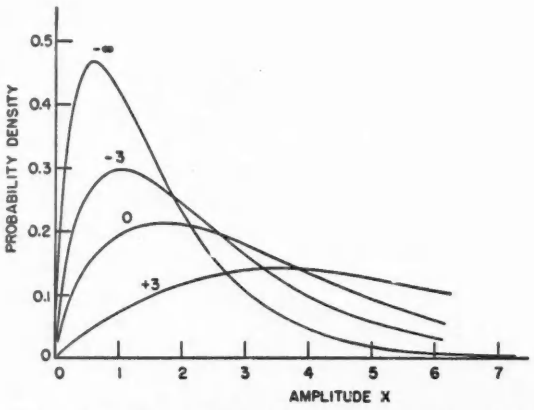

FIG. 6. The product distributions obtained with equal signal to noise ratio in both channels. The four curves are for s_1 or s_2 values ranging from $-\infty$ db. (pure noise) to $+3$ db.

The present curves may also be compared with those of the previous section. They are similar in that the maximum value decreases and shifts to the right. Here however the peak tends to occur at $2s_1s_2$ for values of s_1 and s_2 not less than unity. This location agrees with that obtained in the next section. Estimates of the mean and variance of the -3 db. and 0 db. curves are given in Table II.

VII. VERY LARGE (INDEPENDENT) SIGNALS

Using the asymptotic form for the large signal case, the product distribution may be expressed as

$$\frac{dx}{2\pi}\sqrt{\frac{x}{2s_1s_2}}\,e^{-s_1^2-s_2^2}\int_{-\infty}^{\infty}\exp[-x\cosh 2\theta+2\sqrt{2s_1s_2x}\cosh(\theta+\beta)]d\theta.$$

Without attempting to find the definite integral it can be seen in a general way that we are dealing with a situation that can be described in terms of the noise–noise case with the addition of $\exp[2\sqrt{2s_1s_2x}\cosh(\theta+\beta)]$ as a weighting factor. One might guess that the net result would be a Gaussian-like hump in the region of $x = 2s_1s_2$.

In the limit of infinite signal to noise ratio or zero noise, the product distribution is simply an impulse located at $s = A_1A_2$, which agrees with physical intuition. We may infer that with small amounts of noise present, the otherwise sharp spike of probability will be defocused or smeared into a Gaussian-like hump in the same location and having a width determined by the product of the r.m.s. values of the noises.

Usually the practical limitations of either a piece of graph paper or the dynamic range of an amplifier force us to match our field of view to the significant region of the distribution. When this is recognized it is easy to see how the curves, which in Figs. 2 and 7 show every indication of getting broader and

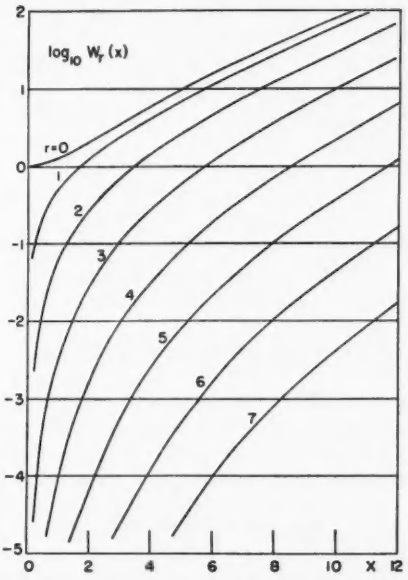

FIG. 7. The function $W_r(x)$ as defined in Appendix I. The curves are intended to show only the general features of the family for orders r of 0 to 7 and in the range $x = 0$ to 12. Semilog coordinates have been used to accommodate the wide range of values involved.

lower, in fact become narrower and taller when we renormalize with respect to the most probable output instead of $\sigma_1\sigma_2$.

VIII. RESUME

We have thus completed our exploration of the first quadrant in the s_1, s_2 plane. At and near the origin the distribution rises very rapidly, then falls exponentially. As we move out from the origin the initial rise is less rapid. There is an axis of symmetry along $s_1 = s_2$ and the distribution changes very slowly across this axis. At points far removed from the origin the distribution takes on some of the appearances of a "delayed" Gaussian hump and finally becomes an impulse function at the point at infinity.

REFERENCES

HUNTINGTON, E. V. 1939. Ann. Math. Statistics, **10**: 195.
JAHNKE, E. and EMDE, F. 1945. Tables of functions. 4th ed. Dover Publications, New York. p. 236.
WATSON, G. N. 1952. Theory of Bessel functions. 2nd ed. Cambridge University Press, London. p. 737.

APPENDIX I

The definite integral which occurs in Section IV is repeated here with $s_1 = a$ and $s_2 = b$:

$$\int_{-\infty}^{\infty} \exp(-x\cosh\theta)\, I_0(\sqrt{2x}\, ae^{\theta})\, I_0(\sqrt{2x}\, be^{-\theta})d\theta.$$

A solution may be obtained by expressing the Bessel functions as series, multiplying term by term, and regrouping as:

$$\sum_{n=0}^{\infty} \frac{(\frac{1}{2}abx)^{2n}}{n^4!} + \sum_{n=0}^{\infty} \frac{(\frac{1}{2}abx)^{2n+1}}{n!^2(n+1)!^2} 2\cosh(2\theta+\beta) + \sum_{n=0}^{\infty} \frac{(\frac{1}{2}abx)^{2n+2}}{n!^2(n+2)!^2} 2\cosh 2(2\theta+\beta) + \ldots$$

where $e^{\beta} = a/b$. Using this expression and interchanging the order of integration and summation, we obtain a series of terms that are the products of infinite sums and known definite integrals of the form

$$\int_{-\infty}^{\infty} \exp(-x\cosh 2\theta)\cosh r(2\theta+\beta)\, d(2\theta).$$

The integrals may be readily reduced to $2\cosh(r\beta)K_r(x)$ where $K_r(x)$ represents modified Bessel functions of the second kind and order r. This formula holds for all integral r except $r = 0$ where the factor 2 is missing.

The infinite sums have the general form

$$W_r(abx) = \sum_{n=0}^{\infty} \frac{(\frac{1}{2}abx)^{2n+r}}{n!^2(n+r)!^2}$$

and may be compared with the series for modified Bessel functions of the first kind,

$$I_r(abx) = \sum_{n=0}^{\infty} \frac{(\frac{1}{2}abx)^{2n+r}}{n!(n+r)!},$$

TABLE I

VALUES OF $W_r(x) = \sum_{n=0}^{\infty} \frac{(\frac{1}{2}x)^{2n+r}}{n!^2\,(n+r)!^2}$ AS COMPUTED FROM THE SERIES

The device 2.503 −3 has been employed to denote 2.503×10^{-3} or 0.002503

x	$W_0(x)$	$W_1(x)$	$W_2(x)$	$W_3(x)$	$W_4(x)$	$W_5(x)$	$W_6(x)$	$W_7(x)$
0.2	1.0100	0.10025	2.503 −3	2.779 −5	1.737 −7	6.946 −10	1.929 −12	3.938 −15
0.4	1.0401	0.2020	1.004 −2	2.220 −4	2.782 −6	2.220 −8	1.235 −10	5.04 −13
1.0	1.2539	0.5314	6.42 −2	3.529 −3	1.096 −4	2.185 −6	3.029 −8	3.07 −10
2.0	2.0633	1.2570	2.782 −1	2.955 −2	1.806 −3	7.138 −5	1.969 −6	4.00 −8
4.0	6.054	4.227	1.463	2.800 −1	3.236 −2	2.474 −3	1.342 −4	5.35 −6
6.0	15.64	11.55	4.828	1.211	1.945 −1	2.129 −2	1.677 −3	9.87 −5
8.0	36.35	27.93	12.98	3.855	7.51 −1	1.055 −1	1.065 −2	8.15 −4
10.0	78.3	61.9	31.17	10.39	2.37	3.879 −1	4.702 −2	4.37 −3
12.0	159.4	127.6	68.7	24.5	6.36	1.186	1.658 −1	1.79 −2
16.0	584	482	280	115	34.8	7.81	1.344	1.83 −1
20.0	1849	1571	966	436	146.5	37.9	7.63	1.22
24.0	5361		2983	1436	528	151	34.3	6.25

in which the factorials appear to the first power only. It is quite evident that the present sums must converge. In fact the whole family of functions, which might be defined by raising the factorials to progressively higher powers, would all converge with increasing rapidity. No application is envisioned for these higher members at the present. For the sake of simplicity of notation we represented the present sums by $W_r(x)$, although $I_r^{(2)}(x)$ might be more logical. The solution obtained for the original integral is

$$K_0(x)W_0(abx)+2\sum_1^\infty K_r(x)W_r(abx)\cosh(r\beta)$$

in which the hyperbolic cosines may also be written as

$$2\cosh(r\beta) = (a/b)^r+(b/a)^r.$$

In order to compute values for the complete expression it is of course necessary to compute and tabulate sufficient W_r functions. This has been done for orders $r = 0$ through 7 and over the range of the variable $x = 0.2$ to 24, and Table I is the result. It will be noted that a wide range of values is covered even on a logarithmic scale. The curves in Fig. 7 show the general features of these functions.

The $W_r(x)$ functions may be considered as solutions to differential equations. When treated as such it was determined that they obey a recurrence formula

$$W_{r-1}(x)-W_{r+1}(x) = 2r\frac{d}{dx}W_r(x).$$

It was also found that the differential equation is fourth order and of the form

$$W_r''''+\frac{6}{x}W_r'''-\frac{2r^2-7}{x^2}W_r''-\frac{2r^2-1}{x^3}W_r'+\frac{r^4-4x^2}{x^4}W_r = 0,$$

which differs from any we have seen to date. This has been taken as an indication that the $W_r(x)$ function may not have been previously tabulated.

APPENDIX II. MEAN AND VARIANCE BY TEMPLATE METHOD

The mean may be found from the center of gravity of a template containing as much as practical of the area under the probability density curve. Likewise the variance may be found from the moment of inertia about a vertical axis through the mean. The various distributions were carefully cut from a sheet of brass and the center of gravity found by balancing on a knife edge. After the mean was established, each shape was suspended by a fine steel wire to form a torsion pendulum. The square of the period of oscillation provides a measure of the moment of inertia. A rectangular test piece whose rotational inertia could be easily computed was used to calibrate the system. Normal precautions were observed to maintain equal areas under each curve and first-order corrections for thickness variations were made.

It was convenient to employ a scale of ordinates expanded by a factor of 10. This of course did not alter the mean, but did multiply the measured variance by 10. Even with this expansion it was impractical to include as much of the highly skew right-hand tail as might be desirable. It is almost certain that the

estimated values of mean and variance are low and the variance error may be quite large. Only those cases where the curves could be reasonably extrapolated beyond the computed points are included in Table II. It is interesting to note that for signal to noise ratios less than unity there are roughly linear relations between the mean, the variance, and the signal to noise power ratio. The rates of increase of mean and variance in the case of equal ratios in both channels are about twice the corresponding rates for signal in one channel only.

TABLE II

ESTIMATED VALUES OF MEAN AND VARIANCE OBTAINED FROM CENTER OF GRAVITY AND MOMENT OF INERTIA MEASUREMENTS

Signal/noise ratio (db.)		Mean	Variance
Channel 1	Channel 2	$M\{x\}$	$\sigma^2\{x\}$
$-\infty$	$-\infty$	1.57	1.52
$-\infty$	$-\infty$	1.571*	1.533*
$-\infty$	−3	1.95	2.24
$-\infty$	0	2.36	3.12
$-\infty$	+3	2.90	3.91
−3	−3	2.37	2.84
0	0	3.12	4.08

*Computed values.

CORRELATION TENSORS IN STATISTICAL HYDRODYNAMICS IN POROUS MEDIA[1]

By A. E. Scheidegger

ABSTRACT

The author's statistical theory of flow through porous media, based upon an extremely simple model in which pressure fluctuations are being neglected, has been criticized because velocity correlation tensors had not been introduced as dynamical variables. It is shown in the present paper that the introduction of such variables is not useful in the author's theory. This is due to the particularly simple nature of the model employed and does not imply that the use of correlation tensors may not lead to something useful in other conceivable statistical theories.

1. INTRODUCTION

Statistical methods have proved to be very successful in the mathematical description of various flow phenomena, such as in the theory of isotropic turbulence and in the theory of flow through porous media. As these statistical methods are somewhat analogous in the two cases, it is of interest to investigate whether the methods successful in the one, i.e., in the treatment of turbulence, could not be applied in the other, i.e., in the theory of flow through porous media. Thus, the occurrence of dispersion in laminar flow through porous media has been interpreted by Yuhara (1954) as analogous to velocity fluctuation during eddy motion in turbulent flow of bulk masses of fluid.

The only statistical theory of flow through porous media existing to date is that proposed by the author (Scheidegger 1954, 1955), which is based upon an extremely simple model. It has been criticized (Lighthill 1955) for not using velocity correlation tensors as variables. To introduce velocity correlation tensors amounts, in physical terms, to comparing the author's theory with the theory of turbulence since such tensors are of fundamental importance there. It is thus of interest to investigate the possible use of introducing velocity correlation tensors into the author's simple statistical theory.

The statistical theory of isotropic turbulence has been recently reviewed in a monograph by Batchelor (1953). In this theory, the turbulent motion is treated as an actual statistical process with the instantaneous velocity at any one point being a possible dynamical variable.

The writer's simple statistical theory of flow through porous media has been recently reviewed in a monograph (Scheidegger 1956). In this theory, the fundamental problem is to determine the equations of motion for the probability density of the position of all the particles (i.e., geometrical points) of the fluid as a function of time. Pressure fluctuations are neglected. The notion of "probability" is understood with respect to a fictitious ensemble

[1]Manuscript received January 16, 1956.
Contribution No. 24, Vol. 1, from the Dominion Observatory, Ottawa.
Published by permission of the Acting Deputy Minister, Department of Mines and Technical Surveys, Ottawa.
Paper presented orally at the 1956 meeting of the American Geophysical Union, in Washington, D. C.

of porous media consisting of a great number of similar pieces with identical macroscopic properties and dimensions.

If one considers a particle and its probable flow path (in the ensemble), the fundamental probability distribution function v has been assumed as Gaussian

$$v(\mathbf{x}, t) = (4\pi Dt)^{-3/2}\exp\{-(\mathbf{x}-\langle\mathbf{x}\rangle_{Av})^2/(4Dt)\} \tag{1.1}$$

where $\mathbf{x}$ is the position co-ordinate of the particle, t is the time, $\langle\mathbf{x}\rangle_{Av}$ is the vector of the average position (over the ensemble) of the fluid particle, and D is a measure of dispersion.

The assumption of a Gaussian probability distribution is an outcome of the central limit theorem of probability calculus if one reasons that the likelihood of deviation of a particle from the mean displacement vector during a time step τ is the same in every direction (isotropic porous media).

It will be shown in the present paper that the velocity correlation tensor, a significant dynamical variable in turbulence, is unsuitable as such a variable in the statistical hydrodynamics in porous media, if the simplest such theory is used. If pressure fluctuations are neglected, the correlation tensor depends only in a trivial way on the pressure term. It does depend, however, on the geometry of the porous medium and is thus suitable to characterize the latter rather than the flow through the same medium. It thus appears that the analogy between turbulent flow and the author's particular model of flow through porous media is not very complete, in spite of the fact that the contrary has been claimed. This, however, does not imply that the use of velocity correlation tensors may not lead to something useful in other conceivable statistical theories.

2. KINEMATICS OF VELOCITY CORRELATION

In analogy with the statistical theory of turbulence, we shall consider the local (pore) velocity $\mathbf{v}$ as fundamental dynamical variable. From this, the displacement $\mathbf{x}$ of each particle can later be calculated. The values of the components of $\mathbf{v}$ (i.e. v_i) are, then, within the ensemble, random functions of the position $\mathbf{x}$. However, in contrast with the theory of turbulence, it should be noted that in any one particular realization of the fluid motion through a porous medium, $\mathbf{v}(\mathbf{x})$ is a function which is zero in most places—i.e. wherever one is outside the pore space of that particular medium.

It is a well-known premise of probability theory that a random function, such as $\mathbf{v}(\mathbf{x})$, is determined statistically by the complete system of joint-probability distributions of the function of any n values of the argument, where n may take any integral value.

The simplest velocity correlation is obtained by choosing n equal to 1. One then has the average local velocity $\langle\mathbf{v}(\mathbf{x})\rangle_{Av}$ which is equal to the filter velocity $\mathbf{q}$. The filter velocity $\mathbf{q}$ (obtained in this manner) is that quantity which is the subject of most investigations on the flow through porous media (e.g. Darcy's law refers to it). If one is, essentially, interested in deviations from Darcy's law, it is often useful to make a transformation of variables to a (steadily) moving system where the average of $\mathbf{v}$ at any point is identically zero.

The next step is to consider two-point correlations. This leads one to the commonly considered "correlation tensor" defined as follows:

$$R_{ik}(\mathbf{r}) = \langle v_i(\mathbf{x})\, v_k(\mathbf{x}+\mathbf{r})\rangle_{\text{Av}}. \tag{2.1}$$

If we assume that the porous medium and the pressure drop across it are homogeneous, then the tensor R_{ik} is indeed independent of the choice of $\mathbf{x}$.

The kinematics pertaining to the tensor R_{ik} defined above is identical to the kinematics of the analogous tensor in the theory of homogeneous turbulence (cf. Batchelor 1953). Considering steady-state flow, one may always consider $\mathbf{v}$ as the deviation from the mean velocity vector instead of as total velocity, as outlined earlier.

The kinematics of the tensor R_{ik}, thus, may be taken over verbatim from the statistical theory of turbulence. We thus introduce the spectrum tensor by the following relation:

$$R_{ij}(\mathbf{r}) = \int \phi_{ij}(\boldsymbol{\kappa}) \exp(i\boldsymbol{\kappa}\mathbf{r})d\boldsymbol{\kappa} \tag{2.2}$$

where ϕ_{ij} is a complex hermitean tensor. The inverse relationship is

$$\phi_{ij}(\boldsymbol{\kappa}) = \frac{1}{8\pi^3}\int R_{ij}(\mathbf{r}) \exp(-i\boldsymbol{\kappa}\mathbf{r})d\mathbf{r}. \tag{2.3}$$

When $|r| = 0$, the first of these equations becomes

$$R_{ij}(0) = \langle v_i(\mathbf{x})\, v_j(\mathbf{x})\rangle_{\text{Av}} = \int \phi_{ij}(\boldsymbol{\kappa})d\boldsymbol{\kappa} \tag{2.4}$$

showing that $\phi(\boldsymbol{\kappa})$ represents a density of contributions to $\langle v_i(\mathbf{x})v_j(\mathbf{x})\rangle_{\text{Av}}$ in $\boldsymbol{\kappa}$-space. A knowledge of all components of the tensor $R_{ij}(0)$ is necessary and sufficient to determine the energy (per unit volume) associated with an arbitrary component of the velocity, and it is therefore called the energy tensor. Accordingly, $\phi_{ij}(\boldsymbol{\kappa})$ is the energy-spectrum tensor.

3. DYNAMICS OF LAMINAR FLOW

In order to investigate the properties of the velocity correlation tensor in the author's simple theory of flow through porous media, it is necessary to introduce the appropriate dynamical laws.

Thus, let us consider viscous, laminar flow. Assuming narrow channels, the law of viscous flow (corresponding to the Hagen–Poiseuille equation) can be written as follows:

$$v_i = -\frac{b_{ik}}{\mu}\frac{\partial p}{\partial x_k} \tag{3.1}$$

expressing the fact that, in narrow channels, the flow is proportional to the driving force. Pressure fluctuations will be neglected.

The formulas of Section 2 refer to a system where the mean velocity is zero. Assuming a homogeneous velocity gradient, the mean velocity is expressed as follows:

$$q_i = \langle v_i\rangle_{\text{Av}} = -\frac{1}{\mu}\frac{\partial p}{\partial x_k}\langle b_{ik}\rangle_{\text{Av}} = -\frac{1}{\mu}k_{ik}\frac{\partial p}{\partial x_k} \tag{3.2}$$

where q_i are the components of the "filter-velocity" and

$$k_{ik} = \langle b_{ik} \rangle_{Av} \tag{3.3}$$

is called "permeability-tensor". The latter is a function of the porous medium only, obtained by forming the required averages.

Thus, the velocity of interest is

$$v_i = v_{i\,\text{actual}} - \langle v_i \rangle_{Av} = -\frac{1}{\mu} \frac{\partial p}{\partial x_k} (b_{ik} - \langle b_{ik} \rangle_{Av}). \tag{3.4}$$

Forming now the correlation tensor, we get

$$\begin{aligned} R_{ik}(\mathbf{r}) = \frac{1}{\mu^2} \frac{\partial p}{\partial x_l} \frac{\partial p}{\partial x_m} \langle & b_{il}(\mathbf{x}) b_{km}(\mathbf{x}+\mathbf{r}) - b_{il}(\mathbf{x}) \langle b_{km}(\mathbf{x}+\mathbf{r}) \rangle_{Av} \\ & - b_{km}(\mathbf{x}+\mathbf{r}) \langle b_{il}(\mathbf{x}) \rangle_{Av} + \langle b_{il}(\mathbf{x}) \rangle_{Av} \langle b_{km}(\mathbf{x}+\mathbf{r}) \rangle_{Av} \rangle_{Av}. \end{aligned} \tag{3.5}$$

If we assume that the porous medium is homogeneous, this formula can be simplified to yield

$$R_{ik}(\mathbf{r}) = \frac{1}{\mu^2} \frac{\partial p}{\partial x_l} \frac{\partial p}{\partial x_m} \{ \langle b_{il}(\mathbf{x}) b_{km}(\mathbf{x}+\mathbf{r}) \rangle_{Av} - \langle b_{il} \rangle_{Av} \langle b_{km} \rangle_{Av} \}. \tag{3.6}$$

For abbreviation we set

$$\begin{aligned} b_{iklm} &= \langle b_{il}(\mathbf{x}) b_{km}(\mathbf{x}+\mathbf{r}) \rangle_{Av} - \langle b_{il} \rangle_{Av} \langle b_{km} \rangle_{Av} \\ &= \langle b_{il}(\mathbf{x}) b_{km}(\mathbf{x}+\mathbf{r}) \rangle_{Av} - k_{il} k_{km}. \end{aligned} \tag{3.7}$$

As is easily seen, the tensor b_{iklm} is a tensor which depends on the porous medium only. It is obtained by forming the required averages. From the definition of R_{ik} it is obvious that b_{iklm} must be symmetrical in the indices l and m. Furthermore,

$$b_{iklm}(r) = b_{kilm}(-r), \tag{3.8}$$

as the same property holds for R_{ik}.

The Fourier transform (spectrum function) of R_{ik} turns out to be given by the following expression

$$\begin{aligned} \phi_{ik}(\boldsymbol{\kappa}) &= \frac{1}{8\pi^3} \int R_{ik}(\mathbf{r}) \exp(-i\boldsymbol{\kappa}\mathbf{r}) d\mathbf{r} \\ &= \frac{1}{\mu^2} \frac{\partial p}{\partial x_l} \frac{\partial p}{\partial x_m} \beta_{iklm}(\boldsymbol{\kappa}) \end{aligned} \tag{3.9}$$

with

$$\beta_{iklm}(\boldsymbol{\kappa}) = \frac{1}{8\pi^3} \int b_{iklm}(\mathbf{r}) \exp(-i\boldsymbol{\kappa}\mathbf{r}) d\mathbf{r} \tag{3.10}$$

where ϕ_{ik} (and thus β_{iklm} in the indices i and k) is a tensor with hermitean symmetry.

The inverse formulas are

$$R_{ik} = \int \phi_{ik}(\boldsymbol{\kappa}) \exp(i\boldsymbol{\kappa}\mathbf{r}) d\boldsymbol{\kappa}, \tag{3.11}$$

$$b_{iklm} = \int \beta_{iklm}(\boldsymbol{\kappa}) \exp(i\boldsymbol{\kappa}\mathbf{r}) d\boldsymbol{\kappa}. \tag{3.12}$$

For $r = 0$ this becomes

$$R_{ik}(0) = \langle v_i(\mathbf{x})v_k(\mathbf{x})\rangle_{\text{Av}} = \int \phi_{ik}(\boldsymbol{\kappa})d\boldsymbol{\kappa} \tag{3.13}$$

showing that ϕ_{ik} is a density of energy. This energy density is, according to the earlier formula (3.9), given as follows:

$$\phi_{ik} = \frac{1}{\mu^2}\beta_{iklm}\frac{\partial p}{\partial x_l}\frac{\partial p}{\partial x_m} \tag{3.14}$$

where β is a function of the porous medium only. The dispersive energy content (i.e. the energy content other than that owing to average motion) of a fluid-filled volume of porous medium depends, thus, on the one hand on the pressure gradient in a very special, almost trivial, way, and, on the other hand, on a tensor determined by the porous medium only.

In the case of isotropic porous media, it is known that the permeability must be expressible as a scalar

$$k_{il} = \delta_{il}k. \tag{3.15}$$

In isotropic porous media, the actual velocity, in terms of the pressure gradient, is expressible as follows:

$$v_i = -\frac{B}{\mu}\frac{\partial p}{\partial x_l}n_l n_i \tag{3.16}$$

where $\mathbf{n}$ denotes a unit vector in the direction of instantaneous flow channels as prescribed by the porous medium. As has been shown in previous publications, the filter velocity is

$$\langle \mathbf{v}_{\text{actual}}\rangle_{\text{Av}} = \mathbf{q} = -\frac{k}{\mu}\operatorname{grad} p \tag{3.17}$$

where k can duly be expressed in averaged terms of the porous medium:

$$k\delta_{il} = \langle Bn_l n_i\rangle_{\text{Av}}. \tag{3.18}$$

Thus:

$$\begin{aligned} v_i = v_{i\text{act}} - q_i &= -\frac{B}{\mu}\frac{\partial p}{\partial x_l}n_l n_i + \frac{k}{\mu}\frac{\partial p}{\partial x_i} \\ &= -\frac{1}{\mu}\frac{\partial p}{\partial x_l}\{Bn_l n_i - k\delta_{il}\}. \end{aligned} \tag{3.19}$$

Thus, we can at last calculate the correlation tensor R_{ik} which yields

$$R_{ik} = \frac{1}{\mu^2}\frac{\partial p}{\partial x_l}\frac{\partial p}{\partial x_m}\langle[B_z n_i(\mathbf{x})n_l(\mathbf{x}) - k\delta_{il}][B_{z+r}n_k(\mathbf{x}+\mathbf{r})n_m(\mathbf{x}+\mathbf{r}) - k\delta_{km}]\rangle_{\text{Av}} \tag{3.20}$$

and therefore

$$\begin{aligned} b_{iklm} &= \langle B_z B_{z+r}n_i(\mathbf{x})n_l(\mathbf{x})n_k(\mathbf{x}+\mathbf{r})n_m(\mathbf{x}+\mathbf{r})\rangle_{\text{Av}} - \langle Bn_i n_l\rangle_{\text{Av}}k\delta_{km} \\ &\quad - k\delta_{il}\langle Bn_k n_m\rangle_{\text{Av}} + k^2\delta_{il}\delta_{km} \\ &= \langle B_z B_{z+r}n_i(\mathbf{x})n_l(\mathbf{x})n_k(\mathbf{x}+\mathbf{r})n_m(\mathbf{x}+\mathbf{r})\rangle_{\text{Av}} - k^2\delta_{il}\delta_{km} \end{aligned} \tag{3.21}$$

which shows that the velocity correlation in laminar flow through porous media depends, in the present simple theory, only in a trivial way on the dynamical variables (viz. the pressure). The main dependence of this tensor is on the geometry of the porous medium. Owing to the assumed homogeneity of the porous medium, b_{iklm} will not depend on the particular choice of $\mathbf{x}$.

In a similar fashion, one can calculate the spectrum function. Equation (2.3) gives an expression of ϕ_{ik} in terms of a tensor β_{iklm} which, in the case of isotropic, homogeneous porous media sustaining laminar viscous flow, turns out to be expressible as follows:

$$\beta_{iklm} = \frac{1}{8\pi^3}\int \{\langle B_x B_{x+r} n_i(\mathbf{x}) n_l(\mathbf{x}) n_k(\mathbf{x}+\mathbf{r}) n_m(\mathbf{x}+\mathbf{r})\rangle_{\mathrm{Av}} - k^2\delta_{il}\delta_{km}\} \times \exp(-i\boldsymbol{\kappa}\mathbf{r})d\mathbf{r}. \tag{3.22}$$

It therefore turns out that the velocity correlation tensor in laminar flow through porous media, as well as the corresponding spectrum function, depends only in a trivial way on the dynamical variables (viz. the pressure gradient). The main dependence of these tensors is on the geometry of the porous medium. Thus, the velocity correlation tensor, e.g., for a given pressure drop, is defined by a geometrical tensor with four indices describing the statistical configuration of the porous medium. Choosing a particular such tensor, therefore, does not impose any restrictions on the treatment of the dynamics of the problem, but only on the geometry of the porous medium under consideration.

4. CONCLUSION

Porous media are of an extremely complex nature. In order to describe a porous medium completely, it would be necessary to give the "equation" of the internal surface which is bounding the pore space. Needless to say, such an undertaking would be beyond human capacity.

In view of the complex nature of porous media, it must be expected that the flow through them is also of an extremely complex nature. In order to obtain a suitable description thereof, it is therefore necessary to use models. Many kinds of models have been proposed by many authors, most of them based upon the replacement of a porous medium by bundles of capillaries. Whereas these models have been more or less useful to explain the permeability of a porous medium, they have never been able to explain the experimentally observed *dispersion* of a fluid in passing through a porous medium.

The writer, therefore, proposed that statistical mechanics should be applied to the flow through porous media and investigated an extremely simple model along these lines: the fundamental dynamical variable was the displacement undergone by a fluid particle in a finite time interval; pressure fluctuations were neglected. In spite of the obvious limitations and shortcomings of the author's model, it *does* yield the result that dispersion must occur in fluids passing through porous media and, furthermore, indications are that this dispersion is described correctly (Day 1956). It appears therefore worth while to investigate further the implications and possible extensions of the author's

model. With regard to this, the result of the present study is that a superficial analogy between that model and turbulent flow of bulk masses of fluids does, in fact, not hold.

In conclusion, the writer wishes to thank Dr. L. Massé of the Magnolia Petroleum Company in Dallas, Texas, and Dr. G. M. Volkoff of the University of British Columbia in Vancouver, B.C., for stimulating discussions about the subject matter of this paper. Their kind criticisms and comments proved to be invaluable.

REFERENCES

BATCHELOR, G. K. 1953. The theory of homogeneous turbulence. Cambridge University Press, London.

DAY, P. R. 1956. Trans. Am. Geophys. Union. In press. (Paper presented in December at the 1955 West Coast meeting of the A.G.U.)

LIGHTHILL, M. J. 1955. Math. Revs. **16**: 190.

SCHEIDEGGER, A. E. 1954. J. Appl. Phys. **25**: 994.

——— 1955. Geofis. pura e appl. **30**: 17.

——— 1956. The physics of flow through porous media. University of Toronto Press, Toronto.

YUHARA, K. 1954. Geophysics (Kyoto Univ.), **9**: 127.

SOME RESULTS OF THE HIGH DISPERSION ELECTRONIC EMISSION SPECTRUM OF FORMALDEHYDE[1]

By G. Wilse Robinson

ABSTRACT

It has been possible to obtain the emission spectrum in the near ultraviolet region of formaldehyde in a discharge tube at sufficiently high resolution and purity so that the rotational structure can be studied. Some preliminary results of the analysis are discussed, especially with regard to the vibrational assignment of the emission and absorption systems and to the nature of the upper electronic state. An examination of the data rather strongly indicates a non-planar equilibrium configuration in the excited electronic state. Some of the previous interpretations are shown to be in disagreement with the experimental findings. A long path length absorption study of the gas revealed a number of new bands, some of which may belong to a second electronic transition.

1. INTRODUCTION

In formaldehyde vapor an absorption system extends from λ3700 to lower wave lengths (Henri and Schou 1928; Dieke and Kistiakowsky 1934; Dyne 1952), and an emission system lies on the long wave length side of λ3400 (Herzberg and Franz 1932; Gradstein 1933). These systems have been studied at relatively low dispersion by Brand (1950, 1951), and recent papers by Walsh (1953) and Cohen and Reid (1956) have presented proposed analyses of the vibrational structure of the bands.

An understanding of the rotational and vibrational intricacies of these systems has presented some rather difficult problems. Inadequate resolution in absorption of the rotational structure in the neighborhood of the band origins, where the effect of asymmetry is greatest, has prevented a really complete rotational analysis, although some of the pertinent properties of the transition have been obtained in spite of this. Before the present work the emission spectrum had never been produced at a sufficient intensity to be photographed at high resolution. The many difficulties met in obtaining a satisfactory vibrational analysis of the systems are rather unexpected in view of the simplicity of the molecule and the amount of information known about the ground and excited states.

Besides the interesting vibrational problem, another incentive for further

[1]Manuscript received March 21, 1956.

Contribution from the Department of Chemistry, The Johns Hopkins University, Baltimore, Maryland, U.S.A. This work was supported in part by the Office of Ordnance Research, U.S. Army, under Project No. TB2-0001 of Contract No. DA-36-034-ORD-2169.

Note.—In this paper we shall follow the recommendations of the recent report on the notation for spectra of polyatomic molecules (J. Chem. Phys. 1955. **23**: 1997). This unfortunately introduces yet another set of labels for the normal antisymmetric modes in formaldehyde. The various notations to date are as follows:

	Out-of-plane bend	Species	In-plane bend	Species	CH stretch	Species
(*a*)	ν_6	b_2	ν_5	b_1	ν_4	b_1
(*b*)	ν_6	b_1	ν_5	b_2	ν_4	b_2
(*c*)	ν_5	b_2	ν_6	b_1	ν_4	b_1
(*d*)	ν_6	b_1	ν_5	b_2	ν_3	b_2

(*a*) Herzberg; Ebers and Nielsen; Brand. (*b*) Mulliken; Walsh; McMurry. (*c*) Cohen and Reid. (*d*) Recommended.

extensive work on formaldehyde is the fact that the triplet state has often been mentioned as a possible upper state of the molecule (Walsh 1953). It is hoped that some evidence can be found for or against the singlet–triplet hypothesis in this particular instance and thus shed some light on the more general problem of singlet–triplet transitions in polyatomic molecules. Moreover, a complete analysis of the spectrum would be of interest as a check on the existing qualitative predictions of orbital theories (Mulliken 1935; McMurry 1941) and also as a guide to the interpretation of similar transitions in more complex aldehydes and ketones which are of special interest to the chemist.

It is our present feeling that a more complete rotational study of the absorption and emission systems in formaldehyde is necessary in order to solve many of the above problems, as well as to afford a new line of attack upon the vibrational assignment through a study of the rotational constants of the various combining levels. The present paper deals with some of the preliminary results of this work, in particular with respect to the high-resolution emission spectrum of the molecule.

2. NATURE OF THE TRANSITION

The long-wave system in formaldehyde, as well as that in the higher aldehydes and ketones, is generally accepted as being due to an electron jump from a non-bonding orbital localized on the oxygen atom to an anti-bonding π^* orbital lying out of the molecular plane and localized in the C–O group (Mulliken 1935). The validity of this interpretation is evidenced by the rather large increase in C–O internuclear distance in the upper state as well as by the sharp drop in the C–O stretching frequency ν_2' to about two-thirds the normal state value. In formaldehyde, if a planar configuration is assumed, the wave function which describes this upper electronic state transforms as species A_2 under the operations of point group C_{2v}, causing the transition to be symmetry forbidden, but gaining intensity through mixing with a neighboring B_2 state. Correspondingly, there should be an absence of $a_1 \leftrightarrow a_1$ vibrational bands. The $^1A_2$ assignment for the absorption bands of Dieke and Kistiakowsky (1934) (hereafter referred to as the *DK*-bands) is also indicated by the fact that they are of type-*B* and that the observed *f*-value is far smaller than that calculated for a symmetry allowed transition (McMurry 1941), yet larger than that usually expected for a multiplicity forbidden one (Cohen and Reid 1956). That the stronger emission bands are also of type-*B* has been definitely established by the high-resolution work presented here.

The emission system includes the α-band at λ3700 which also occurs weakly in absorption. Brand (1950) has shown quite conclusively that the lower state of the α-band (α''), as well as the lower states of most other emission bands, is perturbed by a coriolis perturbation of the type observed by Ebers and Nielsen (1937) in the infrared spectrum of formaldehyde. In particular, he showed that his conclusions were in accord with the theory that α'' is a state in which a single quantum of the out-of-plane bending mode ν_4 is excited. This conclusion was more firmly established by the work of Dyne (1952), who

made a partial rotational analysis of the α-band in absorption. Dyne showed that even K'' subbands were strong, which is just the reverse of that found in the DK-bands. Since, in absorption, the alternation of intensities depends only upon the symmetry properties of the lower state, this then is sufficient proof that an electronic ground state vibration antisymmetric with respect to the operation C_2 is the lower level of the transition. Cohen and Reid (1956) were able to show that the temperature coefficient of the α-band is consistent with a lower level having a Boltzmann factor roughly equivalent to a 1200 cm^{-1} frequency. From the above evidence in conjunction with the *known direction of the coriolis perturbation* and the infrared assignments, it can be concluded unambiguously that the mode in question is $\nu_4 = 1167$ cm^{-1} of species b_1. Thus, to explain the type-B structure, an upper level of total vibronic symmetry A_2 must be invoked. The argument concerning the direction of the coriolis perturbation is a strong one which was apparently overlooked by Cohen and Reid (1956) in their recently proposed analysis. In our opinion, this serves as sufficient reason for invalidating many of their conclusions. Their analysis also requires a revision of the infrared assignments in such a way that the 1280 cm^{-1} frequency would correspond to the out-of-plane bending mode. Such a modification seems not too reasonable in view of the character of the infrared bands in the region of their origins (Ebers and Nielsen 1937) and the fact that the product and sum rules do not fit as well under this assumption (Ebers and Nielsen 1938; Davidson *et al.* 1954; Robinson unpublished). The rotational analysis of the α-band in emission (Robinson and Benedict 1956) has given further positive evidence that the total vibronic symmetry of its upper state is A_2.

The difficulty in correlating the absorption and emission systems arises because the upper level of the α-band (α') lies only 125 cm^{-1} lower than the upper level (A') of the longest wave length DK-band, the A-band. The origins of the two bands lie respectively at 27021 cm^{-1} (Robinson and Benedict 1956) and 28313 cm^{-1} (Dieke and Kistiakowsky 1934). Because of the rather small probability that 125 cm^{-1} represents an upper state fundamental, there is apparently no way of connecting the two systems. For this reason it has often been suggested that at least two upper electronic states are involved. However, it is not difficult to find a number of arguments against this possibility.

The fact that the rotational constant $\frac{1}{2}(b'+c')$ is 1.067 cm^{-1} for both α' and A' seems rather good evidence that the upper electronic states are identical and for that matter involve the same number of quanta of ν_2'. Dyne (1952) in agreement with our results reported $\frac{1}{2}(b'+c')$ for α' to be 1.065 cm^{-1} and also used this fact as indication of a common upper electronic state. The preliminary results obtained by us from the high-resolution emission spectrum yield the following rotational constants for α': $a' = 8.950$ cm^{-1}; $b' = 1.1270$ cm^{-1}; $c' = 1.0070$ cm^{-1}. The constants for A' are given by Dieke and Kistiakowsky (1934) to be: $a' = 8.749$ cm^{-1}; $b' = 1.132$ cm^{-1}; $c' = 1.002$ cm^{-1}. The a-constants are significantly different, after taking into account the rather small experimental errors, but the over-all similarity of the other constants strongly indicates that A' and α' belong to the same electronic state. Further evidence

for a common upper electronic state lies in the fact that the C–O stretching frequency is about the same in the two series of bands.

Though it is not entirely possible to rule out the existence of two upper electronic states on the basis of rotational constants alone, an important consequence of the above comparison of the a constants is that any previous interpretation based upon the assumption that A' and α' are identical vibronic levels (Walsh 1953; Cohen and Reid 1956) can now be definitely discarded. Furthermore, since our measurements show the exact origin of the α-band to be 15 cm^{-1} lower than the previously reported value, the $A-\alpha$ separation becomes 1292 cm^{-1} rather than 1277 cm^{-1}. The temptation to attach significance to the near coincidence of this quantity with the ν_6'' in-plane bending frequency (1279 cm^{-1}) is greatly lessened. Another point to be considered is that all prominent DK-bands can be explained on the basis of combinations of $A+824$ cm^{-1}, $A+1321$ cm^{-1}, and $A+\sim 2850$ cm^{-1} with various quanta of ν_2', and this scheme can be followed far into the ultraviolet to the strongly predissociated bands near λ2600. Thus any attempt to divide the DK-bands into a high and a low wave length region of absorption (Walsh 1953) seems unnecessary. The final argument against the two-state hypothesis arises because of an inability to reasonably interpret *any* part of the DK-system as transitions to a second electronic level. The α-series seems to have a much higher transition probability than the A-series either intrinsically or because of the Franck–Condon effect. Thus transitions in absorption from the vibrationless ground state to B_2 vibronic levels of any proposed "α electronic state" should then be by far the most intense absorption bands observed. The fact is, however, that the strongest DK-bands are the very ones which are difficult to fit into the α scheme.

3. EXPERIMENTAL

In a previous paper (Robinson 1954*b*) a technique was described for producing high-intensity, impurity-free emission spectra of polyatomic molecules in a gas discharge tube, and the technique was applied successfully to a number of simple aldehydes and ketones at relatively low dispersion (Robinson 1954*a*, *b*). Extremely sharp vibrational structure was obtained in some instances, suggesting that the method also might be useful for the study of the rotational fine structure in the emission bands of the more simple polyatomic molecules.

Accordingly, we have been able to obtain a number of excellent high-resolution plates of the formaldehyde emission bands in the region λ3400–4400 (Figs. 1 and 2). The resolution in the neighborhood of the band origins was sufficiently great to permit an analysis of the rotational structure of the subbands with $K'' \leqslant 2$ as well as those of greater K''. The low K subbands are described in terms of asymmetric rotor energy levels (King *et al.* 1943; Turner *et al.* 1953; Erlandsson 1955). The complete results of the rotational analysis will be published in another journal (Robinson and Benedict 1956).

The spectrum was photographed in the second order of a 21-ft., 30,000 line-per-inch grating in a Paschen–Runge mounting providing a plate factor of approximately 0.625 Å/mm. The exposures on Eastman 103a-O plates were

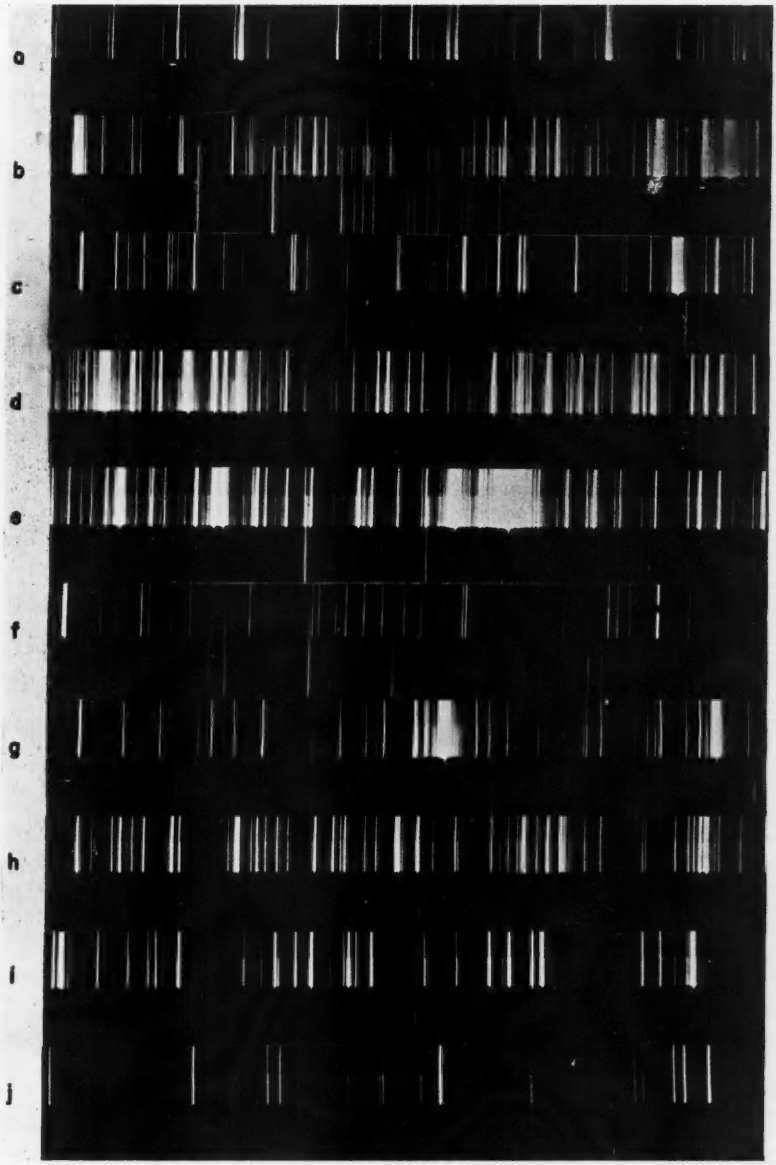

FIG. 1. The emission bands of formaldehyde from λ3400 to λ4347. The frequencies of the heads are given in Table I.

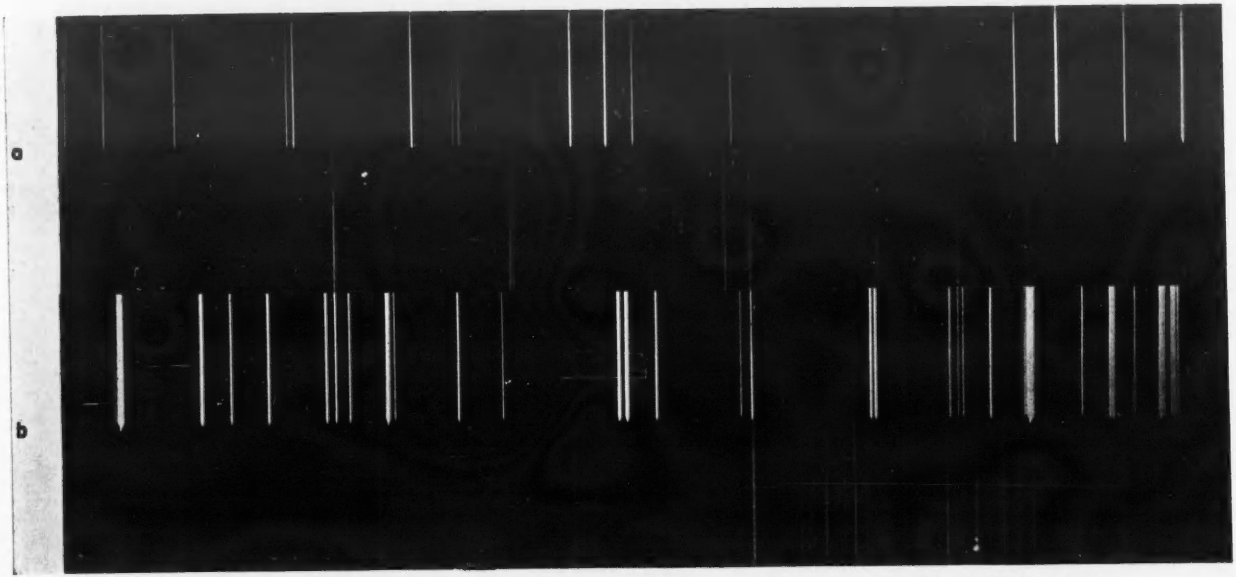

FIG. 2. Details of the rotational structure in emission of (*a*) the band at λ3544 and (*b*) the band at λ3698 (α-band).

from 8 to 24 hr. The comparison spectrum was obtained from an iron hollow-cathode discharge tube filled with neon at a few millimeters pressure (Crosswhite *et al.* 1955). The wave lengths of the iron lines were obtained from the recently published tabulation of vacuum-arc values (Russell and Moore 1944), and the correction to vacuum was made with the help of Edlén's (1953) dispersion formula.

4. RESULTS

Figs. 1 and 2 show photographs of the high-resolution emission spectrum of formaldehyde, and the positions of the ${}^rR$ heads of the observed bands are given in Table I. The measurements are to the nearest tenth of an Angstrom unit except in those cases where there is a great deal of overlapping. While more accurate measurements, of course, are possible, they are meaningless since the position of the heads relative to the origin depends upon the rotational constants of the combining states. Also, it is apparent from the high dispersion work that the actual ΔE of the subbands may differ from the ΔE of the ${}^rR$ heads by as much as a wave number, especially for higher K'' subbands where the heads are less distinct and shifted due to missing $J < K$ lines. In spite of this, the ΔE of the ${}^rR$ heads, accurate to within a wave number, becomes an approximate measure of the coriolis perturbation on the K-structure in the

TABLE I

THE STRONG EMISSION BANDS OF FORMALDEHYDE

Band[a]	$K''=0$			$K''=2$		$K''=4$		$K''=6$		$K''=8$	Assignment		
	λ_{air}[b]	ν_{vac}[c]	$\Delta\nu$	ν_{vac}	$\Delta\nu$	ν_{vac}	$\Delta\nu$	ν_{vac}	$\Delta\nu$	ν_{vac}	n_2''	n_4''	n_2'
a	3404.6	29364 *29359*[d]	36	29400 *29398*	40	29440 *29439*	40	29480 *29478*			0	1	2
b	3543.9	28210 *28207*	37	28247 *28244*	40	28287 *28285*	41	28328 *28324*	39	28367 *28362*	0	1	1
c	3697.7	27036 *27036*	37	27073 *27073*	40	27113 *27114*	42	27155 *27155*	40	27195 *27194*	0	1	0
d	3776.6	26471 *26470*	35	26506	35	26541	34	26575			1	1	1
e	3860.6	25895	41	25936	54	25990	65	26055			0	3	1
f	3951.9	25297 *25297*	35	25332 *25333*	36	25368 *25369*	35	25403 *25403*	30	25433	1	1	0
g	4043.8	24722 *24721*	42	24764	54	24818	65	24883			0	3	0
h	4135.8	24172	38	24210	49	24259	55	24314			1	3	1
i	4239.7	23580 *23579*	33	23613 *23612*	30	23643 *23642*	28	23671 *23670*			2	1	0
	4346.9	22999 *22997*	39	23038	49	23087	55	23142			1	3	0

[a]The labels correspond to Fig. 1.
[b]Angstrom units.
[c]Wave numbers.
[d]Brand's (1950, 1951) measurements in italics.

ground vibrational levels, and thus acts as a good check on any proposed vibrational assignment. The excited state vibrational levels which are involved in emission are not expected to be perturbed because they are overtones of ν_2', all having vibrational symmetry a_1. According to Jahn (1939), their K-structure will be perturbed only by vibrations of species a_2, of which there are, in the low quantum levels, at least, rather few in number by virtue of the fact that they arise only in $b_1 \times b_2$ combinations. Furthermore, perturbations in the J-structure are not expected unless ΔE of the vibrational levels is of the same order of magnitude as the rotational constant $(b'+c')$. It is rather significant that the DK-bands are also void of these perturbations which probably indicates a relatively large difference in frequency of the ν_4' and ν_6' fundamentals in the upper state.*

Table I lists Brand's (1951) low-dispersion subband measurements for comparison purposes. One of the previous objections to Brand's partial interpretation of the vibrational structure rested on the fact that at the dispersion of a medium spectrograph only very rough measurements of the subband heads were possible, and an analysis based on such measurements could be viewed at most as a suggestion. As evidenced from Table I, however, Brand's measurements are, in fact, quite good, and much of his interpretation seems reasonable even in the light of the present high-dispersion work.

In Table II are listed some of the weaker bands in the emission system. There is a great deal of overlapping by strong bands, and for this reason precise measurements were somewhat difficult to make. The bands which involve lower state vibronic levels of species A_1 or A_2 have odd K'' strong and even K'' weak. The $K'' = 0$ heads are more difficult to measure in these cases. Three of these bands were observed by Brand (1951), but the agreement between his results and ours is within only about 10 cm^{-1}. One very interesting point here is that some bands having the same upper vibronic states as certain of the

TABLE II

SOME WEAK EMISSION BANDS OF FORMALDEHYDE

Band[a]	$K''=0$		$K''=2$		$K''=4$					
	λ_{air}[c]	ν_{vac}[d]	$\Delta\nu$	ν_{vac}	$\Delta\nu$	ν_{vac}	n_2''	n_4''	n_2'	n_a'[e]
	3619.0	27624	35	27659	40	27699	1	1	1	0

Band[a]	$K''=0$		$K''=1$		$K''=3$		$K''=5$		$K''=7$					
	λ_{air}	ν_{vac}	$\Delta\nu$	ν_{vac}	$\Delta\nu$	ν_{vac}	$\Delta\nu$	ν_{vac}	$\Delta\nu$	ν_{vac}	n_2''	n_6''	n_2'	n_a'[e]
c'	3679.8	27181	20	27201	40	27241	49	27290	49	27339	0	2	1	1
b'	4120.8	24260	24	24284	41	24325	41	24366			1	2	0	1
e'	3845.1	26000	20	26020	41	26061	48	26109	51	26160	0	2	0	1
A[b]	3529	28328	—	—	—	28371	22	28393	18	28411	0	0	0	1

[a]Labels where present refer to weak bands of Fig. 1.
[b]Quoted from Dieke and Kistiakowsky (1934).
[c]Angstrom units.
[d]Wave numbers.
[e]Upper level of A-band.

*There are possible slight coriolis perturbations in the λ3430 and λ3295 bands.

A-series seem definitely to be involved in emission but with very much lower intensities. The A-band itself is overlapped by the band at 28210 cm^{-1}, and no trace of it appeared even on the strongly exposed photographs. Possible explanations of the very low intensity of the A-series in emission are that the transition probability for predissociation from these levels may be non-zero, or that a considerable Franck–Condon weakening of the A-band results. The possible presence of the latter effect may be evidenced by the rather large difference in the rotational constants a' and a'' of the combining levels of the A-band.

It is fairly easy to obtain a vibrational scheme which explains all of the emission bands. Such an analysis, indicated briefly in Tables I and II, is essentially equivalent to that proposed by Brand (1951). It has been chosen so as to be completely consistent with respect to the K-splitting in the ground state. The fact that the K-splitting is so nicely correlated in this scheme is really quite strong evidence in its favor. It was pointed out earlier that, except for the exact labelling of the upper state normal modes, an equally simple and reasonable analysis can also be made of all the prominent absorption bands from the A-band far down into the ultraviolet. Here, the trends of the rotational constants for the upper levels are a good check on the proposed analysis.

The important facts may now be summarized as follows:

(*a*) Because of symmetry requirements A' must have vibronic symmetry B_2, while α' must have vibronic symmetry A_2.

(*b*) The origin of the A-band lies 1292 cm^{-1} above the origin of the α-band.

(*c*) The lower state of the A-band is the vibrationless ground state, while that of the α-band is a vibrational level in the ground state where one quantum of the out-of-plane bending mode ν_4'' has been excited.

(*d*) Since $\nu_4'' = 1167$ cm^{-1}, A' lies 125 cm^{-1} higher than α'.

(*e*) The α-series occurs strongly in emission, while the A-series occurs only with extremely low intensity in emission.

(*f*) In absorption the intensity of the α-band is lower than that of the A-band because of a Boltzmann factor corresponding to 1167 cm^{-1}. At 400° K. the calculated factor is about 1/70, while the observed factor is roughly 1/20, indicating a probable Franck–Condon enhancement of the α-band.

(*g*) Up to the present, no pertinent absorption bands to the red of the α-band have been found.

Because of (*g*) it has always been assumed that α' is the vibrationless upper electronic state of the molecule. If this is true, then it seems to be required by (*d*) that $\nu_4' = 125$ cm^{-1} assuming a single upper electronic state. The objections to this interpretation are fairly obvious and have been pointed out by several authors (Walsh 1953; Dyne 1952). On the other hand, if α' were not the vibrationless upper state, then new bands, possibly weakened by a large Franck–Condon effect, should occur in absorption somewhere to the red of 28188 cm^{-1} ($A - 125$ cm^{-1}). As a check on this possibility, a 6-ft., 60-mm. diameter absorp-

tion cell was constructed which was suitable for multiple passing. The cell could be heated to avoid polymerization of the formaldehyde. A side tube containing pure formaldehyde polymer was heated independently of the cell and acted as a reservoir for the gas. Six passes through the cell were easily obtained with a White (1942) arrangement, and the spectrum was photographed in the second order of a 15-ft., 15,000-line-per-inch grating in an Eagle mounting. A number of new bands were found, the stronger of which appeared to be double-headed. The double-headed bands were independently discovered by Reid (unpublished) and were interpreted by him to be parallel bands, but a comparison with known parallel bands at shorter wavelengths (Dieke and Kistiakowsky unpublished) showed little resemblance. The approximate positions of these bands as well as the weak perpendicular bands are listed in Table III. All the perpendicular bands arise from excited vibra-

TABLE III

SOME WEAK BANDS FOUND IN THE LONG-PATH-LENGTH ABSORPTION SPECTRUM OF FORMALDEHYDE

λ_{air}[a]	ν_{vac}[b]	Type	Observed in emission?	n_2''	n_1''	n_2'	n_a'[d]	$n_a'+824$
3600	27770	⊥	No	1	0	1	1	0
3616	27650	?	No	–	–	–	–	–
3648	27410	⊥	No	1	0	0	1	1
3680	27181	⊥	Yes	0	2	1	1	0
3760	26590	⊥	No	1	0	0	1	0
3786	26400	?	No	–	–	–	–	–
3845	26000	⊥	Yes	0	2	0	1	0
3878	25780	?	No	–	–	–	–	–
3952	25297	⊥	Yes	1	1	0	0	0
3961	25240	?	No	–	–	–	–	–
A[c]	28328	⊥	No	0	0	0	1	0

[a]Angstrom units.
[b]Wave numbers.
[c]Quoted from Dieke and Kistiakowsky (1934).
[d]Upper level of A-band.

tional levels. They can be fitted readily into the vibrational schemes of the α-series and the A-series, and it can be seen that many of them occur also in emission. It is apparent that the presence of the double-headed bands raises more problems than it solves, since none of the anomalous-appearing ones can be fit into the α- or A-schemes. As a matter of fact, most of the difference frequencies between these bands seem to have nothing in common with the known ground or excited state fundamentals. It must be concluded until further evidence is available that the double-headed bands belong to a different electronic transition from that of the α- and A-bands, possibly singlet–triplet.

The important consequence of the long path length work, then, is that no evidence has been found which contradicts the earlier belief that α' is the vibrationless excited state of the molecule. Because of the presence of the unexplained bands, however, such a possibility can not be definitely excluded.

5. CONCLUSIONS

We feel that the number of plausible solutions to the vibrational problem has been considerably reduced. An assignment based on two upper electronic states may be still tempting to some but, if true, would be somewhat surprising

in view of the facts presented here. If the double-headed bands could in some way be fit into the vibrational scheme or if reasons could be found to explain the absence of otherwise allowed low-lying vibronic transitions, this would mean that α' is not the lowest vibrational level in the upper state and that the entire α-series is in combination with at least one quantum of another upper state vibration. While this description originally was also a very tempting one, it must be discarded for the lack of supporting experimental evidence.

The possibility of an interaction between potential surfaces in the upper states should not be overlooked in polyatomic spectra. The effect may be quite common because of the added degrees of freedom and the less restrictive symmetry selection rules governing such perturbations. These perturbations on the vibrational structure should occur at the same energy for isotopic substituted molecules, except that the region of crossing may be rather extensive in polyatomic molecules. In formaldehyde, A' may correspond to a part of the potential surface in which the H–C–H angle is quite wide, while α' seems characterized by a smaller angle. The two levels then may lie on somewhat different parts of the potential surface and may be affected differently by perturbations of the above type. The fact that the same type of vibrational anomaly occurs in CD_2O (Brand 1951) at a lower energy point on the potential surface weakens the hypothesis in this case, however.

A complication of a different type would arise if the upper electronic state were non-planar (Walsh 1953). According to the analysis of the vibrational structure, a number of quanta of the out-of-plane bending mode are excited. Brand's (1951) vibrational proposal of the emission spectrum of CH_2O and CD_2O also required this interpretation. The intensity of these transitions in the harmonic oscillator approximation depends, among other things, upon the magnitude of the integral

$$\int \psi_m' Q_4 \psi_n'' dQ_4,$$

where ψ_m' and ψ_n'' are vibrational eigenfunctions for the ν_4 modes in the upper and lower electronic states respectively, and Q_4 is the normal coordinate for such a vibration. For ψ_m' and ψ_n' orthogonal, the selection rule is $m = n \pm 1$. Large deviations from this rule can be caused by differences in geometry in upper and lower states, differences in the force constants, and, to a relatively less extent, anharmonicity effects.

If the first effect were operative, it would mean in this instance that the molecule has a non-planar equilibrium configuration in the upper state. The aplanarity could, depending upon the height of the potential barrier, cause an inversion doubling in the vibrational levels of the excited state, each alternate level being symmetric or antisymmetric with respect to a reflection in the (now absent) molecular plane. Only alternate levels would be seen in either the A- or the α-series. Such an interpretation implies then that A' and α' are two members of the lowest lying doublet with splitting 125 cm^{-1}. The relatively large splitting indicates a low barrier and the difference in rotational constants in the two levels does not seem unreasonable (Benedict, private discussion).

Qualitative theoretical arguments can sometimes be used to predict the

directional properties of bonds in polyatomic molecules. In this instance the approximate sp^2 hybridized carbon orbitals in the ground state are modified in the excited state by the addition of the antibonding π^* electron to the C–O double bond. Roughly speaking, this modification would result in the cancellation of the bonding effects of one of the bonding π electrons. The C–O bond would then be essentially a three-electron bond, and the carbon orbitals would have to be described approximately by a hybridization scheme somewhere between the tetrahedral sp^3 and the trigonal sp^2 forms. On the basis of these simplified arguments the non-planar structure would be predicted for formaldehyde in its upper electronic state.

Probably the most striking piece of evidence in favor of the non-planar equilibrium configuration results from a closer examination of the rotational constants of α'. For a planar rigid molecule the inertial defect,

$$\Delta = I_C - I_A - I_B,$$

is zero, while for a non-rigid molecule with a planar equilibrium configuration, Δ is expected to be small and positive because of zero-point vibrations. Formaldehyde in its ground electronic state exhibits an inertial defect equal to +0.057 A.U. (Lawrance and Strandberg 1951), but the inertial defect computed for α' from the rotational constants is −0.101 A.U., which clearly indicates the non-planar character of the upper state. A similar comparison of the inertial defect in the A' level can not be made since the only available rotational constants are those derived on the assumption that $\Delta = 0$ (Dieke and Kistiakowsky 1934).*

The strong probability of a non-planar equilibrium configuration of the molecule in the upper state raises two rather interesting questions. Why doesn't the observed alternation of intensities of the K-structure in emission (Brand 1950; Robinson and Benedict 1956) definitely exclude the non-planar model, and then, how well does one expect the C_{2v} electronic selection rules to hold?

Note added in proof.—While this manuscript was in press a paper by Brand (J. Chem. Soc. 858. 1956) appeared which treats similar topics as discussed here. The slight disagreement in experimental results can be attributed to the low resolution and non-linear dispersion of Brand's instrument. Although we failed to mention it in our paper, we found no evidence for a double α-band as first proposed by Dyne (1952) and discussed in Brand's paper. We also found no evidence for the presence of Brand's a_0, but low dispersion plates may be more suitable for picking out such weak bands among the strong ones. His explanation of b_0 is rather curious, and he gives, it seems to us, no really satisfactory reason why emission bands from the upper state of b_0 are absent, since these, according to the selection rules, should be rather intense. The identification of his 1^+ level then becomes questionable. The apparent non-existence of the 1^+ level has been a problem which has puzzled us for a long time, and at present we can offer no substitute for Brand's proposal. Brand's discussion of the rotational constants, of course, can not be taken as any evidence for the non-planar upper state. Excellent values of the constants must be known for this purpose, and the only unambiguous treatment is that involving the determination of the inertial defect. Brand's asymmetry parameter δ was evidently that given very approximately by Dieke and Kistiakowsky for the 1^-, not the 0^-, band. Furthermore, it must be remembered that the rotational constants reported by Dieke and Kistiakowsky were derived on the hypothesis of rigid planar combining states to begin with. Recently we have been able to assign all the prominent rotational lines of the A-band and have deduced the rotational constants for A' to be: $a' = 8.767$ cm^{-1}; $b' = 1.1223$ cm^{-1}; $c' = 1.0117$ cm^{-1}; $\Delta = -0.280$ A.U.; $\delta = 0.01426$. In all other respects we seem to be in rather close agreement with Brand, although it does not seem to us that the deviation from electronic C_{2v} symmetry is as large as Brand indicates.

If rotational equilibrium has been reached, the alternation of intensities depends only upon the symmetry properties of the initial state (the upper state in the case of emission). The high-dispersion photographs show a surprisingly normal but "alternated" rotational distribution corresponding to a temperature of about 100° C. Certain intensity anomalies are expected and are observed but for the most part the system seems to be very close to rotational (but not vibrational) equilibrium. Since the nuclear wave functions are important only in the small region of space about the nucleus, symmetry properties imposed by their transformation properties under exchange of the nuclei in a rigid molecule must be quite sensitive to small deviations from planarity. However if the non-planar molecule is not rigid but is vibrating through the potential barrier, for inversion the symmetry properties for the planar model must apply. The two members of the inversion doublet will show opposite symmetry character with respect to an exchange of the nuclei, and therefore their rotational levels will possess opposed statistical weight. For the limiting case of the rigid molecule, the doublet splitting goes to zero, and the alternation of intensities in each member of the doublet will cancel that of the other. The second question concerning the transformation properties of the upper electronic state wave functions also arises in the interpretation of the spectra of the higher aldehydes and ketones where neither upper nor lower state possesses strict C_{2v} symmetry. It is generally felt that, since the transition is localized in the C–O bond, the molecular orbitals involved in the transition will be influenced only slightly by asymmetries introduced in a different part of the molecule and the C_{2v} approximation should be a good one. The experimental evidence certainly seems to uphold the argument in the case of formaldehyde. In such molecules as benzaldehyde, however, where large interactions with the rest of the molecule are present, this approximation may not be valid.

In closing we should like to express our gratitude to Professor G. H. Dieke and Dr. H. M. Crosswhite of the Johns Hopkins Physics Department for the use of the spectrographs and for the many helpful discussions throughout the course of the work. We are especially grateful to Dr. W. S. Benedict for pointing out the importance of the negative inertial defect in the upper electronic state, and for many other very helpful discussions.

REFERENCES

BENEDICT, W. S. Private discussion.
BRAND, J. C. D. 1950. Trans. Faraday Soc. **46**: 805.
——— 1951. J. Chem. Phys. **19**: 377.
COHEN, A. D. and REID, C. 1956. J. Chem. Phys. **24**: 85.
CROSSWHITE, H. M., DIEKE, G. H., and LEGAGNEUR, C. S. 1955. J. Opt. Soc. Amer. **45**: 270.
DAVIDSON, D. W., STOICHEFF, B. P., and BERNSTEIN, H. J. 1954. J. Chem. Phys. **22**: 289.
DIEKE, G. H. and KISTIAKOWSKY, G. B. 1934. Phys. Rev. **45**: 4.
——— Unpublished.
DYNE, P. J. 1952. J. Chem. Phys. **20**: 811.
EBERS, E. S. and NIELSEN, H. H. 1937. J. Chem. Phys. **5**: 822.
——— 1938. J. Chem. Phys. **6**: 311.
EDLÉN, B. 1953. J. Opt. Soc. Amer. **43**: 339.
ERLANDSSON, G. 1955. Arkiv Fysik, **10**: 65.
GRADSTEIN, S. 1933. Z. physik. Chem. B, **22**: 384.

HENRI, V. and SCHOU, S. A. 1928. Z. Physik, **49**: 774.
HERZBERG, G. and FRANZ, K. 1932. Z. Physik, **76**: 720.
JAHN, H. A. 1939. Phys. Rev. **56**: 680.
KING, G. W., HAINER, R. M., and CROSS, P. C. 1943. J. Chem. Phys. **11**: 27.
LAWRANCE, R. B. and STRANDBERG, M. W. P. 1951. Phys. Rev. **83**: 363.
MCMURRY, H. L. 1941. J. Chem. Phys. **9**: 231.
MULLIKEN, R. S. 1935. J. Chem. Phys. **3**: 564.
REID, C. Unpublished.
ROBINSON, G. W. 1954*a*. J. Chem. Phys. **22**: 1147.
——— 1954*b*. J. Chem. Phys. **22**: 1384.
——— Unpublished.
ROBINSON, G. W. and BENEDICT, W. S. 1956. J. Chem. Phys. In press.
RUSSELL, H. N. and MOORE, C. E. 1944. Trans. Am. Phil. Soc. **34**: 113.
TURNER, T. E., HICKS, B. L., and REITWIESNER, G. 1953. U.S. Ballistic Research Lab., Report No. 878.
WALSH, A. D. 1953. J. Chem. Soc. 2306.
WHITE, J. U. 1942. J. Opt. Soc. Amer. **32**: 285.

A DOUBLE MAGNETIC FIELD MODULATION PARAMAGNETIC RESONANCE SPECTROMETER[1]

By H. A. Buckmaster[2,3] and H. E. D. Scovil[4]

ABSTRACT

A high sensitivity, wide or narrow band, double magnetic field modulation type paramagnetic resonance spectrometer operating at a wavelength of 1.25 cm. for use at liquid helium temperatures (4°K.) is described. The spectrometer employs a transmission type, cylindrical resonant cavity excited in the H_{111} mode. The magnetic field is modulated simultaneously at 60 c.p.s. and 465 kc. A resonance from 10^{-11} mole of diphenyl trinitro phenyl hydrazyl has been observed with a signal-to-noise ratio of 2:1 at 290°K. in wide band operation (8 kc.) indicating that a sensitivity of $O(10^{-15})$ mole should be possible in narrow band operation (1 c.p.s.) at 4°K. because of its inherent high stability.

INTRODUCTION

The phenomenon of paramagnetic resonance absorption has been studied in great detail by numerous investigators during the past ten years. Comprehensive review articles of the field have been written by Bleaney and Stevens (1953) and by Bowers and Owen (1955). Recently, a book on magnetic resonance has been published by Ingram (1955). This literature summarizes the different types of paramagnetic resonance spectrometers that have been developed. Until recently, not one of these spectrometers has come within several orders of magnitude of achieving the theoretically predicted ultimate sensitivity with the possible exception of a narrow band paramagnetic gas resonance spectrometer described by Beringer and Castle (1950). At the same time as the spectrometer described in this paper was being developed, Feher at the Bell Telephone Laboratories developed a spectrometer possessing such sensitivity using the superheterodyne principle.

With such sensitivity, it should be possible to obtain the nuclear spins and nuclear moments of many radioactive isotopes of elements in the transition groups of the periodic table. The possession of high sensitivity in wide band operation may be of great value in the study of paramagnetic free radicals formed in chemical reactions. Higher order transitions (Bleaney 1951) in phenomena that have already been studied should be observable. This has been realized for gadolinium ethyl sulphate where $\Delta M = \pm 2$ and ± 3 transitions have been observed (Buckmaster 1956). Further work in this direction is in progress at this laboratory. Excited state, impurity center, and color center studies could also benefit from increased sensitivity.

In this paper we describe a 1.2 cm. paramagnetic resonance spectrometer employing a transmission type, cylindrical cavity excited in the H_{111} mode which operates at any temperature between 2°K. and 300°K. by the use of a suitable refrigerant. The magnetic field is modulated at 60 cycles and 462.5 kc.

[1]Manuscript received December 7, 1955.
Contribution from the Department of Physics, University of British Columbia, Vancouver, B.C.
[2]Holder of a Fellowship under the National Research Council of Canada (1954–55).
[3]Present address: Radio-Astronomy Group, Cavendish Laboratory, Cambridge, England.
[4]Present address: Bell Telephone Laboratories, Murray Hill, New Jersey, U.S.A.

If only the low frequency magnetic field modulation of amplitude greater than the line width is employed then it is a single magnetic field modulation or video spectrometer. The sensitivity in wide band operation is then increased by also modulating the magnetic field, to an amplitude less than or equal to the line width of the spectral line being investigated at a frequency where the contribution of the "flicker" or excess low frequency noise in the microwave crystal converter is negligible, thus greatly improving the over-all noise figure of the detection system. The output of the crystal converter is amplified at 462.5 kc., then the low frequency signal components are detected, amplified, and displayed on an oscilloscope whose time base is sinusoidally swept at 60 c.p.s. The r-f. magnetic field is introduced inside the microwave cavity at the crystal site by the following artifice. The cylindrical cavity is partially slotted in a plane through its axis (Fig. 1) and the r-f. modulation current

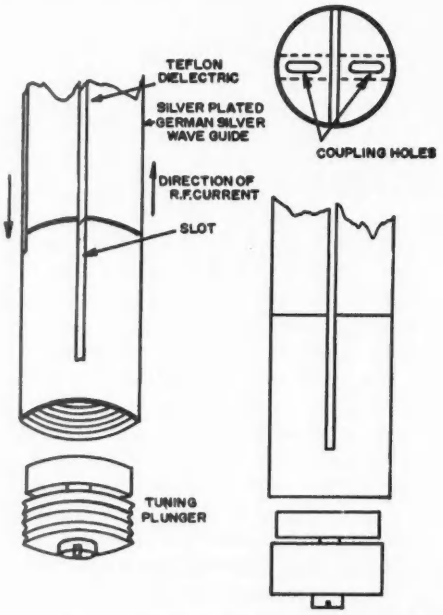

FIG. 1. Diagram showing slotted cylindrical microwave cavity excited in H_{111} mode.

flows around the slot. Only the current flowing on the interior surface of the cavity is effective in producing the r-f. magnetic field. In this manner, r-f. magnetic fields of up to 50 gauss peak-to-peak can be easily produced at the crystal site. Using this technique, signals have been observed from 10^{-9} gm. (10^{-11} mole) of diphenyl trinitro phenyl hydrazyl $(C_6H_5)_2.N\text{–}N.C_6H_2.(NO_2)_3$ with a signal-to-noise ratio of 2 to 1 in wide band (8 kc.) operation at 290°K.

SPECTROMETER DESIGN

In an ideal paramagnetic resonance spectrometer, it should be possible to use either wide or narrow band operation. Wide band operation is useful to gain the initial information required about the spectrum of a substance because of the speed of operation. Many measurements involving various orientations of both the crystal axes and the magnetic field are required. It is essential for any studies involving phenomena of a short lifetime. The higher sensitivity of narrow band operation is only required when information about the fine detail of a spectrum is required. Both modes of operation are possible with the spectrometer to be described.

The main problem to be considered in the design of any paramagnetic resonance spectrometer concerns the elimination of the noise in excess of the thermal and shot noise which is always generated in microwave crystal detectors at low frequencies (Torrey and Whitmer 1948). This "flicker" noise obeys an inverse frequency law. In the spectrometer to be described in this paper, the higher of the two frequencies used to modulate the magnetic field must satisfy two conditions. (1) The frequency must be as high as possible to minimize the "flicker" or excess noise in the crystal converter. This noise is negligible above 10 Mc. and probably above 1 Mc. (2) The frequency must be less than the full line width at half amplitude (Smaller 1951). For the study of most paramagnetic resonance phenomena such as in crystals, and free radicals, the line width is greater than 1 gauss which corresponds to 2.5 Mc. in units of frequency. A frequency of the order of one megacycle satisfies both of the above conditions. When the percentage modulation of the microwave power incident on a crystal converter is small, then the amplitude of the output voltage due to this modulation is proportional to the incident modulation power (the power absorbed by the paramagnetic resonance transition) and is independent of the law of the detector. A comparison of the root-mean-square noise in the same bandwidth at low and radio frequencies, assuming that the major noise component is due to the "flicker" effect, shows that an improvement of $O(10^3)$ in the sensitivity can be obtained when the modulation frequency of the magnetic field is increased from 60 c.p.s. to 500 kc. with a maximum improvement of $O(10^4)$ at 10 Mc.

At frequencies less than 10 Mc. the over-all noise figure of the detection system is usually determined by the noise figure of the crystal converter. In any case, the higher the magnetic field modulation frequency is, the less likely it is that "flicker" noise due to other components such as the klystron and the amplifier will increase the over-all noise figure of the system.

General Description

The spectrometer to be described is of the double magnetic field modulation type. The principle of its operation is not new. It has already been used in microwave gas spectroscopy (Hartz and van der Ziel 1950), and Smaller and Yasaitis (1953) have used it to improve the sensitivity of a paramagnetic resonance spectrometer operating in the frequency range 10–500 Mc. using modulation frequencies of 30 c.p.s. and 10 kc. In their spectrometer, the use

of two frequencies only decreases the noise due to electron tube flicker effect. This is the first time that this principle has been applied to a microwave paramagnetic resonance spectrometer. In this region, the improvement in the signal-to-noise ratio is large because of the elimination of the flicker noise in the crystal converter. This gives a measured improvement in the sensitivity of $O(10^3)$ over a video spectrometer with the same band width. Although the spectrometer described here operates at a wavelength of about 1.25 cm., the technique can, with little modification, be applied to other wavelengths in the microwave region. Since many of the substances of interest can only be studied at low temperatures (less than 90°K.), this spectrometer has been specifically designed for operation in this temperature region. This aspect of the design presents a number of technical complications. We will simplify the discussion by first describing a room temperature spectrometer and will consider the low temperature aspects later.

The essential requirements of any paramagnetic resonance spectrometer are to place a paramagnetic substance in a region where it can absorb microwave radiation, to apply a magnetic field, and to be able to detect any absorption of microwave power as a function of the magnetic field strength. A block diagram of the system to be described is shown in Fig. 2.

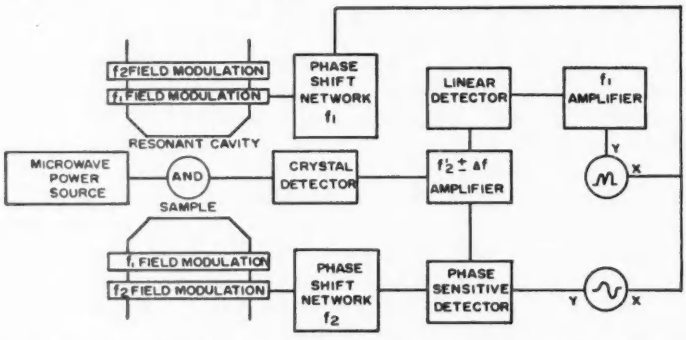

FIG. 2. Block diagram of double field modulation paramagnetic resonance spectrometer.

The system can be divided into three sections for the convenience of explanation: (1) the microwave components; (2) the detection, amplification, and the display units; (3) the magnetic field and magnetic field modulation apparatus.

The microwave frequency components are the same as those required for a video type spectrometer (Bleaney and Stevens 1953). Microwave power from a 2K33A reflex klystron is fed through a transmission type cavity, operated in the H_{111} mode and located in the gap of an electromagnet, to a 1N26 silicon diode crystal converter. On the klystron side of the cavity, provision is made to monitor the microwave power level, to measure the wavelength, and to control the power level.

A high gain amplifier, tuned to 462 kc., amplifies the video signal output of the crystal converter to a level where it can be linearly detected. For wide band operation, the output of either a linear detector or a phase sensitive detector, locked at 462 kc., with a short time constant, can be displayed on an oscilloscope. The former yields the modulus of the derivative of the line shape while the latter gives the derivative. The time-base voltage for the oscilloscope is obtained, via a phase shift network, from the 60 c.p.s. low frequency magnetic field modulation power source. For narrow band operation, the output of the phase sensitive detector, with a long time constant, is fed onto an automatic recorder. The low frequency magnetic field modulation is not required in narrow band operation; the magnetic field is swept slowly and linearly.

The microwave cavity is placed in the gap of an electromagnet whose field is continuously variable. Helmholtz coils, mounted on the poles of the magnet and fed with 60 c.p.s. current, supply the low frequency magnetic field modulation inside the cavity. It is a difficult problem to obtain a sufficient amplitude (20 gauss) of the high frequency magnetic field modulation. Three methods of overcoming this difficulty have been considered. It can be easily shown (Smythe 1950) that the fraction of an external magnetic field at 462 kc. applied perpendicular to the axis of a conducting cylinder that penetrates a practical 1.2 cm. cylindrical cavity is small ($<1\%$) and hence prohibitively large external fields would be required ($O(10^3)$ gauss). This method is further complicated by the presence of large quantities of iron near the cavity necessary to obtain the steady magnetic field. This method is thus not considered practical. Since it is difficult to introduce a coil into the interior of the microwave cavity particularly at 1.2 cm. without drastically affecting the Q of the cavity and the field configuration, this approach to the problem was not considered fruitful either. Fortunately, one other avenue of approach, which we have employed, is possible. If a cavity is partially slotted in a plane through the axis parallel to the planes in which the microwave current flows, then the Q of the cavity is only slightly affected provided that the width of the slot is small compared with the wavelength. If the high frequency magnetic field modulation current flows around the slot, as shown by the arrows in Fig. 1, an r-f. magnetic field will be produced in the interior of the cavity by the fraction of this current flowing on its interior surface. By such an artifice, the high frequency magnetic field modulation is introduced inside the resonant microwave cavity at the crystal site.

Description of Apparatus

1. Microwave Components

(*a*) *Microwave Power Source*

Since all the work has been done at about 1.25 cm., 2K33A klystrons have been used as the microwave power source. The power supply is of the standard regulated type. It has a stabilization factor of better than 10^3 and the ripple is less than one millivolt. It has been found necessary to shield the klystron

with a brass box from the large amount of 462 kc. radiation present. This radiation will cause frequency modulation of the klystron frequency which will result in excess noise appearing in the detector. All of the klystron power leads must be carefully decoupled at both 60 c.p.s. and 462 kc.

(*b*) *Waveguide Components*

Almost all of waveguide components used in this spectrometer are of standard design (Montgomery 1947) for *K* band operation and have been constructed in this laboratory.

The frequency of the klystron is measured using a commercial, transmission type, tuned cavity wavemeter with an accuracy of 0.01%. If greater accuracy in frequency measurement is desired, a microwave frequency standard is available with an accuracy of better than 0.0001%.

Since this spectrometer is designed for low temperature operation, German silver guide $\frac{1}{8}$ in. $\times \frac{1}{4}$ in. I.D. and 0.004 in. wall thick filled with Teflon ($\epsilon = 2.000$) is used to feed the microwave power in and out of the cavity. This reduces the thermal heat leak when the cavity is immersed in liquid helium. The rectangular shape is obtained by drawing 6 mm. diameter German silver tubing with a die. Tapered sections match the standard *K* band guide (0.420 in. $\times$0.170 in. I.D.) to the German silver guide. The outside of the German silver guide is silver plated to a thickness in excess of the skin depth of silver at 462 kc. In our apparatus, the thermal leak before silver plating was $O(1)$ milliwatt (0.10 cc./min.) and the r-f. heating was $O(10)$ watts (100 cc./min.) for a r-f. current of 25 amp. r.m.s. After plating to a thickness of about 0.0005 in., the thermal leak and the r-f. heating effect were both of the same order of magnitude ($O(10^{-1})$ watts (2 cc./min.)) thus minimizing the total heat input to the liquid helium bath. These estimates were based on measurements of the rate of evaporation of liquid helium. The large currents required for the highest sensitivity are only used for short intervals of time and hence the helium boiling rates are not as great as it would initially appear. Since the r-f. current is fed in and out of the cavity on the German silver guide, mica windows and lucite screws are used to insulate this part of the system from the remainder of the waveguide components.

(*c*) *Cavity*

The cavities used are of the cylindrical type and designed to operate in the H_{111} mode which gives a concentration of the microwave magnetic field at the ends of the cavity where the specimen can be conveniently located. Sufficient coupling is used between the cavity and the waveguide to permit the crystal diode to operate as a linear detector.

The cavity has a 1/32 in. slot cut in it as shown in Fig. 1. The presence of this slot has negligible effect on the *Q*. A measurement of the high frequency magnetic field modulation current required to give optimum signal-to-noise ratio shows that the slotted cavity is effectively 0.6 turn.

(*d*) *Crystal Detectors*

In order to assure optimum signal-to-noise ratio, specially selected low noise temperature, low conversion loss 1N26 silicon crystal diodes have been used.

(*e*) *Low Temperature Head*

The photograph in Fig. 4 shows the low temperature head with the dewars removed. The head is mounted on a railway track, permitting the entire unit to be easily moved in and out of the magnetic field. This is particularly advantageous when the cavity is surrounded by dewars filled with liquid

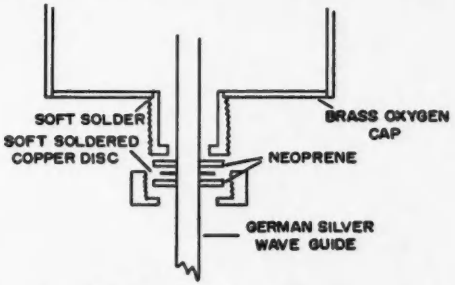

FIG. 3. Diagram of sandwich type, insulated, low temperature vacuum seal.

refrigerants for low temperature operation. Fig. 5 shows the head with the two dewars necessary for liquid helium temperature experiments in the gap of the electromagnet. Flexible waveguide enables the head to be moved without breaking the microwave connection to the detector or the klystron.

The helium dewar has an oxygen cap to reduce the heat leak. Of necessity, the waveguide must pass through the bottom of this cap to the cavity. Since the current for the high frequency magnetic field modulation flows around this part of the waveguide, an insulated vacuum seal which will work when immersed in liquid oxygen is required. Fig. 3 shows a satisfactory method of achieving this.

It is preferable to prevent the refrigerant from entering the cavity. Bubbles in the refrigerant will detune the cavity and cause a modulation of the microwave power level at the crystal converter which will result in serious instabilities. A number of unsuccessful attempts at sealing the slot in the cavity with araldite were made before it was found that a satisfactory seal could be obtained by enclosing the cavity and the waveguide below the oxygen cap in a rubber condom. It is rather surprising that they do not crack when immersed in liquid helium.

2. Amplifier and Detector

A three-stage tuned amplifier of standard design, with band center at 462 kc., has been used to amplify the video signals from the crystal converter. It has a gain of 10^6 and a bandwidth of 8 kc. Care has been taken in the design of the input stage to ensure that the receiver noise figure is small. The phase sensitive detector is of standard design and employs a crystal bridge. Careful electromagnetic shielding of the crystal detector and the entire amplifier is essential because of the large stray radiation field from 462 kc. magnetic field modulation. This has been accomplished by the use of a "water-tight" brass box which contains the crystal converter, amplifier, and detector.

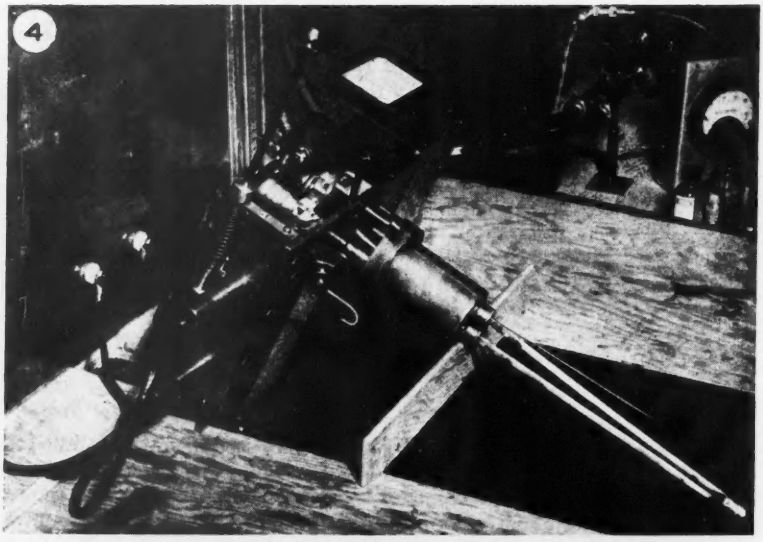

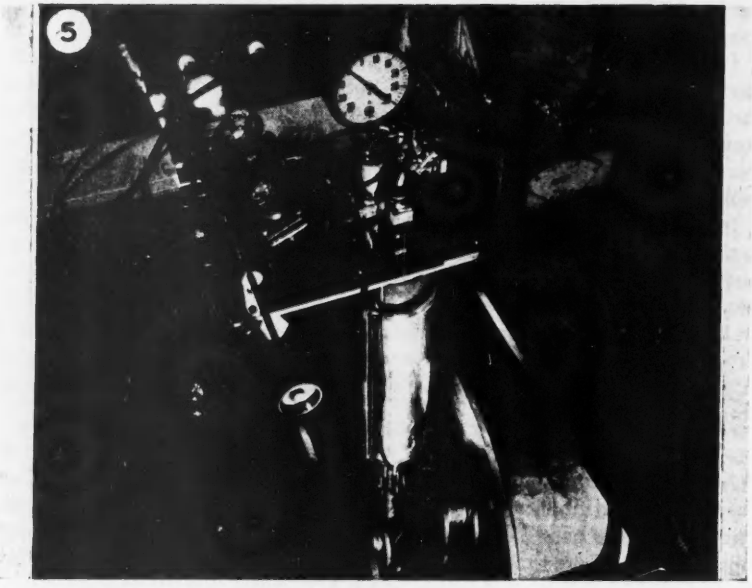

FIG. 4. Photograph of double field modulation paramagnetic resonance spectrometer head showing slotted cavity.

FIG. 5. Photograph showing spectrometer head with liquid oxygen and helium dewars in gap of electromagnet.

3. Magnetic Fields

(*a*) *Magnet and Magnet Power Supply*

A magnet having 4 in. diameter pole faces is used. Adjustable shims permit near optimum magnetic field homogeneity at any desired gap to be achieved. The magnet can be rotated about an axis perpendicular to the direction of the magnetic field to facilitate the study of resonance phenomena as a function of the orientation of the magnetic field. The magnet current is obtained from a d-c. generator and is controlled by a continuously variable electronic current regulator.

(*b*) *Low Frequency Magnetic Field Modulation*

Helmholtz coils mounted on the poles of the magnet supply the 60 c.p.s. field modulation. Sufficient ampere-turns are available to sweep through 400 gauss of magnetic field. The voltage developed across a 1-ohm resistor in series with the modulation coils is used to supply, after proper phase adjustment, the time base for the oscilloscope.

(*c*) *High Frequency Magnetic Field Modulation*

A 300 watt transmitter consisting of a 6AG7 oscillator, 807 buffer, and 4-811A's in parallel supplies the power necessary to obtain the 462 kc. magnetic field modulation. An *LC* network matches the output of the transmitter to the split cavity. This network is shielded to reduce the radiation from it. The split cavity system is tuned to maximize the r-f. current circulating in it. Sufficient power is available to obtain an r-f. current of 75 amp. r.m.s. around the split cavity.

Sensitivity

The operation of this spectrometer has been checked using the organic radical diphenyl trinitro phenyl hydrazyl which exhibits the paramagnetic resonance spectra of an essentially free electron (g radical = 2.0038 ± 0.0002; g electron = 2.0023) (Holden, Kittel, Merritt, and Yager 1950). It is convenient to use because of its narrow line width (3.5 gauss in powder) and its high magnetic concentration.

With about 10^{-5} gm. of this radical at room temperature, a resonance with a signal-to-noise ratio of 50:1 could be observed with the video spectrometer. The same sample gave a resonance with a signal-to-noise ratio of 50,000:1 with the double magnetic field modulation spectrometer described in this paper. In both spectrometers, the amplifier bandwidth was 8 kc. Smaller samples were prepared by successive dilution in benzene. A resonance from 10^{-9} gm. (10^{-11} mole) of the radical prepared in this manner was observed with a signal-to-noise ratio of 2:1. A photograph of this resonance is shown in Fig. 6 while a stronger resonance from 10^{-6} gm. (10^{-9} mole) is shown in Fig. 7. It should be noted that both signals are the modulus of the derivative of the line shape.

Higher order "forbidden" transitions (Bleaney 1951) corresponding to $\Delta M = \pm 2$ and ± 3 have been observed in dilute gadolinium ethyl sulphate

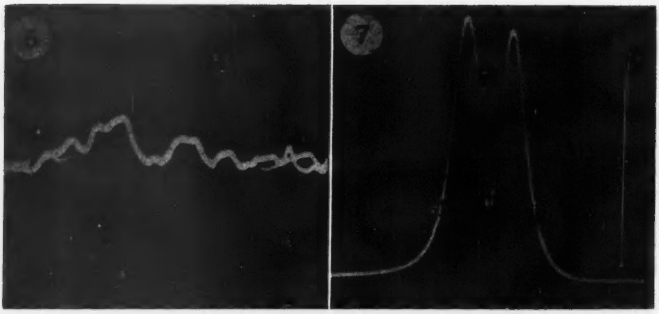

FIG. 6. Resonance signal 10^{-9} gm. "g" marker (S/N = 2:1).
FIG. 7. Typical strong resonance signal from 10^{-8} gm. "g" marker.

(Buckmaster 1956). Previously, only $\Delta M = \pm 1$ transitions have been observed (Bleaney, Scovil, and Trenam 1954). $\Delta M = \pm 2$ transitions have been observed with the double field modulation spectrometer with a signal-to-noise ratio of 1000:1 and $\Delta M = \pm 3$ with 10:1. The intensities of the $\Delta M = \pm 1, \pm 2$, and ± 3 transitions are in the ratio $10^4:10^2:1$. These measurements confirm the relative improvement in the signal-to-noise ratio of the video and double magnetic field modulation spectrometers.

The sensitivity of the double modulation spectrometer is still limited by crystal noise; however we estimate that it is within about a factor of 10 of the limit. It has been found possible to limit the sensitivity of this spectrometer by klystron noise if care is not taken in the choice of the klystron mode and the operating frequency on the mode (Torrey and Whitmer 1948). If paramagnetic substances with line widths of not less than eight gauss are to be studied, the high frequency magnetic field modulation current could be at 10 Mc. rather than 462.5 kc. At this frequency, the theoretical sensitivity should be obtainable.

The present double magnetic field modulation spectrometer has not been used in narrow band operation. However, it should be very easy to change to this mode of operation because of its inherently high stability. The sensitivity in narrow band operation (1 c.p.s.) should be $O(10^{-13})$ moles at 290°K. This stability is due to the fact that the resonance is detected twice, once at microwave frequencies and once at radio frequencies. It can be demonstrated by the observation that it is possible to obtain relatively stable resonance signals even when the cavity is partially full of a liquid refrigerant. Under the same conditions, it was found to be completely impossible to make measurements with a video spectrometer. The stability of the present spectrometer is largely determined by the power stability of our klystron (2K33A).

While there are at present two other paramagnetic resonance spectrometers (Beringer and Castle 1950; Feher unpublished) which possess the theoretical sensitivity, the spectrometer described in this paper is the only one which possesses all of the following advantages: (1) The adjustment is not critical. (2) The stability is good. (3) The apparatus required is relatively simple.

(4) It can be used for both wide and narrow band operation. Unfortunately, the theoretical sensitivity can only be obtained when line widths of about 10 gauss or greater are studied. This is not a very severe limitation because this is the commonest situation.

ACKNOWLEDGMENTS

This research was supported through financial grants from the National Research Council and one of the authors (H.A.B.) is indebted to the National Research Council of Canada for the award of a Fellowship for 1954–55.

REFERENCES

BERINGER, R. and CASTLE, J. G., JR. 1950. Phys. Rev. **78**: 581.
BLEANEY, B. 1951. Phil. Mag. **42**: 441.
BLEANEY, B., SCOVIL, H. E. D., and TRENAM, R. S. 1954. Proc. Roy. Soc. A, **223**: 15.
BLEANEY, B. and STEVENS, K. W. H. 1953. Repts. Progr. Phys. **16**: 108.
BOWERS, K. D. and OWEN, J. 1955. Repts. Progr. Phys. **18**: 304.
BUCKMASTER, H. A. 1956. Can. J. Phys. **34**: 150, 341.
FEHER, G. Unpublished.
HARTZ, T. R. and VAN DER ZIEL, A. 1950. Phys. Rev. **78**: 473.
HOLDEN, A. N., KITTEL, C., MERRITT, F. R., and YAGER, W. A. 1950. Phys. Rev. **77**: 147.
INGRAM, D. J. E. 1955. Spectroscopy at radio and microwave frequencies. Butterworth Scientific Publications, London.
MONTGOMERY, C. A. 1947. Technique of microwave measurements. Vol. 11. M.I.T. Radiation Lab. Series. McGraw-Hill Book Company, Inc., New York.
SMALLER, B. 1951. Phys. Rev. **83**: 812.
SMALLER, B. and YASAITIS, E. L. 1953. Rev. Sci. Instr. **24**: 991.
SMYTHE, W. R. 1950. Static and dynamic electricity. McGraw-Hill Book Company, Inc., New York.
TORREY, H. E. and WHITMER, C. A. 1948. Crystal rectifiers. Vol. 15. M.I.T. Radiation Lab. Series. McGraw-Hill Book Company, Inc., New York.

NOTES

A NEW LOOK AT THE REYNOLDS' STRESSES

By R. W. Stewart

It is the purpose of this note to make explicit a point of view which is implied in much of current work in turbulent shear flows. It will not seem particularly surprising to those who have been studying such flows with special emphasis on the detailed turbulent motion, but to those whose interest is almost entirely restricted to the effect of the turbulence on the mean flow, the ideas may be novel and even startling. This work has been stimulated by the valuable monograph by Townsend (1955) in which is stated the new approach to shear flow problems necessitated by the body of detailed information about turbulent flow which has accumulated in the last decade or so.

Let us write the Navier–Stokes equation for incompressible flow in tensor form (cf. Kármán and Howarth 1938)

$$\frac{\partial V_i}{\partial t}+V_j\frac{\partial V_i}{\partial x_j}+\frac{1}{\rho}\frac{\partial P}{\partial x_i}-\frac{\partial}{\partial x_j}\left(\nu\frac{\partial V_i}{\partial x_j}\right)=X_i \tag{1}$$

where V_i is the ith component of the total velocity vector relative to some steadily moving frame of reference, P is the local instantaneous pressure defined as the pressure experienced by a minute particle moving with the fluid, ρ is the local density, ν the kinematic viscosity, and X_i the ith component of an external body force (usually gravity).

We adapt the tensor summation convention to apply when an index explicitly occurs exactly twice in any term.

Following Reynolds (1894), we take V_i and P divided into two parts:

$$\begin{aligned} V_i &= U_i+u_i, \\ P &= \bar{P}+p \text{ (bars represent averaging)}, \end{aligned} \tag{2}$$

where $\overline{u_i}=\bar{p}=0$ in the sense that $(1/T)\int_T u_i\,dT$ converges stochastically to zero as T approaches some value small compared with the total extent of the flow. For flows in a steady state, or quasi steady state, T will be a time; otherwise it will be a length, area, or volume over which there is some symmetry; or if necessary a summation over a number of hypothetical flow realizations. The problem of suitable averages provides many philosophical and some mathematical difficulties, but is seldom of much importance in measurements of real flows, except in some meteorological and oceanographic examples.

Putting (2) in (1) and averaging over intervals of magnitude T, we find:

$$\frac{\partial U_i}{\partial t}+U_i\frac{\partial U_i}{\partial x_j}+\frac{1}{\rho}\frac{\partial \bar{P}}{\partial x_i}+\frac{\partial \overline{u_iu_j}}{\partial x_j}-\frac{\partial}{\partial x_j}\left(\nu\frac{\partial U_i}{\partial x_j}\right)=\overline{X}_i, \tag{3}$$

where we have made use of the continuity condition for incompressible flow in a uniform medium:

$$\partial u_j/\partial x_j = 0.$$

The $\overline{u_i u_j}$ are the well-known Reynolds' stresses, and represent the entire effect of the turbulence on the flow.

Now the fact that turbulence can transfer momentum in a direction perpendicular to the mean flow and down a mean velocity gradient has led many workers, starting with Reynolds himself, to treat it as producing a virtual viscosity, or "eddy viscosity" ν_e, and in essence

$$-\overline{u_i u_j} \text{ is put equal to } \nu_e \, \partial U_i/\partial x_j.$$

The momentum and vorticity transport theories of Prandtl and Taylor with their "mixing length" concept, crystallized this viewpoint and it is still in wide use (Goldstein 1938; and many other works). In an analogy with the Kinetic Theory of Gases' theory of viscosity, ν_e was thought of as the product of a turbulent velocity (analogous to the molecular velocity) and a mixing length (analogous to the mean free path). The essential problem of turbulent flow has been conceived to be to determine, from the mean flow distribution, values for a mixing length and a turbulent velocity. The product is the eddy viscosity which operates on $\partial U_i/\partial x_j$. This leads to some anomalous situations. For example if $\partial U_i/\partial x_j$ is zero, but $\overline{u_i u_j}$ is non zero, we must think of ν_e as being infinite.

It is most important, however, to observe that $\overline{u_i u_j}$ does not contain any *length*,* i.e. equally energetic small eddies are just as effective in the transport of momentum as large eddies. This is quite contrary to the physical picture visualized by the mixing length idea. Probably the chief objection to the eddy viscosity concept in its usual "mixing length" form is the misleading physical picture it brings to mind.

If it is likely to be misleading to think of the Reynolds' stresses as producing a virtual viscosity, how can they best be thought of? To answer this question, it is only necessary to note that $\overline{u_i u_j}$ is a second order symmetric tensor, so it is always possible to find at any point three orthogonal directions such that if they are made co-ordinate directions, the tensor $\overline{u_i u_j}$ in these co-ordinates is diagonalized, i.e. $\overline{u_i u_j} = 0$, $i \neq j$ (e.g. Green and Zerna 1954, p. 24).

In these special co-ordinates equation (3) becomes

$$\frac{\partial U_i}{\partial t} + U_j \frac{\partial U_i}{\partial x_j} + \frac{1}{\rho}\frac{\partial \overline{P}}{\partial x_i} + \frac{\partial (\overline{u_i u_i})}{\partial x_i} - \frac{\partial}{\partial x_j}\left(\nu \frac{\partial U_i}{\partial x_j}\right) = \overline{X}_i. \tag{4}$$

We now have no cross components of the type $\overline{u_1 u_2}$ in which the correlation between u_2 and u_1 can be thought of as transporting 1-directed momentum in the 2 direction. All we have is the term $\overline{u_i^2}$ † or twice the contribution to the turbulent energy per unit mass from motions in the i direction. Yet these terms still describe the entire effect of the turbulence on the motion! It is now

*This fact was observed by Lamb (1945, p. 677) in another connection.

†Our summation convention implies summation for $\partial \overline{u_i^2}/\partial x_i$ and $\overline{u_i u_i}$ but not for $\overline{u_i^2}$ and $\partial(\overline{u_i u_i})/\partial x_i$.

evident that the Reynolds' stresses belong not with the viscosity, but with the pressure term. If the density can be taken as constant we may combine the two into

$$\frac{1}{\rho}\frac{\partial}{\partial x_i}(\bar{P}+\rho\overline{u_i u_i})$$

and we see that the effect of the turbulence can be represented by an additional pressure $\rho\overline{u_i^2}$ acting in the i direction. If the turbulence is isotropic in the most elementary sense that the intensity is the same in all directions, then $\overline{u_i u_j} = \overline{u^2}\,\delta_{ij}$, where δ_{ij} is the Kronecker delta symbol. In this case the turbulence has no effect whatever on the flow except that the fluid will expand the amount required for the value of $\bar{P}$ to decrease by $\rho\overline{u^2}$ from its non-turbulent value.

When, however, the $\overline{u_i^2}$ are different, we shall have different effective pressures in different directions, and the flow will be modified accordingly.

We now see that the Reynolds' stresses express the effect of the anisotropy of the turbulence on the flow—and that only. To complete the physical picture, the situation is as follows:

The mean velocity gradients $\partial U_i/\partial x_j$ imply mean rates of strain.

These mean rates of strain act on the turbulence so as to stretch vortex tubes in the direction of positive rates of strain and compress them in the direction of negative rates of strain. This produces increased vorticity in the direction of positive rates of strain and decreased vorticity in the direction of negative rate of strain (Kármán and Howarth 1938).

Both theoretically and experimentally this can be shown (Townsend 1955, Chapter 4) to result in turbulent intensities low in the direction of positive rate of strain and high in the direction of negative rate of strain, i.e. the turbulence becomes anisotropic, with the preferred directions determined by the mean flow gradients.

The anisotropic turbulence, acting like a pressure different in different directions, modifies the mean flow.

This picture is very similar to and owes much to the ideas presented by Townsend (1955). The difference in point of view from that of the traditional eddy viscosity idea is, however, striking, and the two salient differences will bear repeating for emphasis:

1. The scale of the turbulence is of no consequence as far as its effects on the mean flow are concerned.

2. Isotropic turbulence produces no influence. The Reynolds' stresses are only important in that they express the amount and orientation of the anisotropy of the turbulence.

Thus it is seen that although the mixing length concepts have been very successful in supplying a foundation for empirical formulae in such situations as wake and pipe flows, the physical picture they invoke is inaccurate, and the model is likely to give false impressions when applied to other situations such as occur in meteorology and oceanography. It is preferable to regard the Reynolds' stresses as pressures, for it is then much easier to keep in mind that they are in fact only manifestations of the anisotropy of the turbulence.

It is hoped to deal with some oceanographic aspects of these concepts in a forthcoming paper.

GOLDSTEIN, S. *Editor*. 1938. Modern developments in fluid dynamics. The Clarendon Press, Oxford.
GREEN, A. E. and ZERNA, W. 1954. Theoretical elasticity. The Clarendon Press, Oxford.
KÁRMÁN, T. VON and HOWARTH, L. 1938. Proc. Roy. Soc. A, **164**: 192.
LAMB, H. 1945. Hydrodynamics. 6th ed. Dover Publications, New York.
REYNOLDS, O. 1894. Trans. Roy. Soc. A, **186**: 123.
TOWNSEND, A. A. 1955. The structure of turbulent shear flow. Cambridge University Press, Cambridge.

RECEIVED FEBRUARY 29, 1956.
DEPARTMENT OF PHYSICS,
UNIVERSITY OF BRITISH COLUMBIA,
VANCOUVER, B.C.

CURRENT DEPENDENCE OF THE SUPERCONDUCTING TRANSITION

BY D. C. BAIRD

The superconducting transition of wire carrying a current is of interest as an example of the intermediate state. Two equivalent experiments are possible. de Haas and Voogd (1931) and Haley and Andrews (1953) measured the resistance versus temperature curves for various currents and Scott (1948) measured the variation of resistance with current for constant temperature. The work of Scott shows that the hypothesis of Silsbee (1916) regarding the critical current for the onset of the intermediate state is borne out. However, the actual value of the resistance in the intermediate state in both sets of experiments is unsatisfactory. The treatment by London (1950) of a current-carrying superconductor suggests that the sudden rise on the destruction of superconductivity by a current should be to a resistance, R, half the total value R_0 but Scott's results show a rise to a value higher than this suggesting the existence of some source of resistance other than the mesh of normal and superconducting regions postulated by London. The work of Haley and Andrews showed that for columbium nitride the variation of current with the square of that temperature for which $R = \frac{1}{2}R_0$ did not follow the linear form predicted by London. This is not necessarily equivalent to the discrepancy found by Scott but tends to confirm the inadequacy of the London picture. The present report deals with preliminary experiments on the behavior of a current-carrying superconductor designed to investigate the resistance in the intermediate state.

The sample consisted of extruded tin wire of diameter 0.5 mm. and purity about 99.99% wound non-inductively and strain-free on a plexiglass frame. Its resistance was measured by a Leeds and Northrup galvanometer which operated a split-cell amplifier with negative feedback finally recording on a Beckman photo-pen recorder. The temperature was simultaneously recorded while the sample was cooled slowly through the transition. The resistance R

expressed as a fraction of the residual resistance R_0 is shown as a function of temperature and current in Fig. 1.

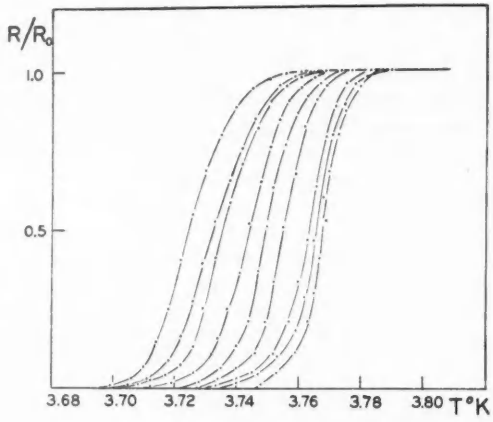

FIG. 1. Resistance, expressed as a fraction of the residual resistance, as a function of temperature and current. The curves refer (left to right) to currents of 600, 435, 328, 229, 142, 81, 20, 10, and 1 ma.

Silsbee postulated that the transition should take place between the intermediate state and the superconducting state when the current-produced field equals H_c at the surface of the wire. On the London model, which involves triangular laminae of normal and superconducting states, this results in a resistance $R = \frac{1}{2}R_0$. This means that for the point $R = \frac{1}{2}R_0$ on a curve for current i in a wire of radius a

$$H_c = 2i/a,$$

whence, using the parabolic critical field form,

$$H_c = H_0(1-(T/T_c)^2),$$

$$i = \tfrac{1}{2}aH_0-(aH_0/2T_c^2)T^2.$$

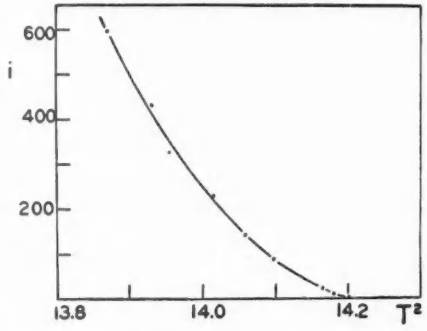

FIG. 2. Current in ma. versus the square of the temperature for which $R = \frac{1}{2}R_0$.

The plot of i versus T^2 is given in Fig. 2. The departure from linearity is obvious and the slope can be used to find the region in which the fit is best. The calculated slope $aH_0/2T_c^2$ is 0.274, and from the graph the slopes are 0.275 and 0.045 at the top and bottom of the curve respectively. The disagreement with theory therefore lies at the low current end and the curve for higher currents may become the straight line suggested by the theory.

While the transitions are comparatively broad on account of the polycrystalline nature of the specimen, it is difficult to see how this will affect any current variation. It can be seen that the shape of the lower part of the transition, which arises from the crystal structure of the specimen and lies outside the scope of the theory, is not altered substantially by the increased current and it appeared to be justified, on that account, to accept the shift of the half-resistance point as arising genuinely from the altered current.

This is the same effect as observed by Haley and Andrews. Their interpretation was based on the fact that their material was columbium nitride. Superconducting alloys are known to have intermediate state structures different from those found in pure superconductors and it seemed not unreasonable to attribute this current effect to the anomalous magnetic behavior. However the present results suggest that this anomalous effect is a feature of the current-carrying superconductor in general and is not restricted to alloys.

If it is a general property of the current-carrying superconductor, we must regard the effect as confirmation of the inadequacy of the London model. The London treatment specifies the shape of the intermediate state zones within the wire, on the assumption that ideal conditions are obtained. Observations of Meshkovsky (1949) and Schawlow *et al.* (1954) on the structure of the intermediate state show that it is on a scale much larger than that expected from intermediate state theory. This means that the much finer structure derived by London is not stable and it is not surprising, therefore, that the London value of the resistance in the intermediate state is unsatisfactory for wires of diameter less than 1 mm.

Preliminary experiments on 1 mm. wire indicate that the curvature, if it exists, of the i vs. $T^2_{R=\frac{1}{2}R_0}$ characteristic is very much smaller than that for $\frac{1}{2}$ mm. wire, which tends to confirm the suggestion that these anomalous features arise from the scale of the intermediate state structure.

DE HAAS, W. J. and VOOGD, J. 1931. Communs. Kamerlingh Onnes Lab. Univ. Leiden, No. **214c**.
HALEY, F. C. and ANDREWS, D. H. 1953. Phys. Rev. **89**: 821.
LONDON, F. 1950. Superfluids. 1st ed. John Wiley & Sons, Inc., New York. pp. 120–124.
MESHKOVSKY, A. G. 1949. J. Exptl. Theoret. Phys. (U.S.S.R.), **19**: 1.
SCHAWLOW, A. L., MATTHIAS, B. T., LEWIS, H. W., and DEVLIN, G. E. 1954. Phys. Rev. **95**: 1344.
SCOTT, R. B. 1948. J. Research Natl. Bur. Standards, **41**: 581.
SILSBEE, F. B. 1916. J. Wash. Acad. Sci. **6**: 597.

RECEIVED MARCH 27, 1956.
DEPARTMENT OF PHYSICS,
ROYAL MILITARY COLLEGE OF CANADA,
KINGSTON, ONTARIO.

LETTERS TO THE EDITOR

Under this heading brief reports of important discoveries in physics may be published. These reports should not exceed 600 words and, for any issue, should be submitted not later than six weeks previous to the first day of the month of issue. No proof will be sent to the authors.

V.H.F. Auroral Noise

Radio frequency radiation from the aurora was reported by Forsyth, Petrie, and Currie (1949). Covington (1947, 1950), at about the same time, also reported radiation from the sky, which was associated with geomagnetic and ionospheric disturbances. However, further investigations by other workers (Chapman and Currie 1953; Harang and Landmark 1954) failed to show that noise emissions were being received from the aurora, and Chapman and Currie (1953) suggested that the effect may be linked to the sunspot cycle. Consequently, as the time of sunspot maximum is now approaching, it should be possible to verify this hypothesis.

At the Radio Physics Laboratory apparatus designed to record continuously the 50 Mc./s. radiation from the radio star in Cassiopeia (Hartz 1955) has recorded in recent months increased radiation on numerous occasions. A more intensive study using auxiliary receiving equipment has not only ruled out the possibility of interference from local sources or from distant transmitters, but has established that the additional radiation occurs when there is positive evidence of the presence of aurora.

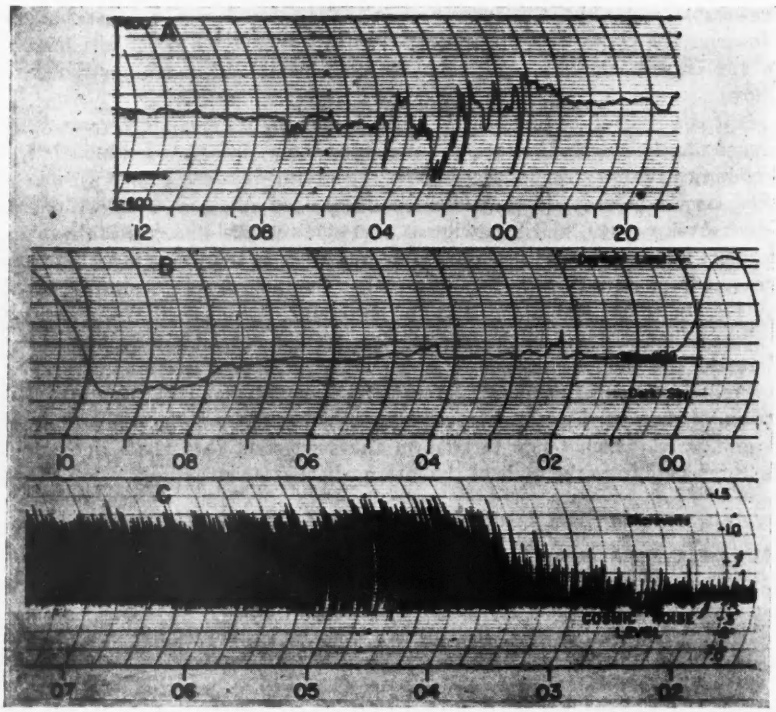

FIG. 1. Example of 32 Mc./s. noise associated with the aurora. A—magnetometer record, B—record from photomultiplier, C—record from 32 Mc./s. noise receiver.

The occurrence of aurora is established by visual observation by an observer, by recordings from a photomultiplier system directed at the northern sky, by magnetometer recordings which show large deviations, and by the appearance of a greatly enhanced signal from a V.H.F. transmitter at a distance of 500 miles.

On several occasions, when the presence of aurora was indicated by all of the above means, radio frequency noise was recorded at frequencies of 32, 50, and 53 Mc./s. of an intensity greater than the cosmic noise level. In some, but not in all cases, some evidence of sporadic absorption of cosmic or radio star radiation was present at the same time. The enhanced signal, when displayed on an oscilloscope or listened to on headphones, appeared to have the characteristics of white noise, and in no case was a signal from a transmitter heard.

In Fig. 1 examples are given of the records obtained on the night of 21–22 March, 1956, when aurora was observed. All times in the figure are Universal Time. The magnetometer record is shown in part A, while part B shows the chart from the photomultiplier auroral recorder. Part C of the diagram shows the record from a 32 Mc./s. receiver which has a vertically directed antenna (beam width approximately 40° to 3 db. points). The presence of enhanced noise radiation can be seen above the cosmic noise level on this latter record.

While the occurrence of terrestrial noise interference originating at some distant point and being reflected by the aurora might explain the observed phenomena, this is considered highly unlikely in view of the very large recorded signal. Likewise, the simultaneous occurrence at three frequencies would rule out a distant transmitting station. It is concluded, then, that radio frequency emissions are being recorded which are associated with the aurora, and hence originate either in the aurora or in the disturbed ionosphere at times of aurora.

This work was carried out under the Defence Research Board project PCC-D48-28-01-02.

CHAPMAN, R. P. and CURRIE, B. W. 1953. J. Geophys. Research, **58**: 363.
COVINGTON, A. E. 1947. Terrestrial Magnetism and Atm. Elec. **52**: 339.
——— 1950. J. Geophys. Research, **55**: 33.
FORSYTH, P. A., PETRIE, W., and CURRIE, B. W. 1949. Nature, **164**: 453.
HARANG, L. and LANDMARK, B. 1954. J. Atm. Terrest. Phys. **4**: 333.
HARTZ, T. R. 1955. Can. J. Phys. **33**: 476.

RECEIVED APRIL 30, 1956.
DEFENCE RESEARCH TELECOMMUNICATIONS ESTABLISHMENT,
RADIO PHYSICS LABORATORY,
DEFENCE RESEARCH BOARD,
SHIRLEY BAY,
OTTAWA, ONTARIO.

T. R. HARTZ
G. C. REID
E. L. VOGAN

Alloy Dendritic Growth

This article has been written to clear up any possible misconception concerning the work of Tiller and Rutter (1956) with regard to their treatment of the transition from a cellular to a dendritic interface in a lead–tin alloy.

It was observed during the course of the experimental work that when crystals of different crystallographic orientation exhibited an interface composed of cells, the shape of the cells depended upon the orientation of the interface. Fig. 18 of the above-mentioned article shows that the cell size may differ by a factor of three or four owing to the difference in the crystallographic orientation of the interface presented to the liquid. Tiller (1955) has shown that this size difference of the cells produces a large interface step between a crystal of high index orientation interface and a crystal of low index orientation interface. Rosenberg and Tiller (1956) discuss this phenomenon and show how it produces the preferred orientation of the columnar zone of a casting.

Because of the different cell size on the crystals of different orientation the interfaces of these crystals become unstable and break down into dendrites under very different growth conditions. The first interface to develop side branches was the interface which exhibited the largest cells; this was the high index orientation interface. The last interface to develop side branches was the interface which exhibited the small regular cells; this was the (100) interface.

In order to study the development of side branching on these interfaces polycrystalline samples containing between five and ten crystallites were grown under various conditions. It was observed that generally one of the crystallites would have an orientation which falls near the center of the stereographic triangle of a standard (100) projection, and another would have an orientation near the dendrite orientation. X-Rays were not taken to determine these orientations because experience allowed one to estimate the orientation of the interface relative to the dendrite orientation by the shape of the cells.

The results plotted in Fig. 8 of the article were determined by observing the conditions for which the first cellular crystallite became unstable, and the conditions for which the last cellular crystallite became unstable. In this way it was possible to find the breakdown conditions for crystals with orientations falling in the center of the stereographic triangle and for crystals of the dendrite orientation. This provided a band of conditions between which inter-

faces of all possible orientations may become unstable for the proper growth conditions. To determine the exact breakdown conditions for interfaces of any other orientation than the two extremes it would be necessary to incorporate an X-ray study of the crystallites. This was definitely not done by Tiller and Rutter (1956) as they were interested only in the two extremes.

The breakdown ratio $G/R^{\frac{1}{2}}$, which describes the transition from a cellular to a dendritic interface, will be not only orientation and concentration dependent, but it will depend very markedly on the type of solute present. The characteristic of the solute to be considered in this case is the k-value as this determines the concentration of solute in the liquid at the interface. Consideration of the theory of redistribution of solute during solidification suggests that the equation describing the breakdown of a cellular interface to a dendritic interface would be of the form

$$G/R^{\frac{1}{2}} = A_\theta C_0/k,$$

where A_θ is the proportionality constant for any particular orientation θ.

It is possible to estimate the variation of A_θ with θ by considering the relative sizes of the cells on interfaces of different θ. The way in which the cells relieve the constitutional supercooling at the interface is that they trap solute at the cell boundaries that would otherwise reside in the solute-rich layer of liquid adjacent to the interface. This decreases the constitutional supercooling by lowering the solute concentration at the interface. The amount of cell boundary per unit area of the interface will vary inversely as the cell size. Therefore, the solute concentration at the interface will vary inversely as the cell size. This accounts for the interface step between a crystal having large cells and a crystal having small cells, and also leads to the relationship

$$A_\theta = A' d_\theta$$

where d_θ is the width of the cell at breakdown.

An estimation of the variation of d_θ with θ involves the consideration of the platelet mechanism of solidification as studied by Rosenberg (1956), and the solute configuration ahead of a cellular interface. This will be discussed in a subsequent publication. However, the ratio of the slopes of the breakdown curves for the two extremes of orientation in Fig. 8 is about 3.5. This is approximately the ratio of the cell sizes for the two extremes of orientation also.

ROSENBERG, A. 1956. Ph.D. Thesis, University of Toronto, Toronto, Ont.
ROSENBERG, A. and TILLER, W. A. 1956. To be published.
TILLER, W. A. 1955. Ph D. Thesis, University of Toronto, Toronto, Ont.
TILLER, W. A. and RUTTER, J. W. 1956. Can. J. Phys. **34**: 96.

RECEIVED MAY 4, 1956.
W. A. TILLER
METALLURGY DEPARTMENT,
WESTINGHOUSE ELECTRIC CORPORATION,
BEULAH ROAD, CHURCHILL BORO.,
PITTSBURGH 35, PA.

THE PHYSICAL SOCIETY

MEMBERSHIP of the Society is open to all who are interested in Physics.

FELLOWS pay an Entrance fee of £1 1*s*. ($3.00) and an Annual Subscription of £2 2*s*. ($6.00).

STUDENTS: A candidate for Studentship must be between the ages of 18 and 26, and pays an Annual Subscription of 5*s*. ($0.75).

MEETINGS: Fellows and Students may attend all Meetings of the Society including the annual Exhibition of Scientific Instruments and Apparatus.

PUBLICATIONS include the *Proceedings of the Physical Society*, published monthly in two sections, and *Reports on Progress in Physics*, published annually. Volume XVIII, 1955, is now available (price 50*s*. ($7.15)). Members are entitled to receive many of the Publications at a reduced rate.

Further information can be obtained from:

THE PHYSICAL SOCIETY

1, LOWTHER GARDENS, PRINCE CONSORT ROAD

LONDON, S.W.7, ENGLAND

CANADIAN JOURNAL OF PHYSICS

Notes to Contributors

Manuscripts

(i) ***General.*** Manuscripts, in English or French, should be typewritten, double spaced, on paper 8½ × 11 in. **The original and one copy are to be submitted.** Tables and captions for the figures should be placed at the end of the manuscript. Every sheet of the manuscript should be numbered.

Style, arrangement, spelling, and abbreviations should conform to the usage of this journal. Names of all simple compounds, rather than their formulas, should be used in the text. Greek letters or unusual signs should be written plainly or explained by marginal notes. Superscripts and subscripts must be legible and carefully placed.

Manuscripts and illustrations should be carefully checked before they are submitted. Authors will be charged for unnecessary deviations from the usual format and for changes made in the proof that are considered excessive or unnecessary.

(ii) ***Abstract.*** An abstract of not more than about 200 words, indicating the scope of the work and the principal findings, is required, except in Notes.

(iii) ***References.*** References should be listed **alphabetically by authors' names,** unnumbered, and typed after the text. The form of the citations should be that used in issues of this journal published in '956; in references to papers in periodicals, titles should not be given and only initial page numbers are required. The names of periodicals should be abbreviated in the form given in the most recent *List of Periodicals Abstracted by Chemical Abstracts*. All citations should be checked with the original articles and each one referred to in the text by the authors' names and the year.

(iv) ***Tables.*** Tables should be numbered in roman numerals and each table referred to in the text. Titles should always be given but should be brief; column headings should be brief and descriptive matter in the tables confined to a minimum. Vertical rules should be used only when they are essential. Numerous small tables should be avoided.

Illustrations

(i) ***General.*** All figures (including each figure of the plates) should be numbered consecutively from 1 up, in arabic numerals, and each figure referred to in the text. The author's name, title of the paper, and figure number should be written in the lower left corner of the sheets on which the illustrations appear. Captions should not be written on the illustrations (see Manuscripts (i)).

(ii) ***Line Drawings.*** Drawings should be carefully made with India ink on white drawing paper, blue tracing linen, or co-ordinate paper ruled in blue only; any co-ordinate lines that are to appear in the reproduction should be ruled in black ink. Paper ruled in green, yellow, or red should not be used unless it is desired to have all the co-ordinate lines show. All lines should be of sufficient thickness to reproduce well. Decimal points, periods, and stippled dots should be solid black circles large enough to be reduced if necessary. Letters and numerals should be neatly made, preferably with a stencil (**do NOT use typewriting**) and be of such size that the smallest lettering will be not less than 1 mm. high when reproduced in a cut 3 in. wide.

Many drawings are made too large; originals should not be more than 2 or 3 times the size of the desired reproduction. In large drawings or groups of drawings the ratio of height to width should conform to that of a journal page but the height should be adjusted to make allowance for the caption.

The original drawings and one set of clear copies (e.g. small photographs) are to be submitted.

(iii) ***Photographs.*** Prints should be made on glossy paper, with strong contrasts. They should be trimmed so that essential features only are shown and mounted carefully, with rubber cement, on white cardboard with no space or only a **very** small space (less than 1 mm.) between them. In mounting, full use of the space available should be made (to reduce the number of cuts required) and the ratio of height to width should correspond to that of a journal page (4¾ × 7½ in.); however, allowance must be made for the captions. Photographs or groups of photographs should not be more than 2 or 3 times the size of the desired reproduction.

Photographs are to be submitted in duplicate; if they are to be reproduced in groups one set should be mounted, the duplicate set unmounted.

Reprints

A total of 50 reprints of each paper, without covers, are supplied free. Additional reprints, with or without covers, may be purchased.

Charges for reprints are based on the number of printed pages, which may be calculated approximately by multiplying by 0.6 the number of manuscript pages (double-spaced typewritten sheets, 8½ × 11 in.) and including the space occupied by illustrations. An additional charge is made for illustrations that appear as coated inserts. The cost per page is given on the reprint requisition which accompanies the galley.

Any reprints required in addition to those requested on the author's reprint requisition form must be ordered officially as soon as the paper has been accepted for publication.

Contents

Page

Meteoric Echoes Observed Simultaneously by Back Scatter and Forward Scatter—*D. W. R. McKinley and A. G. McNamara* 625

Radiation Patterns of a Dielectric-coated Axially-slotted Cylinder—*R. A. Hurd* - - - - - - - - - - - - - - - - 638

Absorption Spectra of Ethylene and Ethylene-d_4 in the Vacuum Ultraviolet. II—*P. G. Wilkinson* - - - - - - - - - - 643

Spin Echoes in Alcohols and Derivatives—*G. J. B. Crawford and J. S. Foster* - - - - - - - - - - - - - - - - 653

The Oscillating Sphere at Large Amplitudes in Liquid Helium—*C. B. Benson and A. C. Hollis Hallett* - - - - - - - - 668

On the Distribution of the Product of Diode Detector Waveforms—*E. L. R. Webb* - - - - - - - - - - - - - - - - 679

Correlation Tensors in Statistical Hydrodynamics in Porous Media—*A. E. Scheidegger* - - - - - - - - - - - - 692

Some Results of the High Dispersion Electronic Emission Spectrum of Formaldehyde—*G. Wilse Robinson* - - - -- - - 699

A Double Magnetic Field Modulation Paramagnetic Resonance Spectrometer—*H. A. Buckmaster and H. E. D. Scovil* - - - 711

Notes:

A New Look at the Reynolds' Stresses—*R. W. Stewart* - - - 722

Current Dependence of the Superconducting Transition—*D. C. Baird* - - - - - - - - - - - - - - - - - - 725

Letters to the Editor:

V.H.F. Auroral Noise—*T. R. Hartz, G. C. Reid, and E. L. Vogan* 728

Alloy Dendritic Growth—*W. A. Tiller* - - - - - - - - 729

Printed in Canada *by* University of Toronto Press